

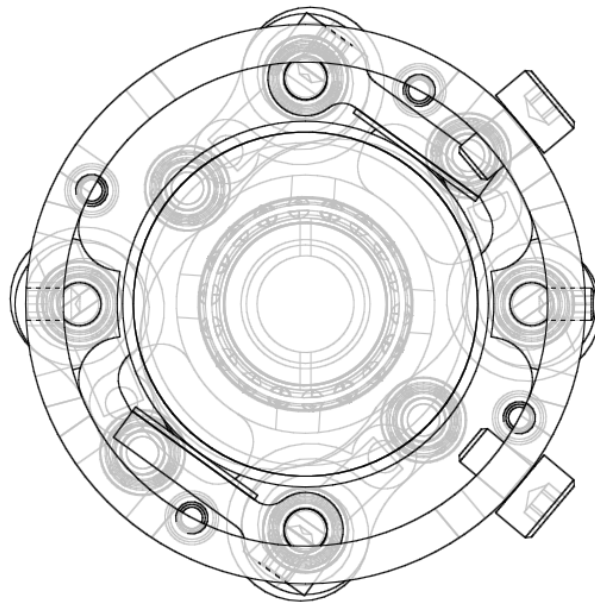
Statically balanced singular-friction locking

Tom van der Hoeven (1519786)

Master thesis

Delft University of Technology
Mechanical Engineering, BioInspired Technology

April 29, 2015



Foreword

At the very beginning of this thesis I would like to take the opportunity to write a personal note on the experience of studying over the last few years. A few things have become clear near the end of my time as a student. First, I have come to think that the questions never disappear when knowledge is gained, they just become more sophisticated or are replaced with new, often more difficult questions. This phenomena will either cause feelings of misery or happiness, depending on the curiosity and self-confidence of the researcher and his external guidance. Curiosity is something we tend to forget every now and then and needs some triggering to regain it. Self-confidence is a skill that can be taught. Ivan Joseph uses the definition of self-confidence to be *the ability or the belief to believe in yourself, to accomplish any task, no matter the odds, no matter the difficulty, no matter the adversity. The belief that you can accomplish it.* I very much enjoy that definition since I think it resembles much of the idea of the second master year. That does however not mean that the task you are to believe in is always clear, certainly not when you have to determine it yourself. That is where the master thesis comes in again, because it is mostly up to you what you make out of it. Last years curiosity, self-confidence and external guidance have led to the work you are about to read, up to the standards that I hope to use as a future engineer. I am happy and satisfied with my graduation project and I am curious to learn how my standards are valued by the examination committee.

Of course this thesis, this master and this bachelor could not have been without the support of friends, family, supervisors, professors and other TU employees. First, I would like to greatly thank my parents, brothers and sisters for their mental, physical and (definitely) financial support during my entire study career. Secondly, many thanks to Michiel for supervising my project with great care. I very much enjoyed the last 12 months for the inspirational talks, the philosophical discussions, the jokes, the Friday afternoon games, and your endless ability to trigger me into working harder and digging deeper into the subject. Thirdly, I also would like to thank the entire RAP project group for their inspirational work, their questions and their comments during the two-weekly meetings. Special thanks to Wouter and Michiel for proofreading my thesis and the comments on how to improve the thesis. Fourthly, many thanks to Jan, Nisse, Reinier, Sjoerd, Jaap and all the others working in the workshop. I am jealous of your skill and ability to make anything your eyes see with the (extreme) quality that your hands are capable of in such short time. Without you and your fast, accurate and beautiful work there would not have been a prototype, let alone a working one, at all. Fifthly, many thanks to my graduation committee members prof. dr. ir. Just Herder and prof. dr. ir. Frans van der Helm. I am honoured to

have you in my graduation committee and as you will read during the rest of this thesis, your work has been a great source of inspiration. Lastly but definitely not least, many thanks to my friends. Whether I met you through my addiction to speedskating, through my affections with (jazz) music, through cycling, through my initial motivation for mechanics (steam engines), through study, just in a bar with good Belgian beer or in a bunch of other situations: without you I would *never* have come this close to graduating.

Abstract

Locking mechanisms are used in a wide range of applications including energy saving mechanisms in the field of robotics. In this thesis a new class of locking mechanisms is investigated: a combination between a singular- and a friction locking mechanism (singular-friction locker) which is statically balanced with one additional spring. This combination of three types of locking mechanisms results in a locking mechanism that has an infinite number of locking positions, can unlock well under load and has an absolute zero actuation force in a singular configuration. In all other configurations the mechanism is theoretically in static balance.

The first part of this thesis investigates rigid body type statically balanced singular-friction lockers (SBS-FLs) and works towards a classification of all possible classes of SBS-FLs. This classification contains nine types of rigid body SBS-FLs, consisting of one linkage type class of lockers and eight cam type classes of lockers.

In the second part of this thesis different embodiments of SBS-FL mechanisms are investigated on their ability to become a very compact locking device. From five different concepts the highest compactness is obtained by a locking mechanism with a rotational cam input and a rotational follower connected to torsion springs. This mechanism is build and all design aspects are reported.

In the third and last part of this thesis the performance and the characteristics of the prototype are investigated. The locking device has a zero actuation torque in the 'engaged' and 'disengaged' (singular) configurations and a maximum actuation torque of 0.035 Nm when switching 'on' and 'off' in 5 seconds. This is a 97% reduction of the actuation torque compared to a regular brake. The maximum braking torque is 0.83 Nm in clockwise direction and 0.75 Nm in counter clockwise direction. The locking device has a diameter of 55 mm and a length of 23 mm. This efficient and small cam based prototype seems to be the most promising approach to statically balanced locking and can find its use not only in robotics but also for in example cars, trucks, bikes and trains.

Contents

1	Introduction	8
2	Singular configurations in locking mechanisms	13
2.1	Singular configurations in mechanisms	13
2.2	Classification of singular-friction lockers	15
2.3	Performance of the singular-friction locker	16
2.3.1	Transfer ratio	17
2.3.2	Manipulability of the actuation force characteristic	18
2.3.3	Compactness	18
2.4	Conclusion	19
3	Statically balancing singular-friction locking mechanisms	20
3.1	Statically balanced locking device	20
3.2	Removing the actuation force of a singular-friction locker	23
3.2.1	Equation of the summed input forces	23
3.3	Static balancing of linkages	26
3.3.1	Slider input - slider output	27
3.3.2	Rotational input - slider output	29
3.3.3	Rotational input - rotational output	31
3.3.4	Slider input - rotation output	32
3.3.5	Conclusion: linkages	34
3.4	Static balancing of cam mechanisms	35
3.4.1	Energy free locking cam systems	35
3.4.2	Generalization	39
3.5	Conclusion	42
4	Conceptual design	43
4.1	Compact locking device in robotics	43
4.2	Concept selection criteria	45
4.2.1	BIC-PEA	45
4.2.2	Specific selection criteria	45
4.3	Concepts	47
4.3.1	Linkage - Slider input/slider output	48
4.3.2	Cam - Slider cam/slider output	49
4.3.3	Cam - Rotation cam/slider output	51
4.3.4	Cam - Slider cam/rotation output	52

4.3.5	Cam - Rotation cam/rotation output	54
4.4	Concept selection and final concept	56
5	Prototype design	59
5.1	Required locking torque	60
5.2	The torsion springs	61
5.2.1	Material properties and required constants	61
5.2.2	Calculation procedure	62
5.2.3	Resulting spring	63
5.3	Cam design	65
5.3.1	Calculations and model	65
6	Performance evaluation	68
6.1	Performance of a SBS-FL mechanism	68
6.1.1	Performance metrics	68
6.1.2	Measurement variables for a SBS-FL mechanism	69
6.2	Experiments	70
6.2.1	Measurement setup	71
6.2.2	Experiment 1: Spring characteristics	72
6.2.3	Experiment 2: Input torque-angle relationship	76
6.2.4	Experiment 3: Output locking torque characteristic	77
6.3	Conclusion	81
7	Discussion	82
8	Conclusion	84
Appendices		
Appendix A Paper Statically balanced brakes		86
Appendix B Additions to chapter 2		99
B.1	Actuation force singular-friction locker	99
Appendix C Additions to chapter 3		101
C.1	Actuation force of a double singular-friction locker	101
C.2	Flawed SBS-FL	103
Appendix D Additions to chapter 5		104
D.1	Friction disk and arm in reality	104
D.2	Cam surface generation	105
D.3	Follower trajectory and cam model	107
D.4	Other components	109
D.4.1	Main body elements	109
D.4.2	Follower links	110
D.4.3	Locknut	111

Appendix E Additions to chapter 6	112
E.1 Additional images test setup	112
E.2 Calibration: No-load conditions	113
E.3 Single runs	115
E.4 Overview measurement runs	116

List of Figures

1.1	Mechanical locker and singular locker	9
1.2	The singular-friction locking mechanism example	12
2.1	Essential singular-friction locking linkage mechanisms	15
2.2	Essential singular-friction locking cam mechanisms	16
2.3	Actuation force characteristic	17
2.4	Schematic singular-friction locker	18
3.1	The z-force	21
3.2	Working principle z-force	22
3.3	A doubled singular-friction locker	24
3.4	Actuation force characteristics of a doubled singular-friction locker	25
3.5	The balanced ladder	26
3.6	SS type singular-friction locker	27
3.7	SBS-FL in on and off configurations	28
3.8	RS type singular-friction locker	29
3.9	General SBS-FL linkage RS	30
3.10	RR type singular-friction locker	32
3.11	SR type singular-friction locker	33
3.12	Overview SBS-FL linkages	33
3.13	Cam type SBS-FL in SS configuration	35
3.14	Two perfectly balanced cam shapes	36
3.15	Infeasible cam shape	37
3.16	Building blocks for a cam based SBS-FL.	39
3.17	Overview of cam based SBS-FLs	41
3.18	Extension to the overview of cam based SBS-FLs	42
4.1	Flowchart for designing a statically balanced locking mechanism	44
4.2	The design space for designing the locking mechanism for BIC-PEA	47
4.3	Linkage SBS-FL SS configuration	48
4.4	Cam SBS-FL SS configuration	50
4.5	Cam SBS-FL RS configuration	51
4.6	Cam SBS-FL SR configuration	53
4.7	Cam SBS-FL RR configuration	54
4.8	Final concept model	57
4.9	Final concept exploded model	57

4.10	Final concept quarter cut model	58
5.1	The final concept build: the p-brake	59
5.2	Figures to calculate the braking torque	60
5.3	Torsion spring schematic	62
5.4	Torsion spring from matlab	64
5.5	Torsion springs cut from spring steel	64
5.6	Cam surface generation	65
5.7	Cam shape from matlab	67
6.1	Locker in test setup to measure the locking torque	71
6.2	Locker in test setup to measure the input torque-angle relationship	72
6.4	Spring characteristic measured against position	74
6.3	Position trajectory of the motor	74
6.5	Spring characteristic in time	75
6.6	Input torque vs. input angle balanced system	76
6.7	Locking torque of the p-brake	78
6.8	Self engaging locking effect	79
6.9	Cam for proper disengagement	79
6.10	Combined overview figure of the input characteristics of the p-brake	80
B.1	Schematic singular-friction locker	99
C.1	Double singular-friction locker	101
C.2	Problem with SBS-FL linkage RS	103
D.1	Braking disk	104
D.2	Braking lever	105
D.3	Output follower angle versus input angle cam	107
D.4	Summed energy in all four springs	107
D.5	Matlab-solidworks export cam	108
D.6	Cam disk	109
D.7	Main body	110
D.8	Secondary body	110
D.9	Follower link with spring attached	111
D.10	Cam installed on the main body with the locknut	111
E.1	Rendered solidworks image of the test setup	112
E.2	Test setup in reality	113
E.3	No-load conditions at standstill	114
E.4	No-load conditions while moving at 5 rpm	114
E.5	Single run of the spring characteristic versus position	115
E.6	Single run of the locking torque measurement	115
E.7	A single run of the input torque versus the input angle	116

List of Tables

3.1	Performance specifications of the z-force	23
4.1	Linkage SBS-FL SS configuration score	48
4.2	Cam SBS-FL SS configuration score	50
4.3	Cam SBS-FL RS configuration score	52
4.4	Cam SBS-FL SR configuration score	53
4.5	Cam SBS-FL RR configuration score	55
4.6	Combined scores of all concept solutions	56
7.1	Performance of the two statically balanced lockers.	82
E.1	Overview of all measurement runs.	116
E.2	Overview of all measurement runs.	117
E.3	Overview of all measurement runs.	118
E.4	Overview of all measurement runs.	119
E.5	Overview of all measurement runs.	120
E.6	Overview of all measurement runs.	121

Chapter 1

Introduction

Robots have numerous applications, from simple repetitive tasks in factories, to more challenging environments where powered prosthetic devices allow humans to regain some of the complex functionality of the lost limb [1]. In the moving parts of many robots, an actuation force is required to obtain the desired movement. A very common way of providing this actuation force is by using a stiff actuator like an electric motor (when including feedback), which continuously consumes energy to maintain or reach a position.

Over the last 20 years studies in the field of actuator design show the increasing incorporation of elastic elements in the actuator to reach a higher energy efficiency [2,3]. Pratt and Williamson originally proposed the series elastic actuator (SEA) where elastic elements are placed in series with the motor [4].

Instead of placing springs in series with the motor, more recent studies focus on placing springs in parallel with the motor [5,6]. The idea of this parallel elastic actuation (PEA) is that the elastic elements provide most of the nominal torque along the preplanned movement trajectory and that the motor can be used for stabilizing control purposes [7].

The preplanned trajectory is however not always clear and cannot be adjusted due to the fixed spring characteristics. To solve this problem, mechanisms can be used to control the energy storage and release in and from the springs [8].

Timing of energy storage and release is done using locking mechanisms, which make these mechanisms of crucial importance in PEA. A definition or the essential functionality for such a locking device is: A device that switches between allowing and preventing the relative motion between two parts [9]. A great amount of locking mechanisms can be found in literature and a recent survey of locking mechanisms in robotics is given by Plooij et al. [9]. There are three main categories for locking principles of locking devices, which are mechanical locking, friction locking and singularity locking [9].

Mechanical lockers like latches [10], ratchets [1] or intermittent mechanisms [11] lock because one component blocks the mechanism. An example of such a mechanism is depicted in figure 1.1a. Generally mechanical lockers use little energy

and they can lock with high locking torques. Two major downsides of mechanical lockers are that they only have a limited number of locking positions and that they do not easily unlock while under load.

Friction lockers are mostly used in electromagnetic brakes (for example [12]). Other less common examples of friction brakes are bi-stable brakes [13], capstans [14], piezo actuated brakes [15] and statically balanced lockers [16]. They all share the locking principle of a friction force between two surfaces. This locking principle has the advantages that it can unlock under load and that an infinite number of locking positions can be used. The first downside of this principle is the energy consumption. The locking force scales linearly to the normal force on the friction surface when assuming Coulomb friction. The current (energy consumption) of a DC motor scales quadratically to the normal force. The second downside is that the maximum friction force that can be obtained is limited by the (limited) maximum normal force on the friction surface multiplied by a friction coefficient.

Singularity lockers like four bar mechanisms [5] and non-linear spring mechanisms [6] use singular configurations in the mechanism to lock. An example of such a mechanism is depicted in figure 1.1b. In a singular configuration the transfer ratio of the output (locking) force to the input (actuation) force goes to infinity. The advantages of singularity lockers are that they can unlock while under load and that they can produce high locking torques while consuming only little power. A disadvantage is that there usually are only a few singular configurations in which the mechanism locks, so the number of locking positions is very limited.

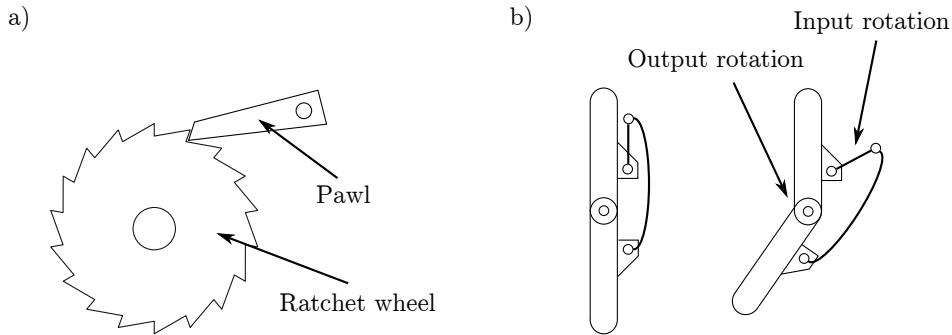


Figure 1.1: A mechanical type locking mechanism (figure a) and a singular type locking mechanism (figure b).

There are five important characteristics that a locking mechanisms must have when it is intended to be used for saving energy in actuators. First it must provide an infinite number of locking positions. Secondly a good unlocking-under-load performance is desired and thirdly low energy consumption is important. Fourthly the mechanism must have a high locking torque and lastly the mechanism must be compact.

There are two types of locking mechanisms that provide an infinite number of locking positions and generally unlock well while under load. The first option is a hydraulic locker, like a valve, which mechanically locks a fluid stream. Hydraulic lockers have a very different nature from all other mechanical lockers because they require a translation between mechanical movement and the fluid stream in the system. Hydraulic systems also require sealing to prevent the fluid from leaking out. The second option is a friction locker. Friction lockers do not have these fluid-related downsides and are therefore favoured to provide an infinite number of locking positions and good unlocking-under-load performance.

As explained, friction lockers often do not perform well on energy consumption. This performance is mainly because of the lack of an efficient source for the normal force on the friction surface. Generally, there are three ways to provide an efficient source for a normal force on a friction surface. The first way is to use a piezo actuator for the normal force. The second way is to decouple the actuation force - locking force relationship in the locking mechanism and the third way is to realize a very large transfer ratio between the actuation force and the locking force.

Piezo actuators do provide a high normal force while consuming only little energy but they require high voltages, a very stiff construction and very precise manufacturing. These downsides reduce the effectiveness of this type of actuator in a friction locking application.

Plooij et al. [16] proposed a static balancing system for a friction locker that is able to decouple the actuation force - locking force relationship in the locking mechanism by using springs with a positive stiffness and (leaf) springs with a negative stiffness. The concept works well, but in practice the mechanism has some internal friction and hysteresis in the springs. Another issue is that the mechanism has a non-perfect static balance. Due to this non-perfect static balance, the brake requires a continuous actuation force when switched 'on' or 'off'. A last issue with this type of locker is the fact that the compliant type leaf springs have the tendency to make the locker big for the amount of locking torque it provides.

The third possibility for providing a large normal force, namely with a large transfer ratio, can be found in the singularity locker class. Such a mechanism with singular configurations can theoretically reach an infinitely large transfer ratio between the actuation and the locking force when the mechanism is in the singular configuration. This solves the problem of a constant transfer ratio based locker that always requires an actuation force for the locker to remain engaged.

The two conceptual innovations I propose in this thesis are first the combination between a singular mechanism and a friction locker (singular-friction locker) and secondly the insight that this type of mechanism can be statically balanced to reduce the energy consumption of the mechanism.

Locking mechanisms that use only a singular configuration can be found in literature [5, 17] but research on a mechanism that combines a friction locker with a singularity locker was not found. This combination between a friction

locker and the use of singular configurations in a mechanism like in figure 1.2 shows interesting advantages. The friction force in the friction surface is in the horizontal singular configuration theoretically infinitely large and no actuation force has to be provided to remain in the singular configuration. However, in non-singular configurations an actuation force still has to be provided. In order to overcome this downside of singular-friction locking, I propose to statically balance singular-friction lockers. This approach will ensure a close-to-zero actuation force in the non-singular configurations considering practical imperfections like imbalance and hysteresis.

The resulting mechanism theoretically has an infinite number of locking positions, a low energy consumption, a high locking force and unlocks well while under load. The fifth criterion, compactness, will have to be investigated. A locking device with these qualities will potentially solve the problem of energy-efficient lockers in robotics.

Up to now only the example in figure 1.2 has been presented for its singular configurations but naturally the question arises what other singular-friction lockers exist and how they potentially can be statically balanced. If there are more singular-friction locking mechanisms that can be statically balanced we will also need to be able to determine 'how good' a specific statically balanced singular-friction locking (SBS-FL) device is compared to another statically balanced singular-friction locker or to a locking mechanisms in general. Last but very important, the size of the locking mechanism is of great importance in robotics. Therefore the research questions of this master thesis are formulated as:

- **What classes of statically balanced singular-friction lockers exist?**
- **Which of these classes contains the most compact statically balanced singular-friction locking device?**
- **What is the performance of this most compact locking device?**

Naturally the terms 'compact' and 'performance' are properly defined in this thesis. This report falls apart in three parts to answer the three research questions. Chapters 2 and 3 form the first part where the theoretical background of the statically balanced singular-friction locker is explored and discussed. The second part is formed by chapters 4 and 5 where the practical implementation from what is learned is brought into practice. Chapter 4 deals with the design aspects and concept solutions for a locking mechanism and chapter 5 describes how the final concept from chapter 4 is detailed and build. The third and last part concerns the verification of the theoretical first part by means of measuring what is designed in the practical second part of the report. In other words, in chapter 6 experiments are designed and conducted to verify whether the measured characteristics from the prototype resembles what was predicted in theory. Finally chapter 7 discusses all findings of this thesis and chapter 8 provides a conclusion and an answer to the research question. Additionally appendix A contains the paper that was written on statically balanced brakes.

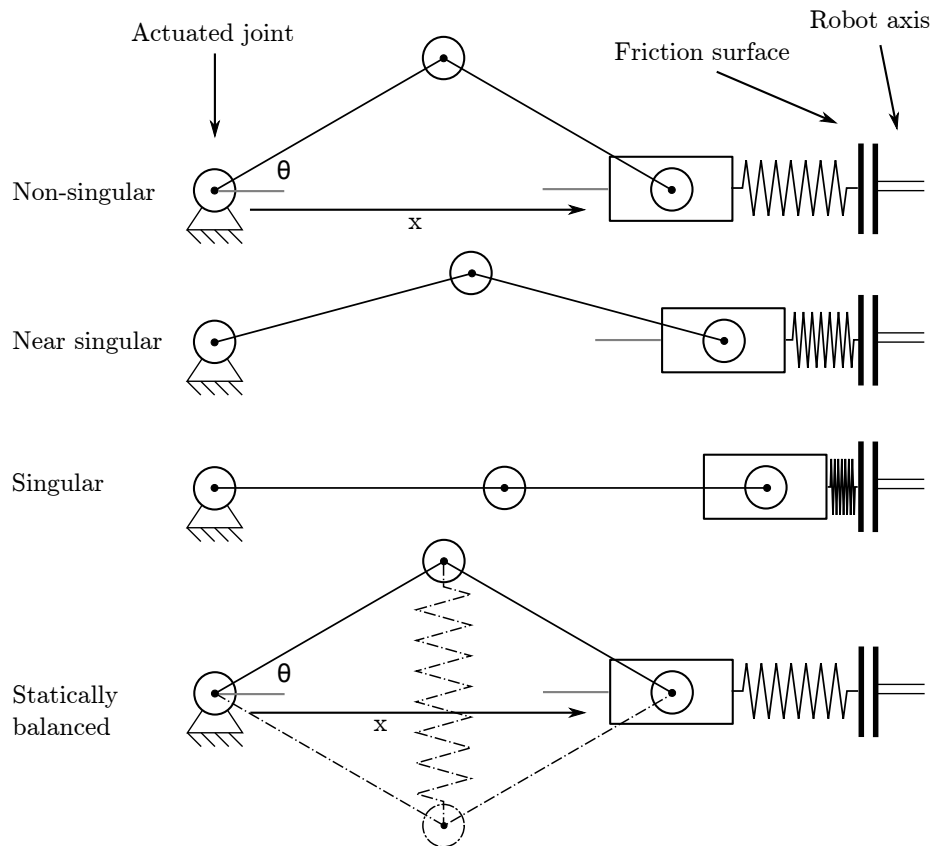


Figure 1.2: A singular-friction locking mechanism example forming the initial motivation for this thesis. Angle θ is the input of the mechanism and length x is the output of the mechanism. If the two bars with a length L align, an infinitely large force can be exerted in the x direction on the output link without exerting or feeling any force at the input link. In the case of this configuration, the magnitude of the locking force that can be obtained in the friction surface is only dependent on the stiffness of the spring that is used. The actuation force to move to the singular configuration is however not zero yet, but with the addition of one extra extension spring as depicted in the bottom figure, this problem might initially be solved.

Chapter 2

Singular configurations in locking mechanisms

As argued in chapter 1, the combination between a singular locking mechanism and a friction locking mechanism has potential to become an energy efficient locking mechanism to be used in robotics. I conducted a literature survey on the subject of singular-friction lockers and the main results are presented in this chapter. For a more detailed and elaborate version, I refer to the original document [18]. The findings and classifications of the survey on singular-friction lockers function as a backbone for the rest of the thesis.

In this chapter, first in section 2.1 a definition and an explanation are presented of what a singular configuration in a mechanism is. Secondly, singular configurations are incorporated in a friction locking mechanisms in section 2.2. The resulting overview of different *classes* of singular-friction locking mechanisms is comprehensively given in tabular form. Thirdly, the performance of a singular friction lockers in terms of actuation force and output locking torque is discussed in section 2.3. All findings are summarized in a concluding section.

2.1 Singular configurations in mechanisms

The term 'singularity' can mean many very different things. In the case of researching singular locking mechanisms, mechanical singularities must be investigated. To understand what a mechanical singularity is we first look at the overall number of degrees of freedom (full cycle mobility) of a mechanism. This full cycle mobility can be determined with the Chebychev–Grübler–Kutzbach criterion [19]:

$$K = 6(k - 1) - \sum_{i=1}^j (6 - f_i) \quad (2.1)$$

in which K is the mobility of the mechanism (number of degrees of freedom), k is the number of bodies (incl. ground) and j is the number of joints with f_i degrees of freedom.

The mobility of a mechanism is however not always equal to the full cycle mobility as determined in equation 2.1. The configuration of the mechanism in the third illustration in figure 1.2 is for example in a special (singular) configuration. In the top- and second configurations of figure 1.2 the slider can slide in horizontal direction but in the singular configuration the slider is blocked and cannot function for example as an input for the mechanism any more. So in this configuration the mechanism seems to have lost the translational degree of freedom (DOF). This number of degrees of freedom in *a certain configuration* is the instantaneous mobility of the mechanism in that configuration. A definition for a singular configuration is therefore: "A configuration in which a mechanism's number of degrees of freedom changes instantaneously" [20] and the instantaneous mobility is not equal to the full cycle mobility any more.

There are many mechanisms that exhibit such a singularity. As mentioned in chapter 1 a very practical use of a singular configuration in a mechanism is that in that configuration the mechanism can resist infinitely large forces on some joints. To illustrate this phenomena we look at the bottom picture in figure 1.2 for a simple example. Let τ denote the torque on the actuated joint and F the horizontal force on the slider. τ and F are related by the Jacobian J of the input rotation θ to the output position x as follows:

$$\tau = J^T F \quad (2.2)$$

The position relation can be written as:

$$x = 2L \cos(\theta)$$

and the Jacobian is:

$$J = \frac{\partial x}{\partial \theta} = 2L \sin(\theta)$$

In the singular configuration θ is equal to 0, which results in $J = 0$. From equation 2.2 we can see that for $J = 0$ any force F results does not lead to a torque τ on the input joint.

There are many types or classes of singularities that can be distinguished in mechanisms. First we must realize that a locking mechanism is a closed-loop kinematic chain. In this case the end-effector is grounded in multiple ways to the same ground as the input joint of the mechanism. A closed-loop kinematic chain is for example a grounded four bar mechanism.

Secondly, there are many different ways to classify singular configurations in closed-loop kinematic chains. In the literature survey three distinctly different approaches are discussed. Gosselin and Angeles [21] define a clasification by only looking at the input and the output of the mechanism, Zlatanov et al. [22] also include all other (passive) joints of the mechanism in their classification while Park and Kim [23] try to identify the causes of why certain singularities occur in closed-loop kinematic chains. Again, a full explanation of their works is included in the original literature survey [18].

2.2 Classification of singular-friction lockers

In the previous section we have become familiar with the term mechanical singularity and we have become aware that there are different singularities which can be classified with different classification approaches. In this section I present a classification of essential configurations for a singular-friction locker.

Basically we must realize that any singular-friction locker must be able to lose a degree-of-freedom at the end-effector to become locked. The actuator of the mechanism must be able to regain this degree-of-freedom, otherwise the mechanism cannot be unlocked.

Another insight for this classification was that the mechanism ideally only has a single degree of freedom. More degrees-of-freedom require more actuators to control them and more undesired singular configurations might occur.

Lastly, the possibilities for the input and output of the singular-friction locker really are limited to a slider and a rotational joint, as these are the only two possibilities to press two surfaces together in a friction locking application.

As for the classification, there were two classes of mechanisms that satisfy the recipe above. These classes of mechanisms are linkages and cam mechanisms. In figures 2.1 and 2.2 the two classifications for those singular-friction locking mechanisms are presented. They are all single degree-of-freedom mechanisms which are capable of losing a DOF at the end-effector without losing control over the entire mechanism. As can be seen all four combinations between a

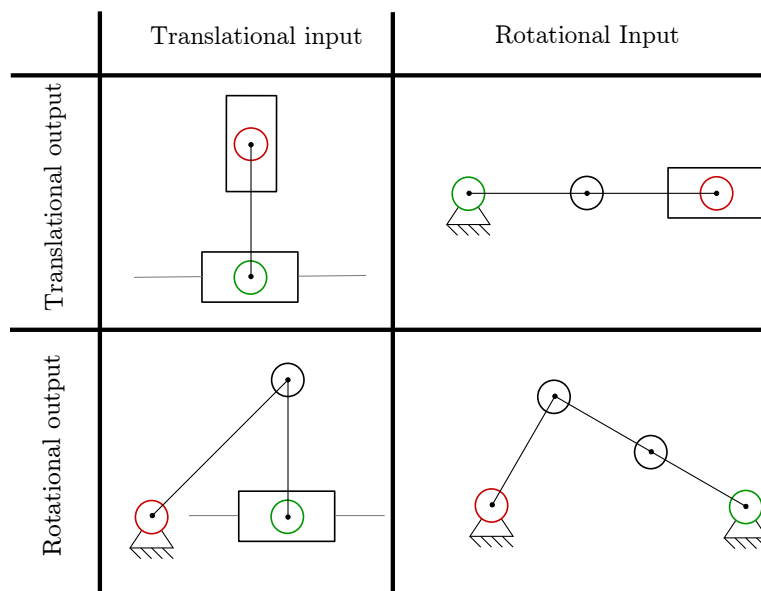


Figure 2.1: Four classes of essential singular-friction locking mechanisms filled in with linkage mechanisms. Horizontally is the input of the mechanism (green in the figures) and vertically is the output of the mechanism (red in the figures).

sliding input and -output and a rotational input and -output are satisfied with mechanisms.

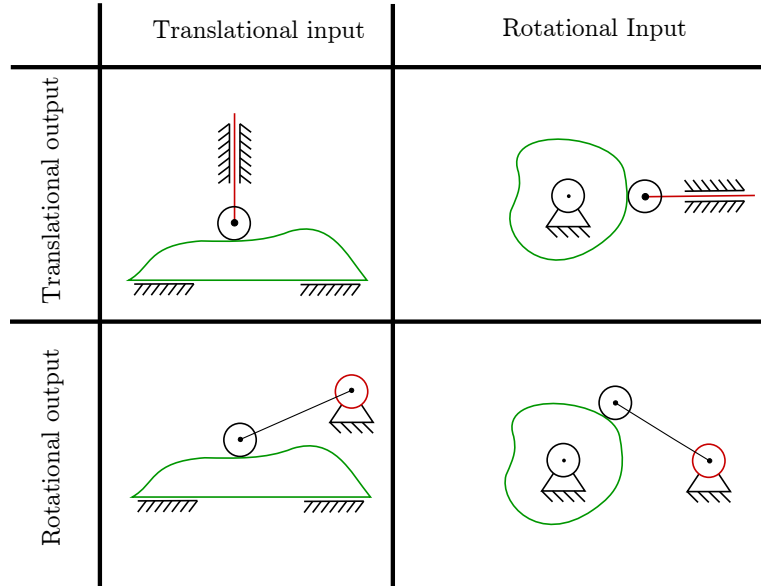


Figure 2.2: Four classes of essential singular-friction locking mechanisms filled in with cam mechanisms. Horizontally is the input of the mechanism (green in the figures) and vertically is the output of the mechanism (red in the figures).

These classifications in figures 2.1 and 2.2 can be used for two purposes. They can serve the purpose of a reference frame for any singular-friction locker found in literature, but they can also be used for synthesizing new singular-friction locking applications.

2.3 Performance of the singular-friction locker

In this section the performance of the singular-friction locker is discussed because in order to assess which singular-friction locker is 'better' than another, reference criteria are required.

As argued in previous sections a singular-friction locker is a very efficient force amplifier. In this section the focus will be on three topics: The transfer ratio between maximum input force and maximum achieved braking force, the manipulability of the actuation force characteristic and the compactness of the mechanism.

2.3.1 Transfer ratio

In order to assess the transfer ratio between the input force and the output force a closer inspection of the actuation force trajectory of a typical singular-friction locking linkage must be made. In figure 2.4 such a typical singular-friction locking linkage is depicted. As can be seen, the input force is directed vertically in downward direction on the middle joint and the output force is generated in horizontal direction on the red joint. With the principle of virtual work, the actuation force characteristic is derived for this typical mechanism. This derivation is presented in appendix B. The mechanism in figure 2.4 has an actuation force characteristic like in fig 2.3. A transfer ratio of the maximum input force, being the peak value, to the maximum braking force can be calculated. This transfer ratio is the first objective measure for comparing one singular-friction locker to another singular-friction locker.

Values used for the calculation:

L1		1
L2		1
α		0-45 [deg]
k		100

Values obtained:

Transfer ratio		2.6266
max output force		42.2065 [N]
max input force		16.0687 [N]

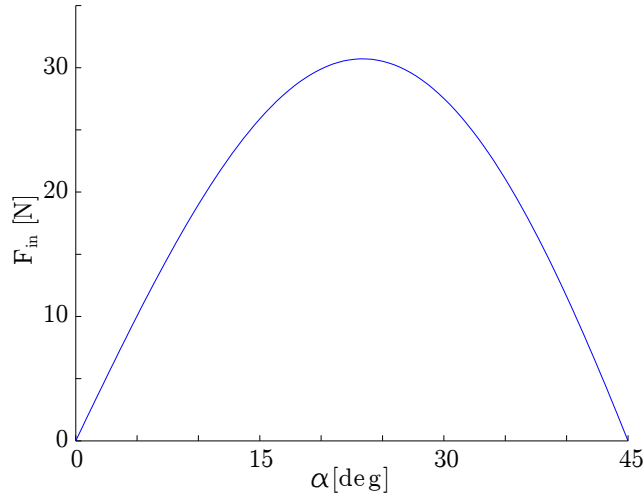


Figure 2.3: Actuation force characteristic of a typical singular-friction locking linkage. On the x-axis is the angle of the actuating link and on the y axis the input force is depicted. Both quantities can be found in figure 2.4.

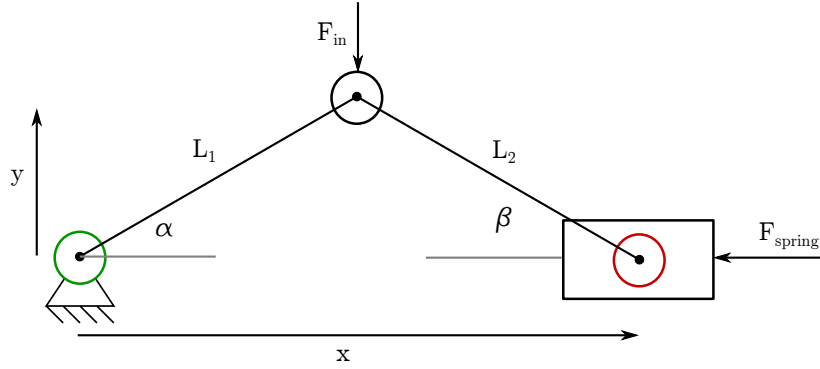


Figure 2.4: A schematic representation of a singular-friction locker with a rotational input (green) and a translational output (red). The resulting actuation force characteristic of this mechanism is depicted in fig 2.3.

2.3.2 Manipulability of the actuation force characteristic

As argued in the previous section, the transfer ratio between the input force and the actuation force provides a comparable quantity between different singular-friction lockers. However, for linkages this actuation force characteristic is hard to fundamentally change of shape. The basic calculations for all linkage singular-friction lockers will result in the same parabolic-looking shape.

Nevertheless it might be beneficial to be able to change this characteristic to a non-parabolic shape to fit exactly fit some desired actuation force characteristic shape. Cam mechanisms have this ability to fundamentally change this actuation force to any desired and physically possible actuation force characteristic. By simply realizing that the cam surface can have any shape, it must be possible to change the actuation force characteristic. This adaptability of the actuation force characteristic of a singular-friction locker is therefore the second performance criterion for a singular-friction locker. This phenomena will play an important role in the rest of this thesis and is further elaborated in chapter 3.

2.3.3 Compactness

The last performance criterion seems quite trivial, however has proven very valuable in chapters 4 and 5. The first reason to look at the compactness of the mechanism is simply because the singular-friction locker can be assessed as a special mechanical lever. However if the arms of the lever are enlarged, the lever becomes more efficient and that seems unfair compared to a smaller mechanism that realizes the same mechanical advantage. As will be seen further in the thesis, some classes have the tendency to remain very small while achieving a very large mechanical advantage. This size-to-mechanical advantage ratio is what I refer to as compactness and is the third important performance criterion for a singular-friction locker.

2.4 Conclusion

The literature survey investigated what types of singular-friction lockers can be extracted from literature and how their performance can be quantified. Firstly we have seen that the only mechanical singularity that can be used for friction locking purposes is a mechanical singularity where the end-effector of the mechanism loses a degree of freedom. Secondly, by looking at different kinematic pairs for the input and the output of a singular-friction locker, a classification with four different essential singular-friction locking functionalities can be constructed. Two classes of mechanisms satisfy this classification, namely linkages and cam mechanisms. Thirdly, the performance of these mechanisms can be quantified by looking at the manipulability of the actuation force characteristic, the overall mechanical advantage of the mechanism and the compactness of the mechanism.

Chapter 3

Statically balancing singular-friction locking mechanisms

From reading chapter 2 the knowledge should be obtained that there is a classification of singular-friction locking mechanisms that can be used to place all existing singular-friction lockers in and from which new singular-friction lockers can be generated. However, as a major downside of the singular-friction lockers the actuation force characteristic of such a device was presented. To find a possible solution to this downside, in this chapter the principle of static balancing is exploited to generate a classification of locking devices with singular configurations that can be statically balanced.

First in section 3.1 the only statically balanced locking device is studied in order to statically balance a singular-friction locker. In the second section (3.2) of this chapter the strategy from section 3.1 is used to try to statically balance singular-friction lockers. Thirdly and fourthly, sections 3.3 and 3.4 are devoted to static balancing of linkage singular-friction lockers and cam singular-friction lockers respectively. Lastly, a conclusion is reached on the static balancing of singular-friction lockers.

3.1 Statically balanced locking device

Plooij et al. [16] discovered a way to obtain a statically balanced locking mechanism. This locking mechanism also performs well on energy consumption, amount of locking force, the number of locking positions and unlocking under load performance. The first and only statically balanced locking device (z-force) was built by Plooij et al. [16] and is depicted in figure 3.1. The main idea of the principle behind this locking device is depicted in figure 3.2. Basically, compliant elements with a positive stiffness are connected in series with compliant elements with a negative stiffness. If the positive and the negative stiffness constants can be fabricated in the exact same magnitude, the system is in static balance over the full range of motion. The z-force is a working locking device and the per-

formance statistics are presented in table 3.1. This locking mechanism has a locking torque of more than 1 Nm and in small applications like a Maxon motor this torque is a standard. However there are also two downsides present in this approach to statically balanced locking.

The first downside is the fact that this locker needs a continuous actuation force of 5.9 N. This implies that whenever the locker is engaged or disengaged, energy has to be transferred into the system resulting in a continuous consumption of power.

The reason for this continuous power consumption lies in the number of singular configurations in this system and their stability. Closer inspection of the z-force leads to the conclusion that it only has *one* singular configuration. This configuration is depicted in the middle figure of figure 3.2. In this configuration the braking spring is fully extended and all energy is stored in the leaf type storage spring which is in its highest tension state. Since all other compression springs are relaxed in this configuration, the leaf spring can be assumed to be in a singular configuration. This singular configuration is unstable, the slightest touch will disrupt the equilibrium. The mechanism is not in a singular configuration when the braking springs are fully compressed.

Singular-friction lockers also have one singular configuration but this singular configuration is used when the locking device is in the 'engaged' state. In order to obtain an absolute zero actuation force when the mechanism is in 'disengaged' state a second singular configurations must be incorporated in the mechanism. In this way the mechanism has a singular configuration in both the 'engaged' and 'disengaged' states which results in an absolute zero actuation force.

From the performance of the z-force the conclusion can be reached that due to manufacturing imperfections or hysteresis in the springs the static balance can deviate from perfect in practise. Therefore the essence of designing a SBS-



Figure 3.1: The second prototype of the z-force as found in the original paper [16].

FL mechanism with a zero continuous power consumption must be to design a mechanism with at least two singular configurations.

The second downside of the z-force is its size, as it is quite large for the amount of locking torque it provides. A reason for this lack of compactness are the negative stiffness (leaf) springs which use a lot of space in the z-force. Possibly the rigid body approach of the SBS-FLs will reduce the size of the overall locking mechanism.

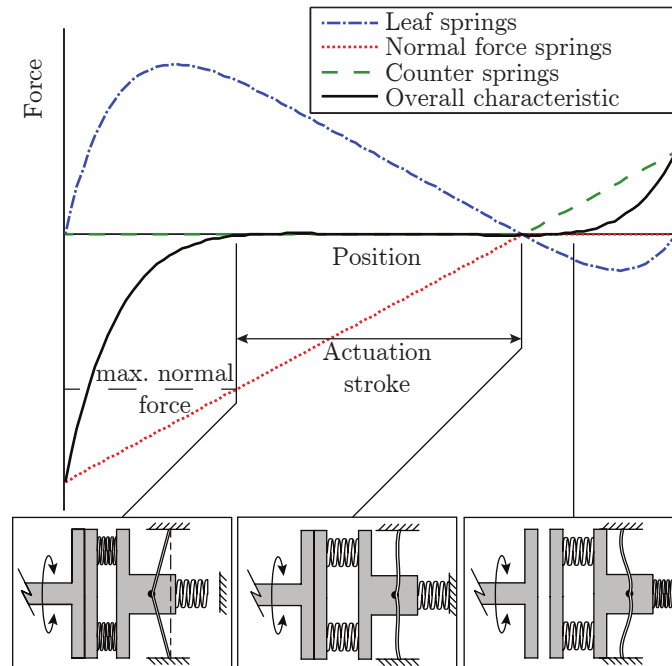


Figure 3.2: The principle behind the z-force locking mechanism by Plooij et al. [16]. In the left picture the z-force is in the locking configuration, in the middle figure the mechanism is unlocked but the friction plates still touch, and in the right configuration the friction plates are free from each other and the mechanism is fully unlocked. As indicated the leaf type springs in the middle provide the negative stiffness, whereas the positive stiffness springs are simply compression springs. Note that the leaf springs have a linear negative stiffness only for a part of their mobility, and during this part this negative stiffness exactly compensates the positive stiffness springs.

Criterion	Performance z-force
Locking Torque	1.08 Nm
(continuous) Actuation force	5.9 N
Size	\varnothing 60 x 59 mm
Mass	170 g

Table 3.1: Performance specifications of the z-force.

3.2 Removing the actuation force of a singular-friction locker

As can be read in chapter 2 the actuation force characteristic of a singular-friction locking mechanism is typically a parabolic-like shape as pictured in figure 2.3. The first idea to try to get rid of the actuation force of such a mechanism is to place a mirrored version of exactly the same mechanism in series with the original mechanism. As was argued in section 3.1 such a mechanism has singular configurations in the 'engaged' and 'disengaged' states. This idea is depicted in figure 3.3. The energy of the unlocking mechanism is simultaneously stored in the mechanism which is locking at the same moment. If the spring on one side is attached to the friction brake and the spring on the other side to the ground, the energy in the system can effectively be transferred between a grounded spring and a braking spring. When the right side of the mechanism is locking ($\alpha \rightarrow 0$), as depicted in the right side of figure 3.3, the red actuation force characteristic is followed by that side of the mechanism. The left side of the mechanism is simultaneously unlocking as depicted in the left side of figure 3.3, and in this case the blue actuation force characteristic is followed by that side of the mechanism. In total, the net actuation force is the sum of the red and the blue actuation force trajectories. This net actuation force is depicted in figure 3.4. The red and the blue graphs correspond to the red and blue graphs in figure 3.3. To illustrate the slight asymmetry in both graphs, the negative projections are depicted in dashed lines.

The resulting actuation force characteristic should be close to zero. The black graph of the net input force in figure 3.4 might give the impression that a perfect static balance can be reached with parameter tweaking of the dimensions of the mechanism to slightly change the actuation force characteristic.

3.2.1 Equation of the summed input forces

In figure 3.4 the input force vector of a single singular-friction locker is flipped reverse and multiplied by -1 to obtain the actuation force characteristic of the mirrored mechanism. The resulting sum gives the total actuation force characteristic of the total mechanism. Interesting is however the equation of this summed actuation force in order to be able to determine how to zero it. To find an analytical formula for the shape of this characteristic, again the principle of virtual work can be used. The mathematical derivation is presented in section

C.1 of appendix C. The resulting expression for the input force is:

$$F_{in} = \frac{F_{spring,r}(-L_1 \sin(\alpha) - L_1 \tan(\beta) \cos(\alpha)) + F_{spring,l}(L_3 \sin(c) + L_3 \tan(d) \cos(c))}{-L_1 \cos(\alpha)}$$

where:

$$\tan(d) = \frac{\frac{L_3 \sin(c)}{L_4}}{\pm \sqrt{1 - \left(\frac{L_3}{L_4}\right)^2 \sin^2(c)}} \quad \tan(\beta) = \frac{\frac{L_1 \sin(\alpha)}{L_2}}{\pm \sqrt{1 - \left(\frac{L_1}{L_2}\right)^2 \sin^2(\alpha)}}$$

This equation can be written in terms of input angle α and the initial value of α , α_0 . The resulting equation is quite long and is therefore in appendix C.1. The main result however is that there is no set of parameters that will result in a zero actuation force for a range of motion of the 'double' singular-friction locker. A set of values can be chosen in order to get an idea what kind of transfer ratios can still be achieved.

L1	1
L2	2
L3	1
L4	2
α	0-60 [deg]
k	100

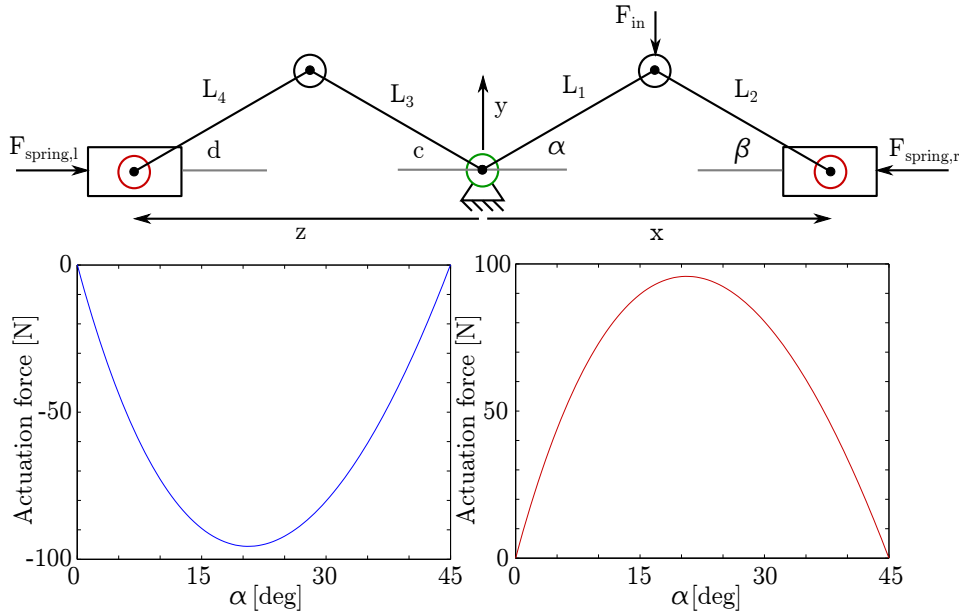


Figure 3.3: A singular-friction locker with a rotational input in the middle. The right side of the mechanism has an actuation force characteristic as depicted in the right red graph. The left side of the mechanism has an actuation force characteristic as depicted in the left blue graph. The total actuation force in the green input joint is the sum of these two action force graphs.

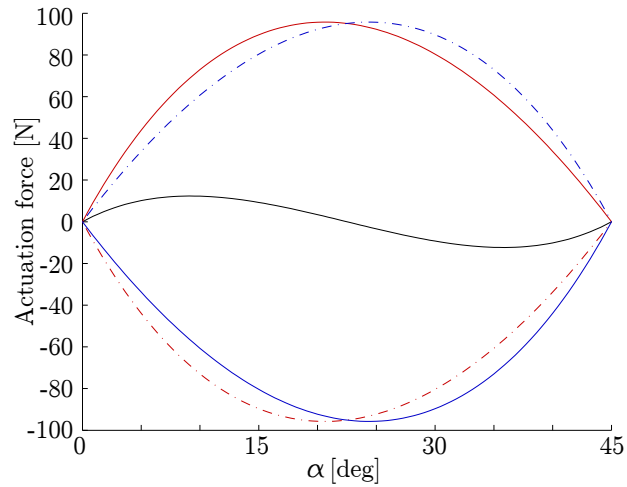


Figure 3.4: The actuation force characteristics of two singular-friction lockers in series. When one locks (red, solid line), the other mechanism unlocks (blue, solid line) for an decreasing input angle α . The resulting actuation force is depicted in black. The dashed lines are presented to emphasize that the actuation force graphs are not symmetrical.

These input values result in the following output values:

Transfer ratio	36.4
max output force	69.7 [N]
max input force	1.9 [N]

From these results the conclusion can be drawn that the transfer ratio of the mechanism is much better than that of a single singular-friction locker, but another conclusion must be that there is no set of parameters for the link lengths that will provide a *perfect* static balance. Therefore the next logic topic to research is that of static balancing of linkages.

3.3 Static balancing of linkages

As concluded from the previous section, there is no analytical solution to perfectly statically balance the singular-friction locking linkages by adding the negative mechanism to the original mechanism in series. However, this is just one initial way to try to achieve the static balance, and in literature solutions to solve the problem might be found. In fact, the doctoral thesis of J.L. Herder [24] will prove to be able to provide insight in how to achieve a perfect static balance in a singular-friction locking mechanism.

Energy-free systems

In this subsection a short literature based summary and explanation is given on the subject of energy-free systems as described in the doctoral thesis of J.L. Herder [24]. One of the insights gained in this thesis is the 'balanced ladder' as depicted in figure 3.5. This 'ladder' with a length L is in perfect static balance in any configuration or angle with the wall when two zero-free-length springs are attached to the top and the bottom of the ladder. The main criterion for this or any system to be in static balance is that the potential energy in the system must always be constant. The analysis for this ladder is quite simple when using this constant energy criterion combined with Pythagoras law. The main result is that this 'ladder' is always in perfect static balance.

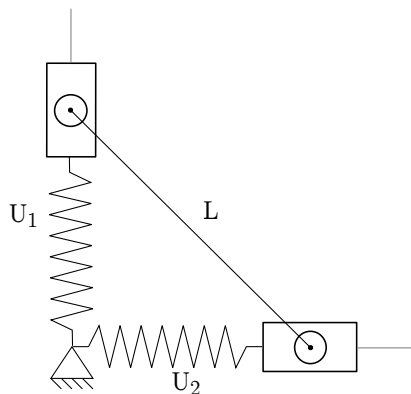


Figure 3.5: Statically balanced ladder. This mechanism is in perfect static balance in every position of the ladder. The springs are zero-free-length tension springs meaning that the springs have no length when they produce zero force. The length of the ladder is of course a constant: L . Compare this figure with figure 3.6 to see the resemblance.

$$\begin{aligned}
 E_{pot} &= E_1 + E_2 \\
 E_1 &= \frac{1}{2}ku_1^2 \\
 E_2 &= \frac{1}{2}ku_2^2 \\
 E_{pot} &= \frac{1}{2}ku_1^2 + \frac{1}{2}ku_2^2 \\
 u_1^2 + u_2^2 &= L^2 \\
 E_{pot} &= \frac{1}{2}ku_1^2 + \frac{1}{2}ku_2^2 = \frac{1}{2}kL^2 = \text{constant}
 \end{aligned}$$

3.3.1 Slider input - slider output

Fortunately this ladder looks very much like one of the classes of singular-friction locker defined in chapter 2, and it is quite simple to transfer this principle into the singular-friction locker. This combination between the statically balanced ladder and the singular-friction locker with a slider input and a slider output is depicted in figure 3.6. The 'engaged' and 'disengaged' singular configurations of the mechanism are depicted in figure 3.7. Note that no matter the imperfections in the springs the actuation force of the mechanism to remain in the singular configurations is always zero.

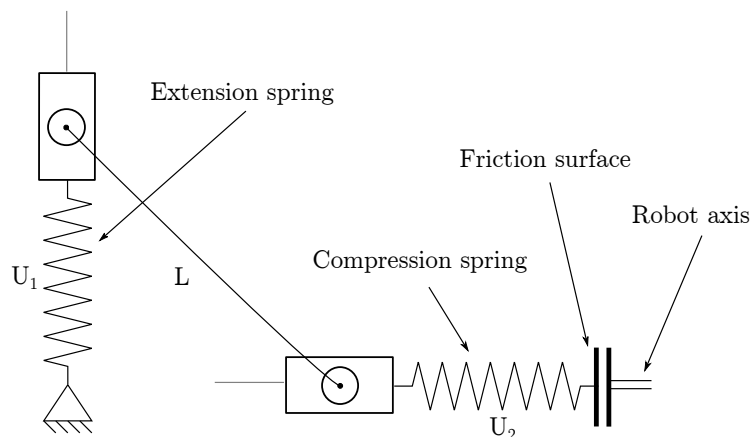


Figure 3.6: A statically balanced singular-friction locker. Bearing in mind figure 3.5 we can see the resemblance with these now balanced singular-friction lockers. Note that the zero-free-length tension springs from figure 3.5 can be interchanged with the compression springs in this picture.

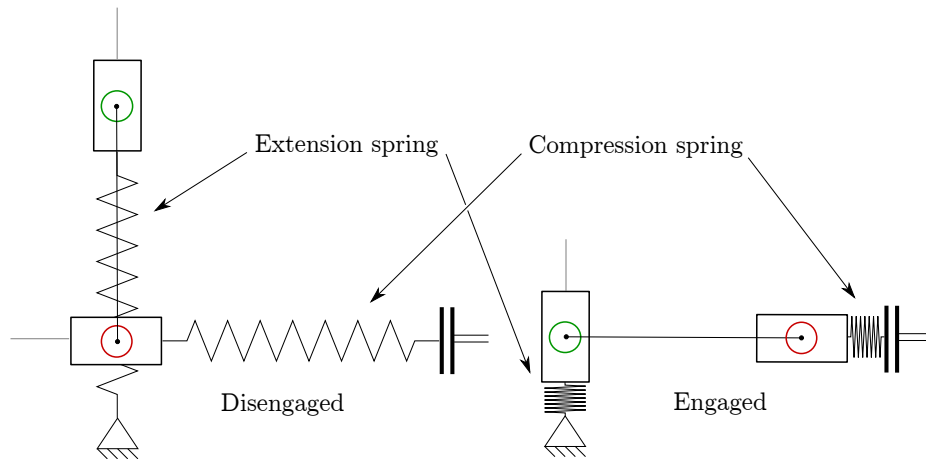


Figure 3.7: The left picture shows the locker fully disengaged and the right picture shows the locker locked. Note that the zero-free-length tension springs from figure 3.5 can be interchanged with the compression and normal extension springs in this picture.

When observing figure 3.7 another problem can be spotted. The storage spring is connected to the green slider where the normal force spring is connected to the red slider. However neither of the two can function as a translational actuated joint. Therefore the actuated degree of freedom has to be a rotation between the link with length L and a slider to avoid losing control over the mechanism. This can be either the red or the green circle in figure 3.7. This linkage type of statically balanced singular-friction locker is therefore labelled *Slider input, slider output, rotational actuator*.

Naturally the question arises whether the other classes of singular-friction lockers can be statically balanced as well. For this classification the following rules are used to keep the focus on small mechanisms:

1. The spring type on the output is the same as the output type (for example a rotational output is connected with a torsion spring to the friction surface of the robot axis).
2. The actuator can be rotational or translational and does not necessarily have to be connected to the input of the mechanism (the joint to which the storage spring is connected).
3. The storage spring type does not have to match the mechanism input type (for example a rotational input can be connected to the ground with an extension spring).
4. The simplest form of the mechanism is evaluated, more links than strictly necessary increases the complexity, the size and the weight of the mechanism and is therefore not considered feasible.

With these rules the classification as presented in figure 2.1 of chapter 2 can be checked for other classes of linkage type singular-friction lockers that can be statically balanced.

3.3.2 Rotational input - slider output

For singular-friction locker with a rotational input and a translational output, as for example depicted in figure 1.2, literature seemed to provide an answer to the question whether this class of singular-friction lockers can be statically balanced.

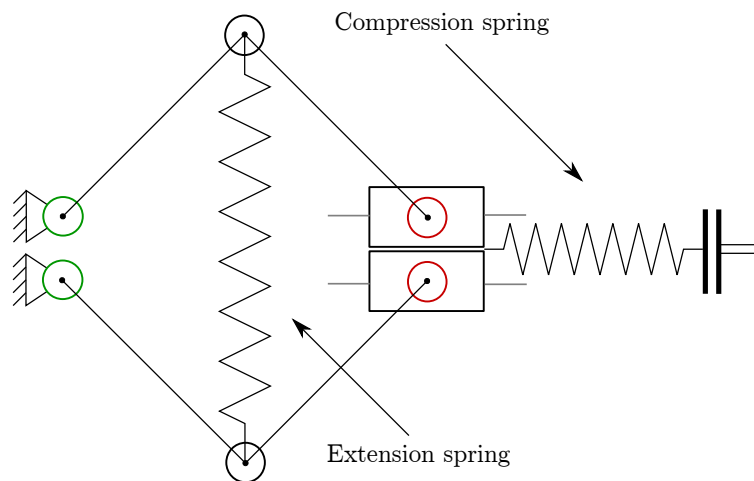


Figure 3.8: Based on the figure by Barents et al. [25], the figure represents the statically balanced mechanism in a friction-locking application where the compression spring presses two friction surfaces together.

Barents et al. [25] provide a mechanism with a rotational input and a translational output which is in perfect static balance for the full range of motion. This mechanism is depicted in figure 3.8. The extension spring is in this case not a zero-free-length spring but a real spring with a rest length L_0 . This mechanism is however technically the same as the 'balanced ladder', because the vertical slider in figure 3.6 is simply replaced with the additional links. For this reason this mechanism can arguably belong to the class of 'translational input - translational output'.

There are two problems with this mechanism. Firstly, there are two links added to the mechanism which is a 'violation' of rule 4. Secondly and more importantly, there is no joint that can be selected to actuate the mechanism that does not lose control over the mechanism in the singular configurations. This problem is graphically explained in figure C.2 of appendix C.

A general case of a singular-friction locking linkage with a rotational input and a translational output is depicted in figure 3.9. According to the rules from section 3.3.1 the only two options for a storage spring (green) are depicted in the figure. The normal force spring (red) has to be in line with the translational output.

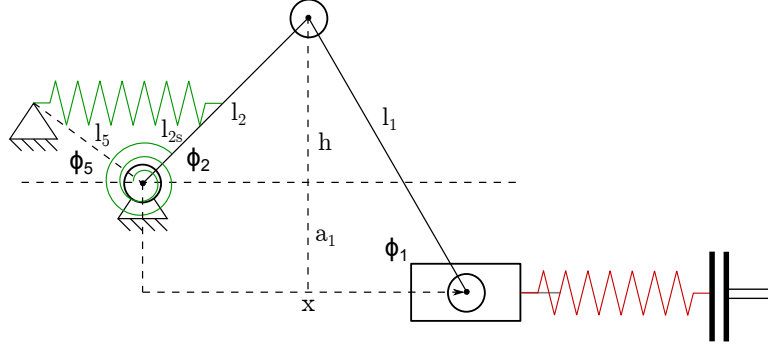


Figure 3.9: A general representation of singular-friction locking linkage with a rotational input and a translational output. The green springs are connected to the rotational input joint, the red spring is the spring that is connected to the friction surface. The actuated joint can be chosen freely such that control over the mechanism is always maintained.

A parametrization for this mechanism as used in figure 3.9 can be used to derive the potential energy function of this mechanism. The actuated angle was chosen to be ϕ_1 because for this choice both singular configurations of the mechanism can be reached without losing control over the mechanism.

$$\begin{aligned}
 h &= l_1 \sin(\phi_1) - a_1 \\
 \phi_2 &= \sin^{-1}\left(\frac{h}{l_2}\right) \\
 x &= l_2 \cos(\phi_2) + l_1 \cos(\phi_1) \\
 l_{spring} &= \sqrt{(l_5 \cos(\phi_5) + l_{2s} \cos(\phi_2))^2 + (l_5 \sin(\phi_5) - l_{2s} \sin(\phi_2))^2} \\
 E &= \frac{1}{2}k_1(\phi_2 - \phi_{2,0})^2 + \frac{1}{2}k_2(x - x_0)^2 + \frac{1}{2}k_3 l_{spring}^2
 \end{aligned}$$

Where $\phi_{2,0}$ is the zero torque angle for the torsion spring and x_0 the zero force length of the extension or compression spring. The full equation for the potential energy as a function of ϕ_1 is very long. However from the energy function E can already be seen that there is no set of parameters that results in a statically balanced system with constant potential energy.

3.3.3 Rotational input - rotational output

In this subsection the focus is on singular-friction locking linkages with a rotational input and a rotational output. The rotational output is always connected to a torsional spring, which is connected to the friction surface. When a normal spring would be used, the output would again be transformed into a translational output, and the mechanism would belong to a different class of SBS-FLs. The research on statical balancing with torsion springs is scarce. There appear to be three attempts to use torsion springs for static balancing purposes. The first work is by Zhu and Lamarche [26] where the torsion spring is only used to counteract static gravity. A second work is by van Osch [27] in the form of a master thesis on static balancing of a weight with torsion bars. A third and more extensive work is presented by Radaelli et al. [28] where a graphical energy approach is presented along with a functional prototype of an approximately statically balanced five bar linkage. Nevertheless there appears to be no trace of work to statically balance the simple linkages I presented as singular-friction lockers with a rotational output.

The representation of this mechanism is a four bar mechanism as depicted in figure 3.10. The output angle which determines the compression in the torsion spring is ϕ_2 . In order to find the potential energy function of this mechanism all position relationships are identified with the parametrization as depicted in figure 3.10. There are two options for the compensation springs (green) when following the rules from section 3.3.1. The output of the mechanism is connected to a friction surface with a torsion spring (red). The actuated rotation is chosen to be θ_4 because for this choice the mechanism can reach both its singular configurations without losing control over the mechanism. The energy analysis of the system can be as done with the parametrization from figure 3.10:

$$\begin{aligned}
 a_1 &= \sqrt{l_3^2 + l_4^2 - 2l_3l_4 \cos(\theta_4)} \\
 \phi_1 &= \cos^{-1}\left(\frac{l_2^2 + l_1^2 - a_1^2}{2l_2l_4}\right) \\
 h &= l_2 \sin(\phi_1) \\
 \theta_1 &= \sin^{-1}\left(\frac{h}{a_1}\right) \\
 \theta_2 &= \cos^{-1}\left(\frac{a_1^2 - l_3^2 + l_4^2}{2a_1l_4}\right) \\
 \phi_2 &= \pi - \theta_1 - \theta_2 \\
 l_{spring} &= \sqrt{(l_5 \cos(\phi_5) + l_{2s} \cos(\phi_1))^2 + (l_5 \sin(\phi_5) - l_{2s} \sin(\phi_1))^2} \\
 E &= \frac{1}{2}k_1(\phi_1 - \phi_{1,0})^2 + \frac{1}{2}k_2(\phi_2 - \phi_{2,0})^2 + \frac{1}{2}k_3l_{spring}^2
 \end{aligned}$$

Where $\phi_{1,0}$ and $\phi_{2,0}$ are the zero torque angles for the torsion springs. The full equation for the potential energy as a function of θ_4 is very long. However from the energy function E can already be seen that there is no set of parameters that results in a statically balanced system with constant potential energy.

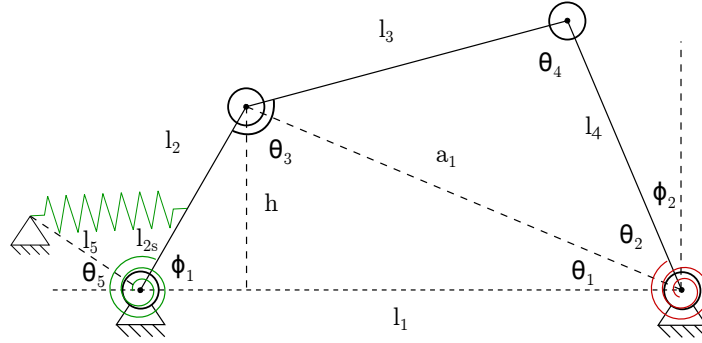


Figure 3.10: Parametrization of a singular-friction locker with a rotational input ϕ_1 and a rotational output ϕ_2 . The actuated joint for this mechanism is chosen to be θ_4 in order not to lose control over the mechanism in both singular configurations.

3.3.4 Slider input - rotation output

In this subsection the static balancing of a singular-friction locker with a translational input and a rotational output is investigated. Again the constraint rules from section 3.3.1 apply for statically balancing this type of mechanism. Furthermore the representation of this mechanism is a slider crank mechanism as depicted in figure 3.11. The output angle which determines the compression in the torsion spring is ϕ_2 . The actuated angle is chosen to be θ_1 . The potential energy function of this mechanism is identified by finding all position relationships with the parametrization as depicted in figure 3.11.

$$\begin{aligned}
 h &= l_1 \sin(\phi_1) - a_1 \\
 \phi_2 &= \sin^{-1}\left(\frac{h}{l_2}\right) \\
 x &= l_2 \cos(\phi_2) + l_1 \cos(\phi_1) \\
 l_{spring} &= \sqrt{(x_1 - x + l_{1s} \cos(\phi_1))^2 + (y_1 - l_{1s} \sin(\phi_1))^2} \\
 E &= \frac{1}{2}k_1(\phi_2 - \phi_{2,0})^2 + \frac{1}{2}k_2 l_{spring}^2
 \end{aligned}$$

Where $\phi_{2,0}$ is the zero torque angle for the torsion spring. The full equation for the potential energy as a function of ϕ_1 is very long. However from the energy function E can already be seen that there is no set of parameters that results in a statically balanced system with constant potential energy.

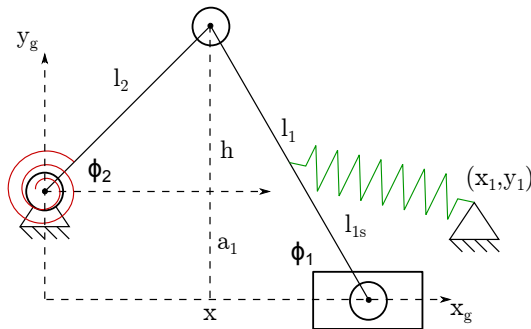


Figure 3.11: Parametrization of a singular-friction locker with a translational input ϕ_1 and a rotational output ϕ_2 . x_g and y_g are the global coordinates in which x_1 and y_1 are defined. The actuated joint for this mechanism is chosen to be ϕ_1 in order not to lose control over the mechanism in both singular configurations.

	Translational input	Rotational Input
Translational output		
Rotational output		

Figure 3.12: Updated overview of section 2.1. In the category of linkage mechanisms the rotation-rotation, the slider-rotation and the rotation-slider singular-friction lockers cannot be statically balanced perfectly. The input is highlighted in green, the output is highlighted in red.

3.3.5 Conclusion: linkages

The conclusion of these calculations is that the singular-friction locking linkages with a rotational output cannot be brought in a static balance for the full range of motion with the addition of a single spring. Also the singular-friction locker with a rotational input and a slider output cannot be brought into static balance. With this information the concluding overview concerning the static balancing of singular-friction locking linkages is depicted in figure 3.12.

3.4 Static balancing of cam mechanisms

From section 3.3 the knowledge is gained that there is one linkage type singular-friction locker that can be statically balanced. From chapter 2 the reader might recall that cam mechanisms are another class of mechanism that can be used in a singular-friction locking application. In this section the question is answered of whether there are classes of cam type singular-friction locking mechanisms that can be statically balanced. First the simple case of a cam type singular-friction locker with a translational cam and a translational output is presented, after which secondly a generalization of the findings is presented.

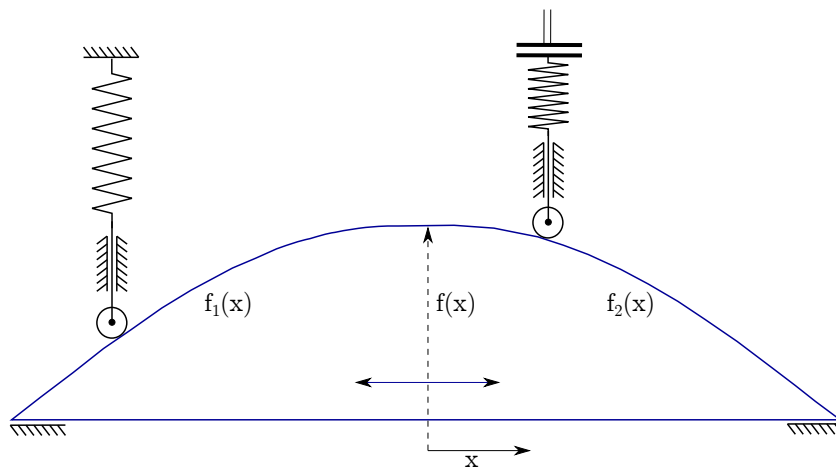


Figure 3.13: A cam type locking device with both a grounded spring and a spring connected to a friction surface rolling over the cam surface.

3.4.1 Energy free locking cam systems

In figure 3.13 a cam surface is presented with two roller followers on it. The blue cam surface can slide horizontally, the followers can slider vertically. When the cam slides for example to the left, the grounded spring is compressed upwards and the spring connected to the friction surface is released downwards. With the functions $f_1(x)$ and $f_2(x)$ the height of the cam surface as a function of the horizontal displacement x can be calculated. These functions basically describe the cam surface and the energy in each of the springs can be determined with these functions. The two springs contain all energy in the system and the constant energy criterion applies for the statically balanced cams: the total energy in the system must be constant. In formula form the following relations for the static balancing of a cam surface can be derived.

$$\begin{aligned}
E_{pot} &= E_1 + E_2 = \text{constant} \\
E_1 &= \frac{1}{2}k_1 f_1(x)^2 \\
E_2 &= \frac{1}{2}k_2 f_2(x)^2 \\
E_{pot} &= \frac{1}{2}k_1 f_1(x)^2 + \frac{1}{2}k_2 f_2(x)^2 \\
f_2(x) &= \pm \sqrt{\frac{E_{pot} - \frac{1}{2}k_1 f_1(x)^2}{\frac{1}{2}k_2}} = \pm \sqrt{\frac{2E_{pot} - k_1 f_1(x)^2}{k_2}} \quad (3.1)
\end{aligned}$$

Where the range of x and the values for E_{pot} and k must be chosen such that no complex function values in $f_2(x)$ are obtained. Technically, this also implies that for any surface function $f_1(x)$ there is a surface function $f_2(x)$ that results in a statically balanced singular-friction locker. Two examples for this rule are depicted in figure 3.14. These cam surfaces can be substituted in the place of the cam surface depicted in figure 3.13.

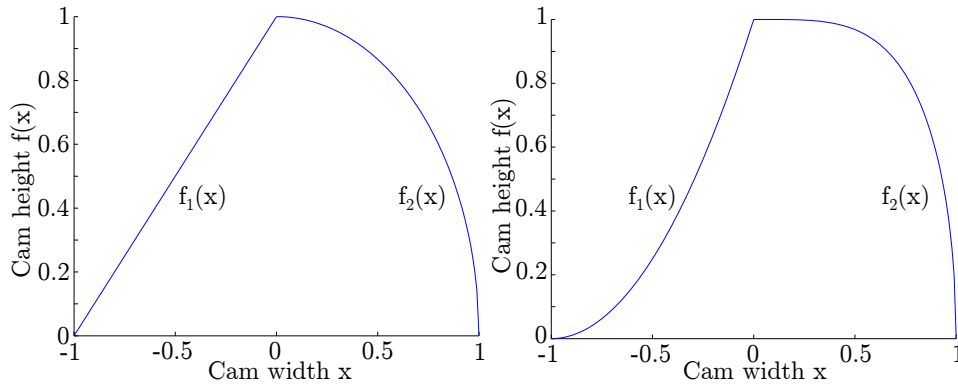


Figure 3.14: A perfectly statically balanced cam shape. On the left $f_1(x) = x$ and $f_2(x) = \pm \sqrt{\frac{E_{pot} - \frac{1}{2}k_1 x^2}{\frac{1}{2}k_2}}$. Choose $E_{pot} = 1$, $k_1 = k_2 = k = 2$ and $x \in [0, 1]$. On the right $f_1(x) = x^2$ and $f_2(x) = \pm \sqrt{\frac{E_{pot} - \frac{1}{2}k_1 x^4}{\frac{1}{2}k_2}}$. Choose $E_{pot} = 1$, $k_1 = k_2 = k = 2$ and $x \in [0, 1]$. These shapes can be substituted for the cam shape of figure 3.13.

When inspecting figure 3.14 a problem might be spotted. In the left figure of figure 3.14 the cam surface with function $f_1(x) = x$ technically represents a horizontal spring. This idea is illustrated in figure 3.15.

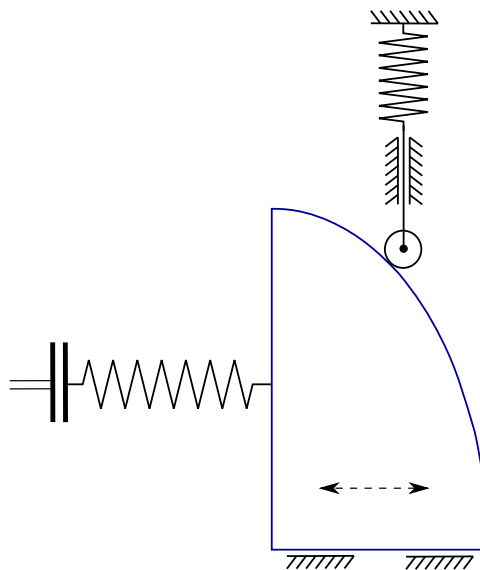


Figure 3.15: A perfectly statically balanced cam mechanism. $f_1(x) = x$ and $f_2(x) = \pm\sqrt{\frac{E_{pot} - \frac{1}{2}k_1x^2}{\frac{1}{2}k_2}}$. Choose $E_{pot} = 1$, $k_1 = k_2 = k = 2$ and $x \in [0, 1]$

When the horizontal braking spring is fully compressed, the grounded spring is fully relaxed. The compressed spring is not in a singular configuration and the other spring is fully relaxed, so what is ensuring that the cam does not move back to the right? The answer lies in the fact that the cam surface in figure 3.15 has *two* singular configurations. This is a problem in the way that when the locker is engaged (the cam is fully to the left), it cannot slide back to the right again! This can also be shown theoretically because the gradient of the cam surface function $f_2(x)$ is infinite in $x = 1$:

$$\begin{aligned} f_2(x) &= \pm\sqrt{\frac{E_{pot} - \frac{1}{2}k_1x^2}{\frac{1}{2}k_2}} \\ f_2(x) &= \pm\sqrt{1 - x^2} \\ f_2'(x) &= \frac{2x}{2\sqrt{1 - x^2}} \\ f_2'(1) &= \infty \end{aligned}$$

This simple example illustrates that not *all* cam surface combinations result in feasible surfaces. *Both* the cam surface for the grounded spring *and* the cam surface for the spring attached to the friction surface have to have singular configurations. Infinite gradients have to be avoided which occur when only one of the cam surfaces has both singular configurations. This obviously results in the uncontrollability of the locker.

An example of a feasible cam surface combination is the sine-cosine combination. This means that similar to the calculations shown earlier in this section the sine and cosine combination is a solution to the constant energy criterion:

$$\begin{aligned}
 E_{pot} &= E_1 + E_2 = \text{constant} \\
 E_1 &= \frac{1}{2}k f_1(x)^2 \\
 E_2 &= \frac{1}{2}k f_2(x)^2 \\
 f_1(x) &= \sin(x) \\
 f_2(x) &= \cos(x) \\
 E_{pot} &= \frac{1}{2}k \sin(x)^2 + \frac{1}{2}k \cos(x)^2 = \text{constant}
 \end{aligned}$$

Visually, this cam surface is depicted in figure 3.13. Note that whenever one of the springs is compressed, it is in a singular configuration and the relaxed spring does not in any way have to compensate for its force.

This approach of statically balancing a slider input - slider output cam type singular-friction locker can be generalized to all cam type singular-friction lockers.

3.4.2 Generalization

The four mechanism in figure 2.2 can function as the building blocks for a statically balanced cam based singular-friction locker. These building blocks and their parametrization are depicted in figure 3.16. To statically balance the system again the equation that must be satisfied is:

$$E = \frac{1}{2}k_1f_1^2 + \frac{1}{2}k_2f_2^2$$

where the functions f_1 and f_2 can be:

$$f_{1,2} = \phi_1(\phi_2), \phi_1(x), s(\phi_2), s(x)$$

It still holds that f_2 can be written as a function of f_1 by means of equation 3.1. Now the cam surfaces can be generated when the desired functions f_1 and f_2 are known.

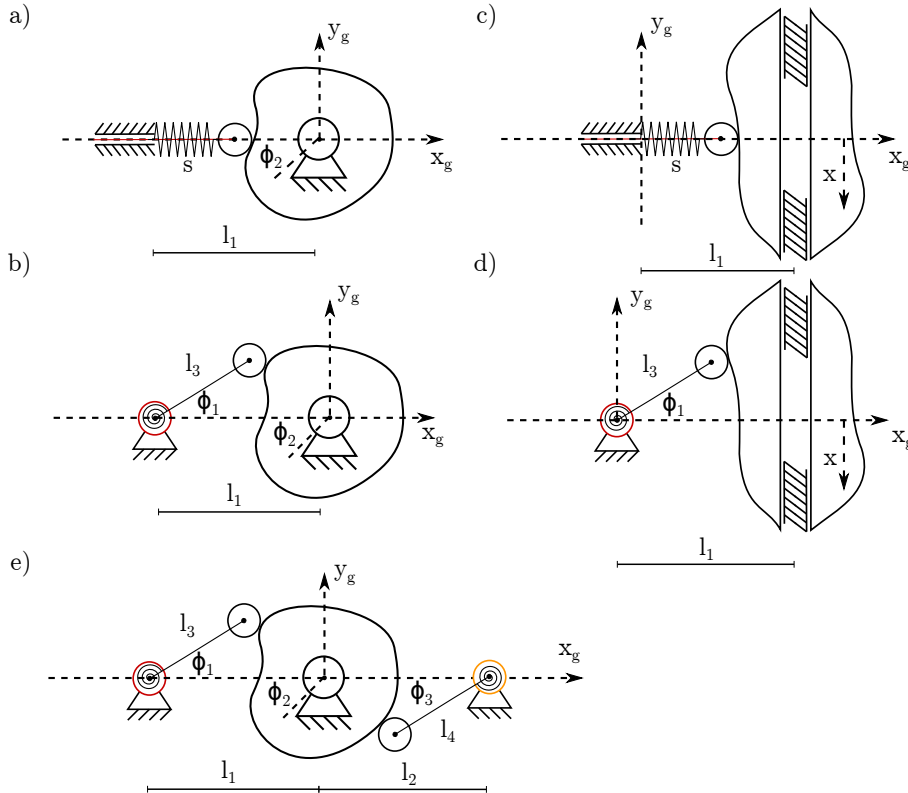


Figure 3.16: Building blocks for a cam based SBS-FL. Figures a, b, c, and d represent the different possibilities of cam type (translational/rotational) and spring type (translational/rotational). The different combinations for the classes of SBS-FL cam mechanisms are: a-a, a-b, b-a, b-b, c-c, c-d, d-c and d-d. The red joints are the outputs of the mechanisms and the orange joint is a storage spring configurations. Figure e presents a combination that belongs to class c-c.

Translational spring - translational cam

An example of such a submechanism is shown in figure 3.16c. The shape of the cam surface for the normal force springs in the global coordinates x_g and y_g can now be obtained with:

$$\begin{bmatrix} x_{cam} \\ y_{cam} \end{bmatrix} = \begin{bmatrix} s(x) \\ x \end{bmatrix}$$

This defines the cam surface for the side with the normal force springs. The side with the compensation springs works the same.

Rotational spring - translational cam

An example of such a submechanism is shown in figure 3.16d. The cam shape can be obtained with:

$$\begin{bmatrix} x_{cam} \\ y_{cam} \end{bmatrix} = \begin{bmatrix} l_3 \cos(\phi_1(x)) \\ l_3 \sin(\phi_1(x)) + x \end{bmatrix}$$

Translational spring - rotational cam

An example of such a submechanism is shown in figure 3.16a. The cam shape can be obtained with:

$$\begin{bmatrix} x_{cam} \\ y_{cam} \end{bmatrix} = \begin{bmatrix} (s(\phi_2) - l_1) \cos(\phi_2) \\ (s(\phi_2) - l_1) \sin(\phi_2) \end{bmatrix}$$

Rotational spring - rotational cam

An example of such a submechanism is shown in figure 3.16b. The cam shape can be obtained with:

$$\begin{bmatrix} x_{cam} \\ y_{cam} \end{bmatrix} = \begin{bmatrix} l_1 \cos(\phi_2) - l_3 \cos(\phi_1 + \phi_2) \\ -l_1 \sin(\phi_2) + l_3 \sin(\phi_1 + \phi_2) \end{bmatrix}$$

By combining one of these classes with another one of these classes, a cam based SBS-FL mechanism can be obtained. Such a combination is depicted in figure 3.16e where a rotational storage spring is connected via a rotational cam to a rotational braking spring. The eight possible combinations for these building blocks can be split into two categories. The first category contains mechanisms with the same type of storage spring as the type of braking spring. These mechanisms are depicted in figure 3.17. The second category contains mechanisms with a different type of storage spring as the type of braking spring. These mechanisms are depicted in figure 3.18.

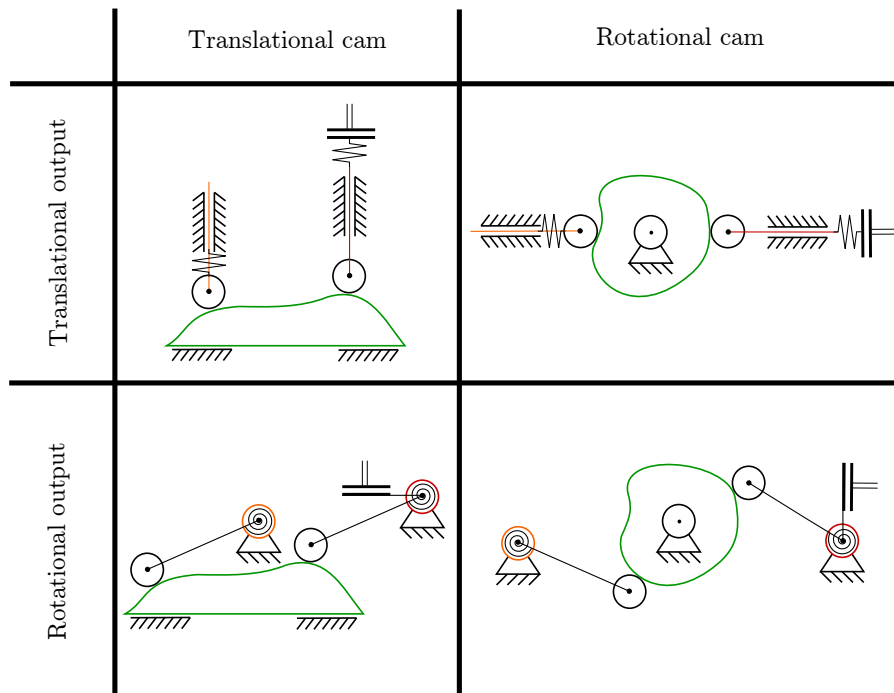


Figure 3.17: Overview of all cam type statically balanced singular-friction lockers with the same configuration for the storage spring (orange) as the braking spring (red). The cams are depicted in green.

In the remainder of this report, and especially in chapter 4, both classifications for the type of storage spring are generally not separately discussed but rather treated as one class.

The reason to do so is the fact that by allowing two types of springs (torsion and extension) on the same cam surface, the cam surface needs to be divided into two surfaces: one for the translational spring and one for the rotational spring. In the case of a translational cam, this is not much different from the other classes with a translational cam since the surface is always divided into two surfaces. As for the rotational cam surfaces, the division of the cam surface comes with the downside that the cam surface can no longer rotate 360 degrees. When fast switching times are required from the locking mechanism, this ability to fully rotate is an advantage. Also the type of actuator and the control of the actuator become simpler as only one rotational direction is required to switch the mechanism between 'engaged' and 'disengaged'.

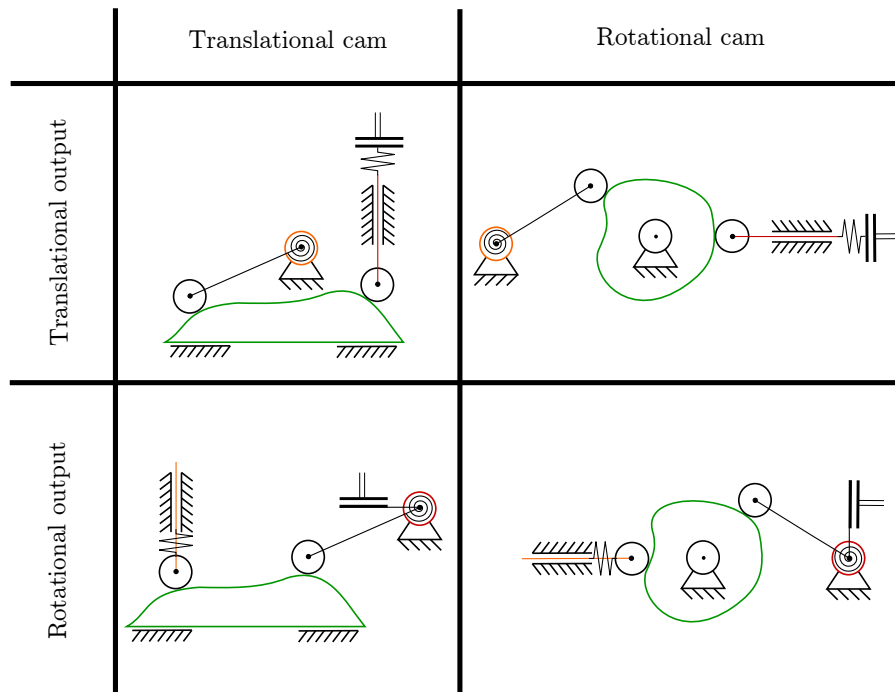


Figure 3.18: Overview of all cam type statically balanced singular-friction lockers with a different configuration for the storage spring (orange) as the braking spring (red).

3.5 Conclusion

In this chapter singular-friction lockers are improved to statically balanced singular-friction lockers. Only one linkage type singular-friction locker can be statically balanced, and all cam type singular-friction lockers can be statically balanced. For the cam type singular-friction lockers there is a restriction concerning the choice of the cam surface functions. When allowing for differences between the types of storage springs and the type of braking springs, eight cam based SBS-FL mechanisms can be identified.

Chapter 4

Conceptual design

In previous chapters statically balanced singular-friction lockers (SBS-FLs) are introduced. In this chapter the goal is to find the most compact form of a statically balanced locking device.

First an overview is presented for statically balanced locking in section 4.1. This section functions as a funnel towards possible concepts for locking devices. Secondly the concept selection criteria for a locking device for the Bidirectional Clutched Parallel Elastic Actuator (BIC-PEA) are derived in section 4.2. The term BIC-PEA, its use and the specific reason for this target object is also clarified in this section.

Thirdly in section 4.3, the concept solutions are generated and evaluated with respect to the concept selection criteria. Lastly in section 4.4 the concept selection is presented along with the elaboration of the final concept. By the end of this chapter the reader will understand what the 'best' SBS-FL mechanism is, what is meant by 'best', what this concept will look like in reality and what the theoretical 'performance' of this concept is.

4.1 Compact locking device in robotics

Previous chapters showed that a statically balanced locking mechanism is a favourable locking mechanism for robotics because it can unlock while under load, it has a high locking force, it has a low energy consumption and it is lockable in any position. What remains to be done is that a statically balanced locking device has to be transformed into a very compact, lightweight and inexpensive locking device with a short switching time.

To narrow down to such a compact locking device the flowchart depicted in figure 4.1 was made. In the category of statically balanced lockers there are two main categories: compliant type lockers and rigid body type lockers.

The main advantage of using a compliant type locker is that there is minimal friction, the downsides are hysteresis and an approximation of a static balance rather than an exact one. Also the pseudo rigid body optimization and the finite element optimization are rather tricky.

The main advantage of using a rigid body approach is that a 'perfect' static balance can analytically be obtained and that singular configurations ensure a zero actuation force in the 'engaged and the 'disengaged' states. However, the downside of this approach is that friction between components might form a problem.

This thesis investigates whether the rigid body type statically balanced lockers will provide a 'better' locking device. The exact definition of 'better' is presented in chapter 6.

Summarizing from figure 4.1 and from chapter 3 there are nine options to make a statically balanced singular-friction locker. However a distinction must be made which of these options will produce the smallest locking device with the lowest actuation force. BIC-PEA will serve as an example device to try to make the locking device as compact as possible. BIC-PEA is a small device that has a rotating axis that must be locked in any angle. In the next section (4.2) the concept selection criteria for a locking device for BIC-PEA are derived after which five different concepts are presented and evaluated on their potential to become the most compact working ideal locking device.

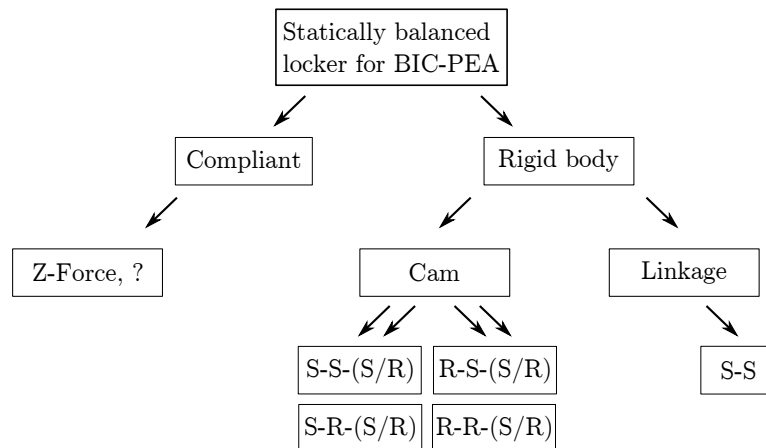


Figure 4.1: Flowchart for designing a statically balanced locking mechanism. 'S' denotes a slider, 'R' denoted a rotational joint. The first letter denotes the input of the mechanism, the second letter denotes the the output of the mechanism and a optional third letter denotes the possible storage spring configurations. In the compliant type mechanisms only one mechanism is known, namely the z-force, but others might exist.

4.2 Concept selection criteria

As stated at the end of the previous section (4.1), in this section the concept selection criteria are derived for a locking device to be used on the BIC-PEA. Two subsections are distinguished: firstly subsection 4.2.1 is devoted to the target application of the locking device (BIC-PEA). Secondly subsection 4.2.2 is devoted to the specific concept selection criteria for the locking device of the BIC-PEA.

4.2.1 BIC-PEA

The Bi Directional Clutched Parallel Elastic Actuator (BIC-PEA) [8] is a device used to save energy in robotic applications. The BIC-PEA can be described as an energy buffer where kinetic energy from a moving robot axis can be stored to and from which this energy can also be released. At any position of a robot axis, the BIC-PEA can connect a spring to the robot axis and store the kinetic energy of a joint in its internal spring such that the joint is decelerated to a standstill (zero velocity). The spring energy can then be released, accelerating the joint again. This acceleration of the joint can be done in both rotational directions because of the incorporation of a differential in the mechanism.

BIC-PEA is a small device: it fits in a cylinder with a diameter of 45 mm and a length of 51mm. Such a small mechanism asks for a locking mechanism that does not increase the size of the BIC-PEA enormously and does not consume the energy that the BIC-PEA is saving.

4.2.2 Specific selection criteria

In this section the specific design requirements are presented for designing a SBS-FL device for the BIC-PEA.

As mentioned in section 4.1 and chapter 1 all SBS-FL mechanisms can unlock while under load, have a high locking force, have a low energy consumption and are lockable in any position. The challenges that are however not completed are to find an embodiment that is most importantly compact and also lightweight, inexpensive and has a fast switching time.

To quantify the desired compactness we must look at the state of the art. In section 3.1 the only other statically balanced locking device is presented with cylindrical dimensions of a diameter of 60 mm and a length of 59 mm. Using two of these locking devices would make the BIC-PEA more than five times bigger than its size without the locking devices. Therefore the desired design space is strongly reduced by 50%, meaning that the locking device must fit in a design space cylinder with a diameter of 60 mm or less and with a length of 30 mm. The BIC-PEA and the design space are depicted in figure 4.2.

The criteria for the weight, the price and the switching time are considered to be of less importance. Weight is closely related to the size of the mechanism

and the number of components. The price will mainly be influenced by the complexity of the parts. The switching time is considered to be more dependent on the type of actuator that is used and no real hard criteria can be distinguished what configuration will have a shorter switching time.

Summarizing the conclusion can be drawn that most of the design criteria naturally follow from the performance criterion on the enclosed volume of the locking device. The specific design requirements that will be used for evaluation of the concept solutions are described in the enumeration below.

- **The compactness of the mechanism**, in a way that the smallest device possible is desired. Firstly the mechanism must fit in the purple design volume indicated in figure 4.2, secondly a smaller mechanism is considered to be better.

A ++ is rewarded if a concept easily fits in the design space, a + is rewarded if a concept just fits in the design space, a - is rewarded if a concept does not fit in the design space and a - - is rewarded if a concept does not fit in the design space by far.

- **The possibility for double execution of the mechanism**. The reason for this requirement is the idea that the bearings of the green braking disk on the BIC-PEA must not suffer unbalanced loads on its bearings.

A ++ is rewarded if a concept easily fits in the design space twice, a + is rewarded if a concept just fits in the design space twice, a - is rewarded if a concept does not fit in the design space twice and a - - is rewarded if a concept does not fit in the design space twice by far.

- **Drum brake or outside disk brake**. An outside disk brake can directly be applied to the outer radius of the green disk of the BIC-PEA and the connection to the sand-coloured ground will be easy in that case. A disadvantage to this configuration of locking is that the moment arm is quite small, so the locking torque will not be as high as a drum brake with a larger moment arm. When an outside disk configuration is not possible for a concept, a drum brake might still be possible. This configuration has the downside that the connection to the sand-coloured ground is difficult, but the advantage that the locking torque will be higher due to the large moment arm. The connection to the sand-coloured ground of the BIC-PEA is difficult because the connection must be made around the braking surface.

A ++ is rewarded for a drum brake that fits in the design space, a + is rewarded for a outside disk brake that fits the design space, a - is rewarded for a drum brake that does not fit the design space and a - - is rewarded for a outside disk brake that does not fit the design space.

- **The position and the type of actuator**. A rotational actuator is favoured over a translational actuator, as rotational actuators are easier to control, widely available and often cheaper than the translational actuators.

A ++ is rewarded if a concept has a rotational actuator that will fit within the design space, a + is rewarded if a concept has a translational actuator that will fit within the design space, a - is rewarded if a concept has a rotational actuator that does not fit within the design space and a - - is rewarded if a concept has a translational actuator that does not fit within the design space or when another very negative actuator related effect is encountered.

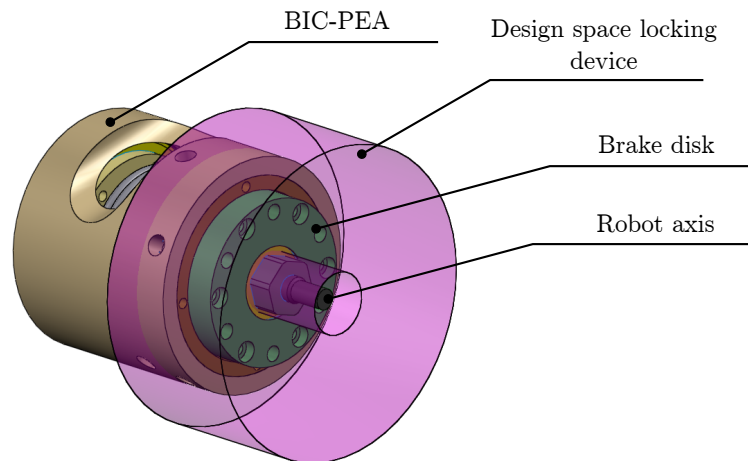


Figure 4.2: The design space for designing the locking mechanism for BIC-PEA. The entire locking device ideally must fit in space indicated with the purple cylinder. This cylinder has an outer diameter of 60mm, an inner diameter of 12mm and a depth of 30mm. The robot axis must pass through the locking mechanism without obstruction. The green disk is the part to be braked with respect to the sand-coloured ground.

4.3 Concepts

In this section the different concept solutions are elaborated on their performance with respect to the concept selection criteria. All concepts theoretically are able to provide a perfect static balance, however in practise difficulties might arise. The design requirements provide the evaluation criteria for each concept. Every concept is dealt with in a separated subsection. These subsections are all structured as follows. First a general note is presented on the concepts solution. Secondly the score of the concept is presented in a table. Thirdly a short textual evaluation is presented to discuss the score of the concept on the performance criteria.

Additionally, a uniform colour scheme is used. The purple parts are the parts that are to be locked with respect to the reference grounds (sand-coloured). Either one of the purple disks can function as a friction surface, however when the outer purple disk is used, the two reference grounds of the locking device and

the BIC-PEA will have to be united. Furthermore green parts are inputs to the mechanism, and orange parts are the parts that are used for the friction interface with purple parts. The translational miniature roller bearings that were used in the concepts had an inner diameter of 3 mm, an outer diameter of 6 mm and a length of 7 mm (NRC L306X). The miniature rotation roller bearings that were used in the concepts had an inner diameter of 4 mm, an outer diameter of 8 mm and a width of 2 mm (SKF W617/4X).

4.3.1 Linkage - Slider input/slider output

In figure 4.3 a rough design of a statically balanced singular-friction locker with a slider input and a slider output is depicted along with its schematic representation. As can be seen this concept appears to work best as a drum brake given the limitations of real components like springs and more importantly, bearings. The sand coloured part is what is to be connected to the reference ground on the BIC-PEA whereas the orange part is what should provide the friction interface.

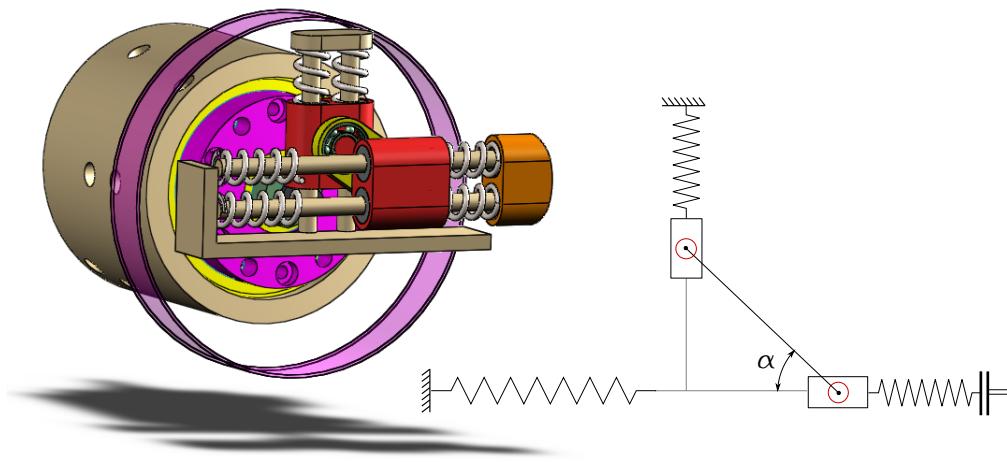


Figure 4.3: A linkage type statically balanced singular-friction locker. On the left a visual representation of what the schematic representation on the right would look like in small dimensions and with real bearing component dimensions.

Score

Criterion	compactness	double execution	brake type	actuator
Score	-	+	-	--

Table 4.1: Score of the concept of a linkage type SBS-FL with a translational input and a translational output.

Evaluation

- **Compactness.** This concept has the ability to just fit inside a disk with the diameter of 60 mm. The orange friction surface should always be perpendicular to the purple disk friction surface to avoid self-engaging behaviour. When looking at the possibility for an axle which can still run through the middle of the design, the conclusion must be that this design runs into trouble. As can be seen from the figure, there is no possibility for anything to pass the locking mechanism in the middle because that is where the two sliders are located.
- **Double execution.** The possibility to execute the concept double is investigated and here the conclusion is that there is indeed a possibility to execute this design double. The leftmost horizontal spring could for example be connected to another orange friction interface and another vertical storage spring could be added at the bottom of the mechanism.
- **Brake type.** As can be seen this concept will only work in a drum brake variant, which should lead to a higher locking torque. The mechanism does not fit in the design space and issues are clearly visible when trying to connect the sand-coloured ground of the locking device to the sand-coloured ground of the BIC-PEA.
- **Actuator.** The position of the actuator has to be determined. Recalling figure 3.6 the conclusion is drawn that the two translational degrees of freedom cannot function as an input as they both move into a singular configuration when the mechanism is turned 'on' or 'off'. Therefore the position of the actuator must for example be the angle α which is depicted in figure 4.3 with the curved arrow. In a way this is good because it is a rotational actuator. However the placement also means that the actuator is continuously moved when the mechanism is switching between locking states. This moving actuator is unfortunately very undesirable and given practical implementation hard to realize. For these reasons a special '- -' is rewarded on this design criterion.

4.3.2 Cam - Slider cam/slider output

In this section a cam type SBS-FL with a translational cam and a translational output is evaluated as depicted in figure 4.4. As can be seen in the right figure, there is a green cam surface which compresses and releases the springs connected to the ground and to the friction surface. In the left figure, an attempt has been made to produce the basis of this concept in a small design space given the limitations of real components.

As can be read in chapter 3 there are two variants of this class of SFS-FL. In this case the variant of this class with a translational storage spring was used. A rotational spring as a storage spring would not give any spatial advantages, so only the single case for this class of SBS-FL is discussed.

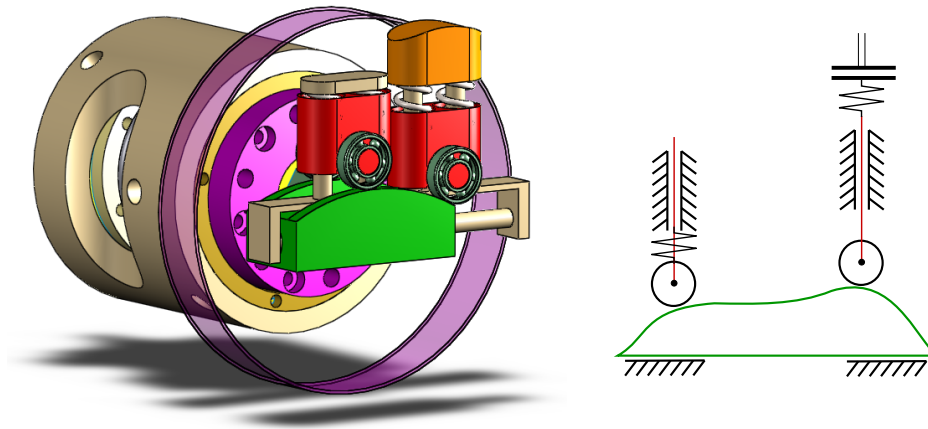


Figure 4.4: A cam type statically balanced singular-friction locker with a translational cam and a translational output. On the left a visual representation of what the schematic representation on the right would look like in small dimensions and with real bearing component dimensions. By translating the green cam to the left and to the right the locking device is engaged and disengaged.

Score

Criterion	compactness	double execution	brake type	actuator
Score	- -	+	-	+

Table 4.2: Score of the concept of a cam type SBS-FL with a translational cam and a translational output.

Evaluation

- **Compactness.** As can be seen from figure 4.4 the concept does not fit in the required design space of a disk with a diameter of 60 mm. The green cam surface can be sled horizontally and a friction force is generated in the orange friction interface. A reason for not fitting the design space is the fact that there appears to be little space for an axle which can still run through the middle of the design. Again from the figure, it becomes clear that the sliding cam surface consumes the space required for an axle to run through the middle of the design.
- **Double execution.** The possibility to execute the concept double and mirrored to reduce the loads on the main bearings is practically achievable. The design can be flipped upside down and attached to the original design. In that way, there are two friction surfaces upwards and downwards which can lock the purple drum disk simultaneously.

- **Brake type.** The brake type of this concept is a drum brake. Due to the size of the concept the sand-coloured grounds of the locking device and the BIC-PEA cannot be connected within the design space.
- **Actuator.** Lastly the position of the actuator must be in line with the sliding direction or even inside the input cam shape. This seems to be a feasible option.

4.3.3 Cam - Rotation cam/slider output

In this section a cam type SBS-FL with a rotational cam and a translational output is evaluated on its possibilities on becoming a compact locking device. A compact version of the concept given real components is depicted in the left picture of figure 4.5. A schematic representation of the same mechanism is depicted in the right picture of the same figure.

As can be read in chapter 3 there are two variants of this class of SFS-FL. In this case the variant of this class with a translational storage spring was used. A rotational spring as a storage spring would not give any spatial advantages and would require the cam surface to be split into two surfaces. For these reasons only the single case with a translational storage spring is discussed for this class of SBS-FL.

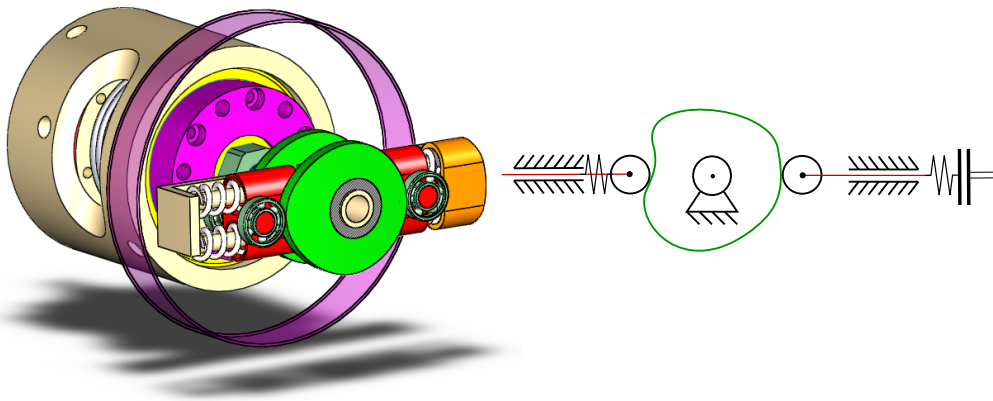


Figure 4.5: A cam type statically balanced singular-friction locker with a rotational cam and a translational output. On the left a visual representation of what the schematic representation on the right would look like in small dimensions and with real bearing component dimensions. The green cam shaft in the left picture is the input to the mechanism. By rotating this cam shaft, the red followers either compress or release the springs connected to the ground or to the friction surface.

Score

Criterion	compactness	double execution	brake type	actuator
Score	-	+	-	++

Table 4.3: Score of the concept of a cam type SBS-FL with a rotational cam and a translational output.

Evaluation

- **Compactness.** When evaluating this type of SBS-FL on its ability to fit inside a disk with the diameter of 60 mm, the conclusion must be that it is only just not possible to do so. The problem lies in the fact that the two grounds of the locking device and the BIC-PEA cannot be connected. As can be seen from figure 4.5 there is some space for a small axle to fit through the middle of the design.
- **Double execution.** The criterion on the possibility to execute the concept double and mirrored to reduce the loads on the main bearings is quite easy to satisfy. The mechanism can be added under a 90 degree angle to the original mechanism without the need of another cam. In that way the springs connected to the orange friction braking part are on the horizontal axis and the springs connected to the ground are connected in vertical direction.
- **Brake type.** This concept is also a drum type locking device. Unfortunately it only just does not meet the compactness criteria to connect the grounds, meaning that the advantages of using a drum type brake are lost.
- **Actuator.** The criterion on the position of the actuator and the feasibility of that position is fully satisfied in this mechanism because a simple rotational actuator can be connected to the green cam shaft.

4.3.4 Cam - Slider cam/rotation output

A cam type SBS-FL with a translational cam and a rotational input is depicted in figure 4.6, where the right image represents the schematic representation of the mechanism on the left. As can be seen from the figure, the mechanism applies the locking force via the orange brake arm to the outside of the green disk. Braking on the inside of the disk will inevitably lead to self-engaging behaviour of the brake as the vector of the friction force will never point through the center of the axle of the braking arm.

As can be read in chapter 3 there are two variants of this class of SFS-FL. In this case the variant of this class with a rotational storage spring was used. A translational spring as a storage spring would not give any spatial advantages, so only the single case for this class of SBS-FL is discussed.

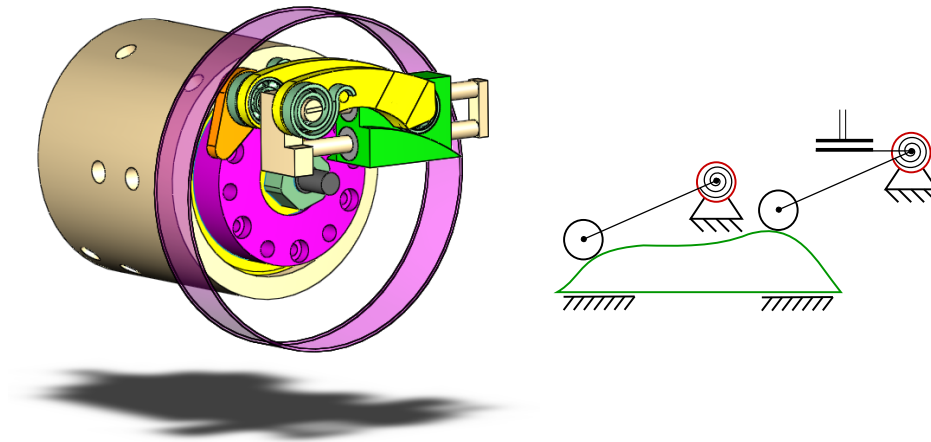


Figure 4.6: A cam type statically balanced singular-friction locker with a translational cam and a rotational output. On the left a visual representation of what the schematic representation on the right would look like in small dimensions and with real bearing component dimensions. Sliding the green cam to the right and to the left will engage and disengage the locking device.

Score

Criterion	compactness	double execution	brake type	actuator
Score	+	+	+	+

Table 4.4: Score of the concept of a cam type SBS-FL with a translational cam and a rotational output.

Evaluation

- **Compactness.** The mechanism brakes on the outside of the 32 mm disk of the BIC-PEA and the mechanism fits in the required design space. One observation to make is that though the mechanism does not consume to much volume in plane, it does consume volume out of plane. This mechanism is already more than 2 cm thick, which is more than most other mechanisms. Another observation that can be made is that the possibility for an axle to run trough the middle of the locking device clearly exists.
- **Double execution.** The possibility to execute the concept double and mirrored to reduce the loads on the main bearings is also satisfied for this locker. By simply flipping the mechanism upside down and coupling the sliders together, a doubled version can be obtained.

- **Brake type.** This concept is the first concept that utilizes outer disk brake configuration. This might result in a lower locking torque but it does ensure that the connection between the sand-coloured ground of the BIC-PEA and the ground of the locking device is easy.
- **Actuator.** The criterion on the position of the actuator and the feasibility of that position should not give problems. Even though a linear actuator is required to actuate the mechanism, there is still plenty of volume to locate it.

4.3.5 Cam - Rotation cam/rotation output

The last concept to be discussed is the cam type SBS-FL with a rotational cam and a rotational output. A representation of such a locking device is depicted in figure 4.7. As can be seen there is an outer cam disk that compresses and releases the torsion springs connected to the followers. The orange axle is connected to the braking arm and the blue axle is connected to the ground.

As can be read in chapter 3 there are two variants of this class of SFS-FL. In this case the variant of this class with a rotational storage spring was used. A translational spring as a storage spring would not give any spatial advantages and requires the cam surface to be split into two cam surfaces. Therefore only the single case for this class of SBS-FL is discussed.

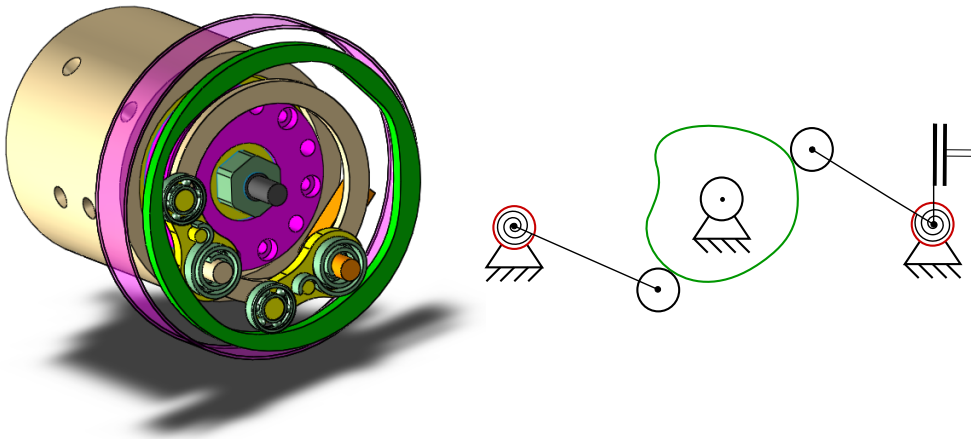


Figure 4.7: A cam type statically balanced singular-friction locker with a rotational cam and a rotational output. On the left a visual representation of what the schematic representation on the right would look like in small dimensions and with real bearing component dimensions. By rotating the green cam disk, the locking mechanism is engaged or disengaged.

Score

Criterion	compactness	double execution	brake type	actuator
Score	++	++	+	++

Table 4.5: Score of the concept of a cam type SBS-FL with a rotational cam and a rotational output.

Evaluation

- **Compactness.** From figure 4.7 the simple conclusion can be drawn that the concepts easily fits in the design space of a disk of 60 mm. Another observation that can be made when comparing the right and left figures of figure 4.7 is that either an inside or an outside cam can be used. No matter the choice, there is always space for an axle to pass through the middle of the locking device. A last observation for this section is that the design, as presented now, is a very slender design of about 1 cm in thickness. Of course more bearings might be needed, but essentially the mechanism shows great potential of providing a very small locking device.
- **Double execution.** The possibility to execute the concept double and mirrored is also present. The two followers only take up half of the space of the cam ring, so two more followers can easily be added to this locking device.
- **Brake type.** This concept utilizes the outside disk brake configuration. Arguably, this is the only type of friction locking configuration that can be used with a rotational output. The reason for this statement is the fact that when using a rotational output in a drum brake, self-engaging behaviour is inevitable.
- **Actuator.** The position of the actuator and the feasibility of that position are also quite clear. A (desirable) rotational actuator can actuate the cam ring or -shaft and there is plenty volume to locate it.

4.4 Concept selection and final concept

In order to make an objective decision which of the concepts will provide the highest locking torque in the smallest volume a performance table can be made. Putting all the scores of the individual concepts together, table 4.6 can be constructed on the performance of the different concepts.

From table 4.6 the conclusion can be drawn that the cam type locking device with a rotational cam, a rotational output and rotational storage springs is the most compact form of a SBS-FL device. The final concept must now be transformed into a real and functional prototype. The working principle of this prototype is depicted in figures 4.8, 4.9 and 4.10. The working principle is explained in more detail in the captions of the figures. The name of the prototype that will be used during the rest of this thesis is the p-brake, because the locking torque is only position dependent.

Criterion	compactness	double execution	brake type	actuator
Linkage SS	-	+	-	--
Cam SS	--	+	-	+
Cam RS	-	+	-	++
Cam SR	+	+	+	+
Cam RR	++	++	+	++

Table 4.6: Table with the combined scores of all concept solutions. 'S' denotes slider and 'R' denotes rotational. The first letter is the cam type and the second letter denotes the output type. Clearly the cam based SBS-FL with a rotational cam and the rotational output (RR) appears to be the concept which shows great potential to be the most compact SBS-FL mechanism.

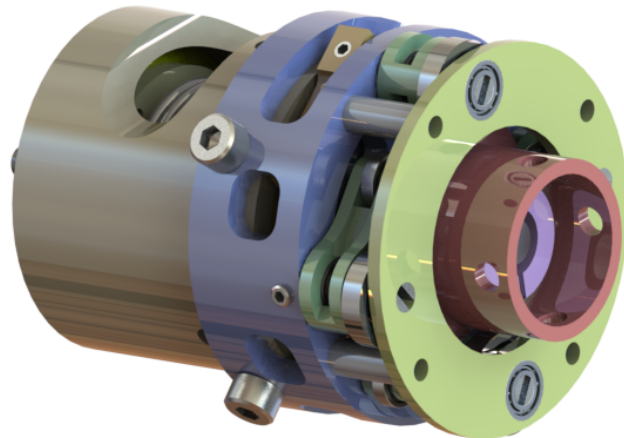


Figure 4.8: The final concept with a diameter of 55 mm and a length of 23 mm. The red part in the middle is the input of the mechanism. This input is in balance in every position. For different positions of the cam, different braking torques are achieved. This is explained further in figure 4.9.

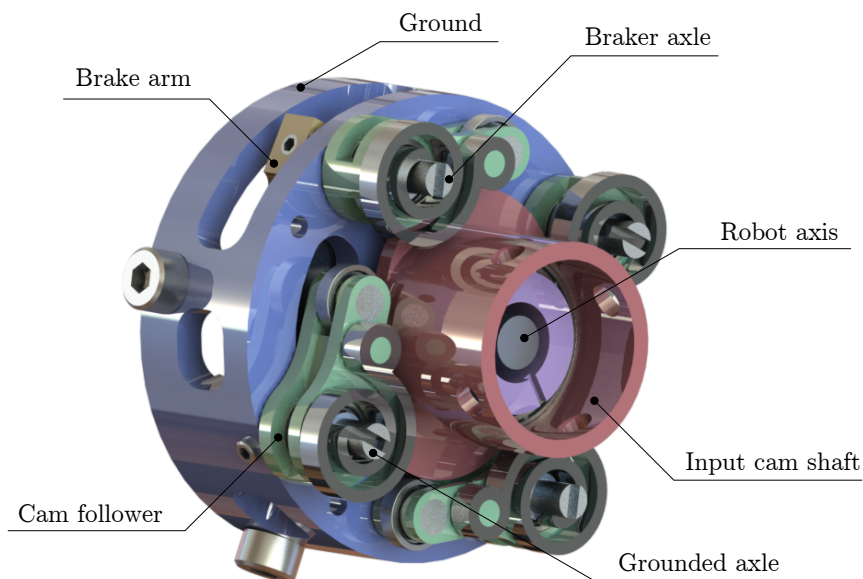


Figure 4.9: The working principle of the final concept. The top and the bottom followers are attached to the axles connected to the braking arms. The left and the right followers are attached to axles connected to the dark blue ground (see also figure 4.10). The followers are connected to the axles by means of the black springs. Energy is transferred from the grounded springs to the braking springs and back via the red cam surface. If this energy transfer from and to the braking springs and the grounded springs is 1:1, the red cam shaft can be turned without applying any torque.

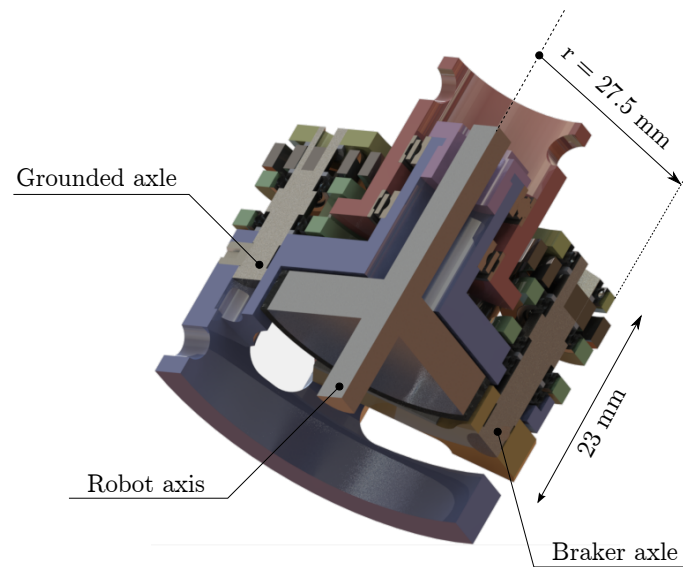


Figure 4.10: The final concept viewed in a sectional view. The grey disk in the middle represents the brake disk on the BIC-PEA which is to be locked. The black ring on the grey disk is a rubber ring to enhance the magnitude of the friction coefficient between the orange brake arm and the brake disk. The orange brake arms can be seen on this braking disk. The main message from this picture is to see the different connections of the axles connected to the torsion springs and the cam followers. The grounded axle is connected to the blue housing. The braker axle is connected to the brake arm. Both run through the green cam followers and are connected to the black springs with a slotted connection. The yellow part functions as a extended housing to deal with any moments that are exerted on the braker- and grounded axles.

Chapter 5

Prototype design

In this chapter the practical implementation of building a first prototype of the concept selected in chapter 4 is presented and discussed. In figure 5.1 the prototype is depicted. All crucial features of the locking mechanism are explained in the report, other details are presented in appendix D.

First in section 5.1 the locking torque and the components required to achieve this locking torque are discussed. Secondly in section 5.2 the torsion spring design, -calculations and -laser manufacturing is presented and discussed. Thirdly in section 5.3 the cam calculations and design are presented along with the manufacturing of the cam shaft. Lastly in section D.4 of appendix D the other components that make up the prototype are presented and discussed on their features.



Figure 5.1: The locking device assembled and fully functional. This image should function as a reference to the parts introduced throughout this chapter.

5.1 Required locking torque

This section the calculations on the locking torque are presented. The real execution of the outcome is presented with extensive photographs in section D.1 of appendix D.

Calculations on the locking torque

In figure 5.2 two figures are depicted to illustrate the calculations in this section. The locking torque that is tried to be achieved is 1.3 Nm. With prior compensation for potential manufacturing errors the design locking torque is corrected to 1.5 Nm. As there are two friction surfaces which provide a friction force on the surface of the brake disk, both levers have to account for 0.75 Nm of locking torque. Furthermore the friction coefficient between the braking shoe (brown) and the braking disk (green) is estimated at 0.8. This estimation is based on findings in prior research by Plooij at al. [16].

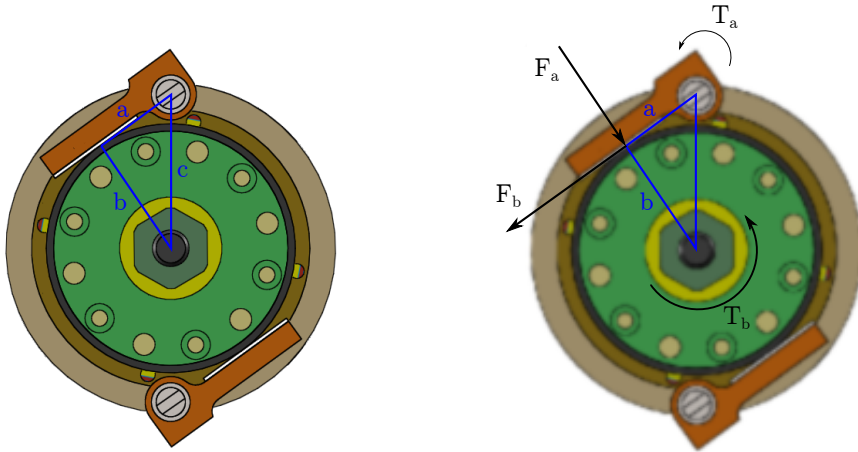


Figure 5.2: Figures with the BIC-PEA and the brake shoes.

Left: Figure to calculate the required torque in the grey axles that are connected to the the braking surfaces. Length c and length b are known and arm length a can now be calculated with $a = \sqrt{c^2 - b^2}$. For $b = 16$ mm and $c = 21$ mm, length a becomes ≈ 13.0 mm.

Right: Figure to calculate the required torque in the grey axles that are connected to the the braking surfaces. Length a and length b are known and equal to $b = 16$ mm and $a = 13.0$ mm. The (Coulomb) friction coefficient is assumed to be equal to 0.8. $T_b = 0.75$ Nm so now T_a can be calculated with: $T_a = \frac{T_b \cdot a}{b \cdot 0.8}$. This results in the required torque from the springs $T_a = 0.797$ Nm.

The effective length of the braking arm a is determined with simple geometry. It is very important that the contact point between the brake arm and the brake disk is chosen such that the vector of the friction force points straight through the axle of the braking arm. If this is not the case, the friction force creates a

moment around the braking arm. This moment is either added to or subtracted from the locking torque depending on the locking direction. This phenomena is known as self-engaging locking. Concluding, the dimensions and the torques can be summarized as:

$$\begin{aligned} T_b &= 0.75 \text{ Nm} \\ a &= 13.6 \text{ mm} \\ b &= 16 \text{ mm} \\ cf &= 0.8 \end{aligned}$$

Naturally the goal is to determine the torque that the torsion springs have to provide on the braking arms. Again, this torque can easily be calculated with the aid of figure 5.2 and the dimensions defined above. The calculated torque T_a is the input for the calculations on the torsion springs in section 5.2.

$$\begin{aligned} F_b &= \frac{T_b}{b} = \frac{0.75}{0.016} = 46.875 \text{ N} \\ F_b &= F_a \cdot cf \\ F_a &= \frac{F_b}{0.8} = \frac{46.875}{0.8} = 58.59 \text{ N} \\ T_a &= F_a \cdot a = 58.59 \cdot 0.0136 = 0.797 \text{ Nm} \end{aligned}$$

5.2 The torsion springs

In this section the numerical calculations are presented based on the work done with Glenn Mathijssen at the VUB in Brussels. This section falls apart in three subsections. First the material properties are defined along with some general torsion spring dimensions and constants. Secondly, the analytical calculation procedure is presented to obtain springs with the required dimensions and the correct stiffness. In the third section theory is brought into practice and the manufacturing of the torsion springs is discussed.

5.2.1 Material properties and required constants

The first thing to be done is to define the material properties of the available spring material and to define the constants required to produce the torsion springs. A safety factor (SF) on the yield strength is incorporated to ensure no plastic deformation will occur. The design torque is obtained from section 5.1 and is labeled T_{max} .

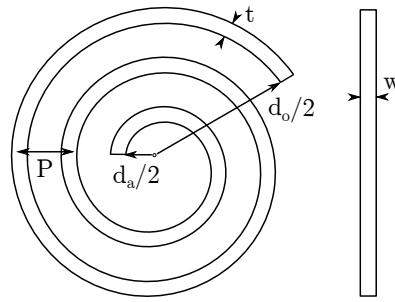


Figure 5.3: A basic representation of a torsion spring where the different parameters like the pitch, the wire thickness and the width of the springs are defined.

$$\begin{aligned}
 \sigma_y &= 1072 \cdot 10^6 \text{ Pa} \\
 \sigma_t &= 1309 \cdot 10^6 \text{ Pa} \\
 SF &= 1.3 \\
 S_y &= \sigma_y / SF \text{ Pa} \\
 E &= 189 \cdot 10^9 \text{ Pa} \\
 \rho &= 7900 \text{ kg/m}^3 \\
 d_a &= 0.004 \text{ m} \\
 \theta_{max} &= 20 \cdot \pi / 180 \text{ rad} \\
 T_{max} &= 0.797 \text{ Nm} \\
 k &= T_{max} / \theta_{max} \\
 w &= 0.003 \text{ m}
 \end{aligned}$$

5.2.2 Calculation procedure

There are several papers describing the design methodology of a torsion spring. For example Knox and Schmiedeler [30] describe something close to the procedure below to calculate the torsion spring characteristics and dimensions.

In general the procedure goes as follows. First the minimum wire thickness t_{min} is calculated along with the minimum length of the spring L_{min} , the minimum mass of the spring m_{min} and the minimum outer diameter $D_{out,min}$. The initial pitch P for further calculations must be chosen just a factor bigger than the minimum wire thickness of the spring. From there on the total wrap angle ϕ_{end} is calculated by solving the equations for the outer diameter D_{out} with helical constants a and b simultaneously with the length of the spring L (where $L = L_{min,0}$). Once the total wrap angle is obtained, the expected outer diameter of the torsion spring can be calculated. If that expected outer diameter is smaller than the minimum required outer diameter, the pitch P must be enlarged manually. This procedure is iteratively done until the expected outer diameter is larger than

the minimum outer diameter of the spring. This constraint is included to ensure that the windings of the spring do not make contact during tensioning of the spring.

$$\begin{aligned}
 t_{min} &= \sqrt{\frac{6 \cdot T_{max}}{w \cdot \sigma_y}} \\
 L_{min} &= \frac{w \cdot t_{min}^3 \cdot E}{12 \cdot k} \\
 m_{min} &= \rho \cdot L_{min} \cdot w \cdot t_{min} \\
 D_{out,min} &= \frac{2 \cdot L_{min}}{\pi \left(\frac{\sqrt{d_a^2 + 1.27 \cdot L_{min} \cdot t_{min} - d_a}}{2 \cdot t_{min}} \right) - \frac{\theta_{max}}{2\pi}} - d_a \\
 D_{out} &= d_a + \text{floor}\left(\frac{\phi_{end}}{2\pi}\right) \cdot 2 \cdot P + \text{round}(\phi_{end} - \text{floor}(\phi_{end})) \cdot P + t_{min} \\
 a &= \frac{(d_a + t_{min})}{2} \\
 b &= \frac{P}{2\pi} \\
 L &= -\frac{1}{2b} \cdot [a \cdot \sqrt{a^2 + b^2} + b^2 \cdot \ln(a + \sqrt{a^2 + b^2}) \\
 &\quad - (a + b \cdot \phi_{end}) \cdot \sqrt{a^2 + b^2 + 2 \cdot a \cdot b \cdot \phi_{end} + b^2 \cdot \phi_{end}^2} \\
 &\quad - b^2 \cdot \ln(a^2 + b^2 + 2 \cdot a \cdot b \cdot \phi_{end} + b^2 \cdot \phi_{end}^2)] \\
 P &= 2.1 \cdot t_{min}
 \end{aligned}$$

5.2.3 Resulting spring

When the procedure from section 5.2.2 is done with the material properties and constants from section 5.2.1, a torsional spring shape is obtained. This torsion spring is depicted in figure 5.4. The dimensions on the axes are the real dimensions of the spring in millimetres. The spring is quite small with a maximum radius of little more than 8 mm, and yet capable of providing the required torque of almost 0.8 Nm.

Once the model is obtained in matlab, there are basically three constants that constrain the helical shape, namely the pitch, the number of coil turns and the wire thickness. These constants are easily obtained from the torsion spring model and can be used in solidworks to produce a 3D model of the torsion springs.

When the basic shape of the springs, namely the helical shape, is achieved, all that remains is to design the attachments to the axle to which the springs are connected. Also a connection for the outer end of the torsion spring must be provided which can be used to tension the spring. It was decided to simply attach the springs to the axle with a slotted connection and a pinned connection on the outer end of the springs.

The torsion springs that were made of 1 mm RVS301 plate and 3 mm RVS301 plate are depicted in figure 5.5. Measurements on the performance of the springs are presented in chapter 6.

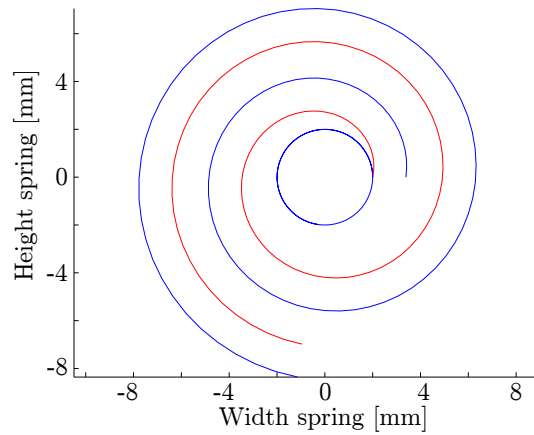


Figure 5.4: Torsion spring as obtained from the model in matlab. The planar dimensions on the axes are in millimetres. The red and the blue lines are to emphasize the inside and outside contours of the spring.



Figure 5.5: Torsion spring in reality. These springs were laser cut from 1 mm RVS301 stainless springsteel and from 3 mm RVS301 sltainless springsteel. The slotted axle connection and the pin follower connection can be seen in this photo.

5.3 Cam design

In this section the procedure is described to obtain a cam shape and follower that will exactly balance the system. The generation of cam surfaces to produce a certain desired follower trajectory is not new and the method chosen for this thesis is described by Tsay and Lin [31]. This procedure is explained briefly as is the generation of the cam which is to be used in the locking device. The real cam emerging from the modelled cam after production is presented in section D.3 of appendix D.

5.3.1 Calculations and model

As mentioned, Tsay and Lin [31] describe a rigid body method to determine the shape of various types of cams given a certain desired follower trajectory. The basic idea, which I will not elaborate in detail, is to rotate the follower by means of the rigid body rotation matrices around the origin of the cam shaft while executing the desired follower trajectory. The basic parameters are presented in figure 5.6.

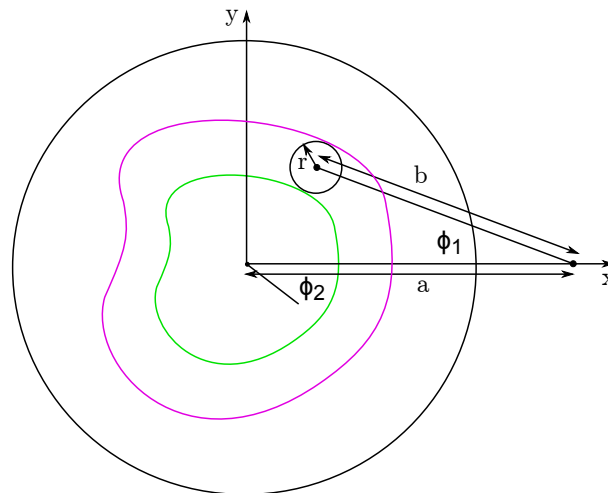


Figure 5.6: Cam surface generation as found in the paper by Tsay and Lin [31]. Length b is the length of the follower arm, length a is the distance from the follower axle to the cam axle and r is the radius of the roller of the follower. Angle ϕ_2 is the rotation of the cam and ϕ_1 is the follower angle.

The exact procedure is described in appendix D.2, but the main equation is presented below. Basically the shape of the cam depends on the parameters a , b and r , the angles ϕ_2 and ϕ_1 but also on the angular velocity ϕ_1' . This means that for the follower trajectory, also the differentiated follower trajectory must

also be known. The cam shape is described in the global coordinates x and y as:

$$\begin{bmatrix} x \\ y \end{bmatrix} = \begin{bmatrix} [a \cos(\phi_2) - b \cos(\phi_1 + \phi_2)] \pm \frac{r[a \cos(\phi_2) - b(1 + \phi_1') \cos(\phi_1 + \phi_2)]}{\sqrt{a^2 - 2ab(1 + \phi_1') \cos(\phi_1) + b^2(1 + \phi_1')^2}} \\ [-a \sin(\phi_2) + b \sin(\phi_1 + \phi_2)] \pm \frac{r[b(1 + \phi_1') \sin(\phi_1 + \phi_2) - \sin(\phi_2)]}{\sqrt{a^2 - 2ab(1 + \phi_1') \cos(\phi_1) + b^2(1 + \phi_1')^2}} \end{bmatrix}$$

The practical generation of the trajectory is constrained to the criterion of constant potential energy in the system. It is therefore important to check for any cam follower trajectory that is used for the generation of a cam shape profile, that the energy in the system remains constant. This means that:

$$E_{pot,total} = \frac{1}{2}k\phi_{spring,ground}^2 + \frac{1}{2}k\phi_{spring,brake}^2 = constant$$

The trajectory for the follower of the cam is chosen to be a modified sine function. First, the design was checked for the ideal minimum- and maximum angles of the follower. These turned out to be -47 degrees and -67 degrees respectively. From these angles, the amplitude constant (b) for the modified sine function can be derived. Furthermore, there have to be four singular configurations on the cam shaft, all spaced 90 degrees apart. The length of the singular configuration was chosen to be 5 degrees on the input cam shaft for each of the singular configurations. This was done to provide a stable zone in the 'on' and 'off' configurations. Four times five degrees are 'lost' on singular configurations, which makes the period of the sine 340 degrees. The c constant for the sine wave is therefore determined. Last but not least, the cam starts with the follower under an angle of -47 degrees, so this angle is an offset to the sine function and is labelled as constant d . All is summarized below, and the resulting energy function fortunately still shows to be constant.

$$\begin{aligned} b &= (-67) - (-47) \frac{\pi}{180} = -\frac{1}{9}\pi \\ c &= \frac{2\pi}{340} = \frac{1}{170}\pi \\ d &= -47 \frac{\pi}{180} = -\frac{47}{180}\pi \\ \phi_{1,ground} &= b \cdot \sin(c \cdot \phi_2) + d = -\frac{1}{9}\pi \sin\left(\frac{1}{170}\pi\phi_2\right) - \frac{47}{180}\pi \\ \phi_{1,brake} &= b \cdot \cos(c \cdot \phi_2) + d = -\frac{1}{9}\pi \sin\left(\frac{1}{170}\pi\phi_2\right) - \frac{47}{180}\pi \\ E_{pot,total} &= \frac{1}{2}k(\phi_{1,ground} - d)^2 + \frac{1}{2}k(\phi_{1,brake} - d)^2 = \frac{1}{162}k\pi^2 \end{aligned}$$

Practically, the trajectory of the follower angles can now be visualized as a function of the input angle ϕ_2 . This relation is depicted in appendix D.3 in figure D.3. To check whether the energy indeed remains constant, figure D.4 in the same appendix shows the potential energy in the system for every angle ϕ_2 of the input cam shaft.

If the trajectory of the followers is known and differentiable, the cam shape can be calculated with the relation provided by Tsay and Lin [31]. In figure 5.7 the generated cam shape is depicted. On both axes are the dimensions of the cam in millimetres. The red trajectory is the nominal trajectory of the follower, but realizing that there is a roller attached to the end of the follower the green line depicts the surface of the cam taking the roller into account.

With the cam shape determined, a 3D model of the cam shape can be made. Unfortunately there appears to be only one cumbersome way to get this procedure done. The graph can only be transported as a discrete number of points by means of an old format .iges file. This point cloud is depicted in figure D.5 in appendix D.3. From there on a 3D model can be obtained in SolidWorks.

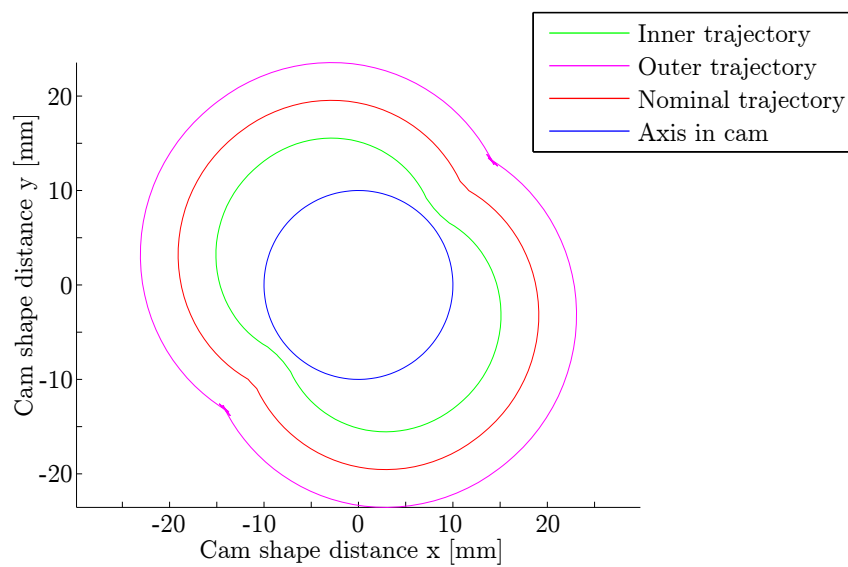


Figure 5.7: The plotted cam surface as calculated in Matlab. The green surface is the cam surface that is used for production. The colours correspond to the colours used in figure 5.6.

Chapter 6

Performance evaluation

The prototype presented in chapter 5 was build in order to be able to see whether theory can be brought into practice. In this chapter the measurement setup, the measurement variables, the experiment execution strategy and of course the results of the experiments are presented and discussed.

First in section 6.1 the properties to judge the performance of the locking device are discussed. Secondly in section 6.2 three experiments are designed to measure the performance. The method, the results and a discussion are presented of each experiment. Lastly in section 6.3 an overall conclusion on the measurements and the performance is presented.

6.1 Performance of a SBS-FL mechanism

In order to compare a specific SBS-FL mechanism to another SBS-FL mechanism or to another locking device, a way to quantify the performance of a SBS-FL must be found. In the first section the performance quantification of a SBS-FL device is described. In the second subsection the physical variables to be measured are introduced.

6.1.1 Performance metrics

Steinthorsson et al. [32] state that there are generally three ways to compare statically balanced mechanisms to other statically balanced mechanisms. The first performance criterion is the amount of energy the mechanism stores per unit volume. The second criterion is the compensated force per unit volume and the last criterion is the statically balanced stroke per unit volume.

The criteria seem not entirely satisfactory for the use on the locking device presented in chapters 4 and 5. There is not really a compensated force but rather a compensated torque. And even about the compensated torque some ambiguity might exist, because there appear to be two options. The first option for the compensated torque is the braking torque provided by the springs in the mechanism. The second option is the torque you feel when the system is unbalanced. This means that only the springs connected to the braking arms are connected and that the storage springs to the ground are disconnected.

Looking at the compensated torque seems to solve the problem for this particular locking mechanism. In order to compare the locking device to the other existing statically balanced locking device, namely the z-force, another issue can be spotted. The z-force is a mechanism with a translational input, so a force is applied on the input. The locking device presented in this thesis has a rotational input cam and therefore an input torque has to be applied. A dimensionless group of the input torque or force divided by the maximum torque or force generated in the springs was chosen to solve this problem.

Lastly the distinction in calculating these dimensionless numbers could be made between the continuous input torque or force or the maximum input torque or force. The continuous input torque is defined as the force or torque required to keep the mechanism engaged or disengaged when it is in either one of those configurations. The dimensionless efficiency numbers could be calculated per unit volume the mechanism incorporates.

$$\frac{\text{Input torque}_{\text{max/cont}}}{\text{Torque in braking springs}} \cdot \frac{1}{\text{Footprint}} \left[\frac{Nm}{Nm} \right] \cdot \left[\frac{1}{mm^3} \right]$$

In the case of a translational input this expression becomes:

$$\frac{\text{Input force}_{\text{max/cont}}}{\text{Force in braking springs}} \cdot \frac{1}{\text{Footprint}} \left[\frac{N}{N} \right] \cdot \left[\frac{1}{mm^3} \right]$$

Of course a last performance metric for a locking device is the amount of locking torque it provides. Last but not least the option exists that the input of the mechanism is for example translational (a force) and the spring type is a torsion spring (a torque). In this case the required input energy can be calculated from the area under the force-position graph and the compensated energy in the braking springs can be calculated in the same manner. This gives the fraction of input energy over braking spring energy, which is also a dimensionless number.

6.1.2 Measurement variables for a SBS-FL mechanism

In the previous section performance metrics are introduced. Some of the quantities to calculate these metrics can be measured directly, others will have to be obtained indirectly. In order to give a clear overview, the two types of measurement variables are described separately.

Direct variables

The direct variables that can be measured directly from the locking device are presented below. These quantities are directly used for calculating the performance metrics in section 6.1.1.

- Maximum input torque (un)balanced system
- Continuous input torque (un)balanced system
- Compensated braking torque
- Footprint/volume

Indirect variables

There are however also some quantities in the performance metrics that cannot be calculated directly.

- Energy
- Torque in braking springs

The maximum torque in the braking springs can be estimated with the maximum input torque of the unbalanced system. This input torque can be compared to the calculated maximum input torque in the model of the torsion springs. This leads to a correction factor for the maximum torque in the torsion springs.

6.2 Experiments

In section 6.1 the way to quantify the performance of a SBS-FL mechanism is described. In order to find the required parameters for these performance metrics, experiments on the p-brake must be conducted. There are three basic questions that must be answered in this chapter to fill in the performance metrics for a SBS-FL mechanism. These are:

1. Is the stiffness in the springs the same as the modelled stiffness?
2. What is the input torque characteristic of the balanced system?
3. What is the locking torque characteristic of the locking device?

The answers to each of these questions are found with three separate experiments, numbered 1, 2 and 3 after the questions they answer. Each experiment is described in a separate section all with the same layout. First the method of the experiments is presented, secondly the results are presented with the aid of graphs, and lastly a discussion is provided on the measurement results.

The results are the final results of the experiments where the locking device is tweaked to show the performance it should regularly show. In appendix E the overview of all measurement runs is presented for completeness and as an index to find measurement data back easily.

The rest of this section is structured as follows. The measurement setup that was used for all experiments and the calibration of the setup are shown in section 6.2.1. The results of experiment 1 are shown in section 6.2.2, the results of experiment 2 are shown in section 6.2.3 and the results of experiment 3 are shown in section 6.2.4.

6.2.1 Measurement setup

In this section the test setup is presented. In figure 6.1 an image of the test setup is depicted. In section E.1 of appendix E additional images of the Solidworks model and the setup are presented. As can be seen a Maxon RE-50 motor (200W, 1:26 gearbox) is present along with two load cells (AE sensors, L6D). These load cells are connected via two cables to an aluminium bridge. This bridge is attached to the outer shell of the motor. The motor is connected to the ground via two large roller bearings. In this way any torque exerted by the motor on its actuated axis can be measured accurately by the two load cells.

The motor is controlled via a control board to which the load cells are also connected. This control board is controlled with a real time target which is connected to the host computer with an Ethernet cable. The real time target communicates with the control board via the CANopen over Ethernet protocol which ensures a fast real time system that operates at 1kHz. The controller on the real time target is configured in Simulink, after which it is compiled and loaded onto the target. All gear and Simulink control was readily available.

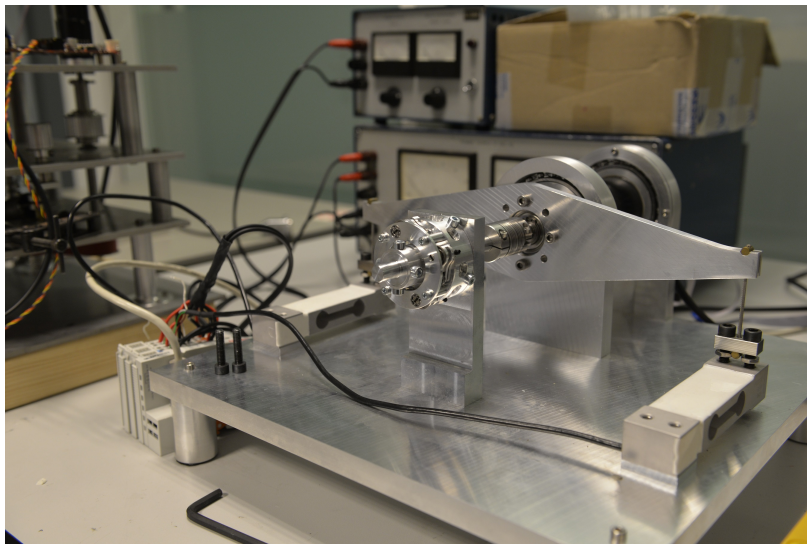


Figure 6.1: Locker in test setup to measure the locking torque. In the middle the locking device can be seen connected with the brake side to the motor. The two load cells and the torque measurement arrangement can also be seen in this photo along with the Maxon motor connected to the load cells. This configuration is used in experiment 3.

Calibration

The measurement setup needs to be calibrated in order to identify any offsets in the data. If there is any imbalance between the load cells or a slight error in their calibration it must be identified. Basically there are two situations: the motor is moving or the motor is at a standstill. In case the motor is at a standstill, purely the static imbalance between the load cells can be identified. In case the motor is moving, any other forms of friction in for example the bearings supporting the motor can be identified. The results of this calibration are presented in more detail in section E.2 of appendix E. The main result is that the static offset in the load cell torque sensor arrangement is identified to be -0.0833 Nm. This offset is corrected in all further measurements.

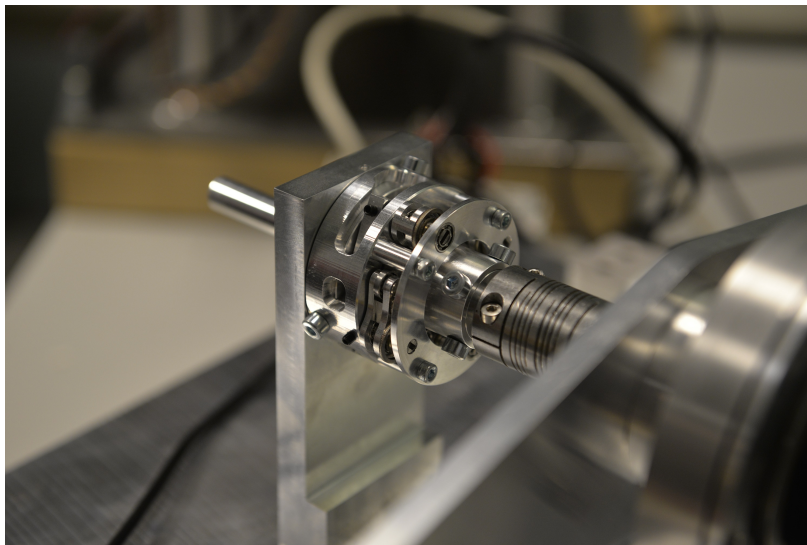


Figure 6.2: Locker in test setup to measure the input torque-angle relationship. In this photo the cam shaft is connected to the motor with a flexible coupling. This configuration is used in experiments 1 and 2.

6.2.2 Experiment 1: Spring characteristics

In this experiment the question that needs to be answered is: Is the stiffness in the springs the same as the modelled stiffness?

Method

The spring characteristics of the springs have to be identified. The locking device has to be put in the measurement setup in the 'input' configuration meaning that the input cam disk is connected to the motor axis. This configuration is depicted in figure 6.2. Only two springs are connected and the other two springs are loose. When the cam shaft is rotated, the force the springs exert on the cam shaft can be felt as a torque on the motor. This torque is measured with the load cells. During a full 360 degree turn the springs are compressed and released

twice. After a full rotation in one direction, the motor must also return in the other direction because in that case the resulting torque-angle relation will show any hysteresis effects in the springs or hysteresis in the form of friction. The torque profile that should ideally be felt on the motor shaft can be generated in matlab and can be used for comparison to the measured reality. Another advantage of using this method is that the cam shape can still be changed if non-linear spring behaviour is identified.

The first thing to be derived is the torque that can be felt in the cam shaft during a full rotation as a result of the springs pressing on the cam shaft. As shown in section 5.3.1, the relation between the follower angle ϕ_1 and the cam angle ϕ_2 in non-singular configurations is chosen as a sine function. This results in a torque on the cam shaft as follows:

$$\begin{aligned}
 b &= (-67) - (-47) \\
 c &= \frac{2\pi}{340} \\
 d &= -47 \\
 \phi_1 &= b \cdot \sin(c \cdot \phi_2) + d \\
 E_{spring,1+2} &= 2 \cdot \frac{1}{2} k \phi_1^2 \\
 T_{non-singular} &= -\frac{\partial E_{spring,1+2}}{\partial \phi_2} \\
 T_{non-singular} &= -2 \cdot b \cdot c \cdot k \cdot \cos(c \cdot \phi_2) \cdot (d + b \cdot \sin(c \cdot \phi_2))
 \end{aligned}$$

Results

The model actuation torque trajectory relationship is depicted in figure 6.4 with the black graph. In this figure the real measurement data are presented as well where again the input torque is presented as a function of the position of the input cam. In order to achieve these graphs, the input cam had to follow a certain trajectory programmed on the motor. This trajectory is depicted in figure 6.3, where the position of the motor is shown as a function of time. This graph is obtained from a real and randomly selected measurement run. Basically the motor makes a full 360 degree turn after which it turns back the full turn to its original position. Every 90 degrees the motor stops in a singular configuration. In the torque-position graph in figure 6.3, it is hard to see what exactly happens in these singular configurations and whether there really is a stable point where the motor does not have to exert any torque to keep the cam shaft in place. Therefore in figure 6.5 the input torque on the cam shaft is depicted as a function of time. Again the same motor position trajectory is followed as depicted in figure 6.3. The figures contain filtered data of several measurement runs. For completeness in figure E.5 in section E.3 of appendix E an individual experiment run is presented with the original non-filtered data.

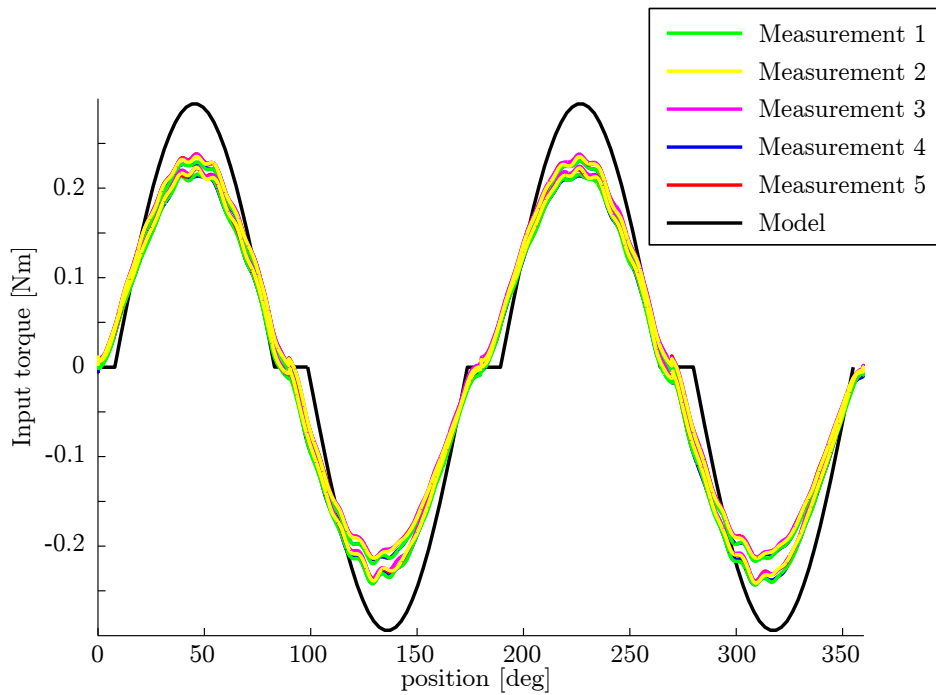


Figure 6.4: Input torque unbalanced system measured against position. Data are filtered with a seventh order lowpass butterworth filter with a cutoff frequency of 5Hz and sample rate of 1000 samples per second. The trajectory of the motor is depicted in figure 6.3 .

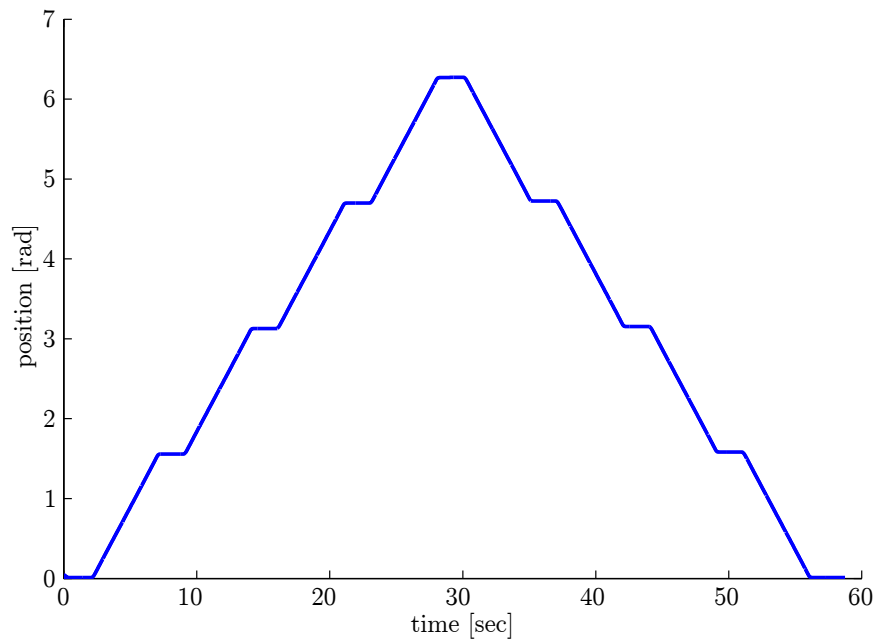


Figure 6.3: Position trajectory of the motor (and the input cam) in time for experiments 2 and 3. This is an actual position trajectory of a random run.

Discussion

When observing figure 6.5 it becomes clear that the singular configurations really work. In positions 0, 90, 180, 270 and 360 of the the input cam shaft there is no actuation force required to maintain that position. Another important observation that must be made is that the the maximum input torque for this experiment is 0.235 Nm. The maximum input torque that was expected from calculations is 0.294 Nm. This leads to the conclusion that the springs have a 20% lower stiffness than expected from the model. The maximum torque the springs produce is therefore corrected to 0.637 Nm per spring instead of the calculated 0.796 Nm. The answer to the experiment question is therefore: The stiffness of the springs is not the same as the modelled stiffness but 20% lower. The shape of the characteristic shows however close similarity.

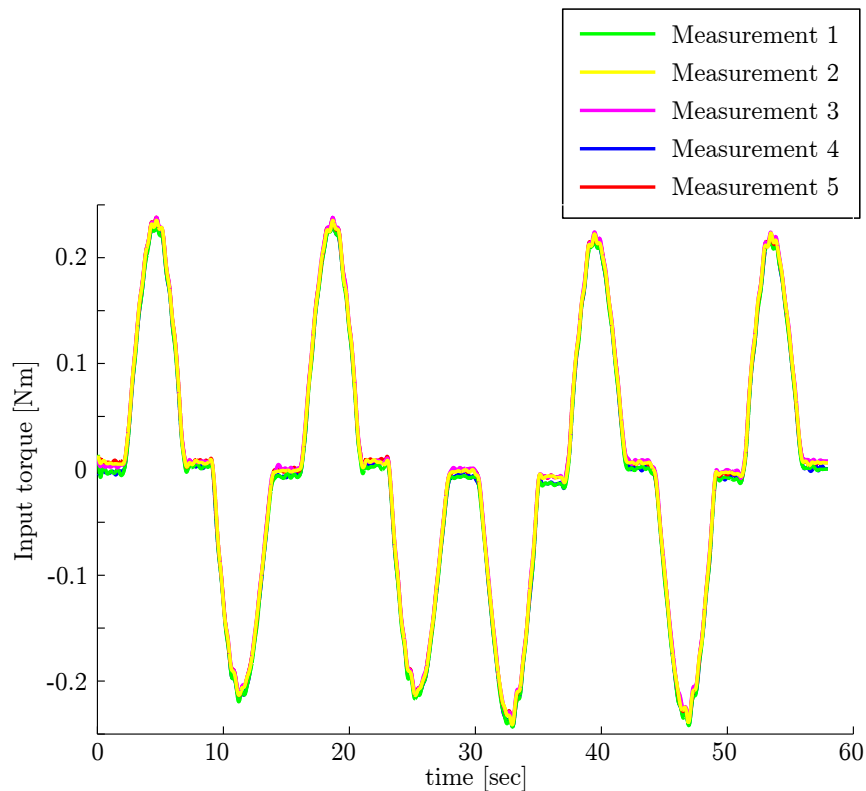


Figure 6.5: Input torque unbalanced system measured over time. Data are filtered with a seventh order lowpass butterworth filter with a cutoff frequency of 5Hz and sample rate of 1000 samples per second. The trajectory of the motor is depicted in figure 6.3 .

6.2.3 Experiment 2: Input torque-angle relationship

In this experiment the question that needs to be answered is: What is the input torque characteristic of the balanced system?

Method

The second experiment to be conducted is the input position measurement against input torque measurement. In experiment 1 only two springs are connected via the cam followers to the cam surface, but in this experiment all four springs are connected to the cam surface via their followers. For this experiment it is very important that all zero-positions are set well, meaning that all surfaces only just make contact when the springs are relaxed. Now the motor must slowly rotate 1 full revolution while measuring the torque required to rotate the input 360 degrees. As an update to this experiment, a stop in all four singular configurations is incorporated. When the input of the locking device is rotated, it is always opposed by a frictional torque. One of the strengths of this type of statically balanced locker is that it has a zero actuation force in the singular configurations. But this absolute zero actuation force is only at stand-still so therefore the motor will stop in all singular configurations to show this phenomena. The result of this experiment is an input angle versus input torque graph. Furthermore, the input torque must be close to zero in non-singular configurations if a static balance was achieved.

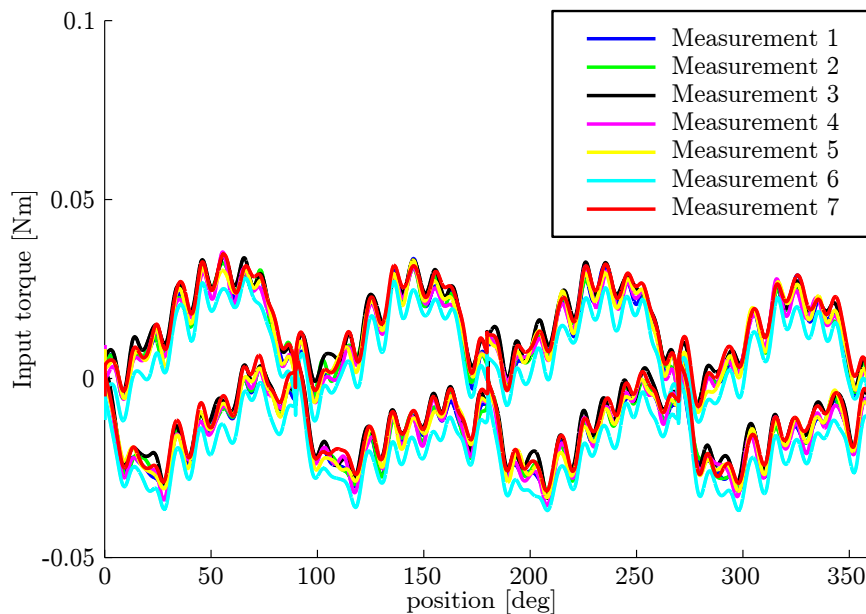


Figure 6.6: Input torque plotted versus the input angle. Data are filtered with a seventh order lowpass butterworth filter with a cut-off frequency of 5Hz and sample rate of 1000 samples per second. The trajectory of the motor is depicted in figure 6.3 .

Results

Theoretically no actuation force should be required to rotate the input cam since it is calculated to be in perfect static balance. However, in that model, hysteresis effects in the springs and friction are not taken into account. To identify the magnitude of these effects the input characteristic of the locking device has been measured. The results of this experiment are presented in figure 6.6. Seven runs of the same experiment were performed to identify differences between runs. Similar to experiment 1 the motor makes a full 360 degree turn after which it turns back the full turn to its original position. This procedure was done to identify hysteresis effects and imperfections in the static balance. For completeness in figure E.6 in section E.3 of appendix E an individual experiment run is presented with the original non-filtered data.

Discussion

From these measurements the conclusion can be drawn that the maximum continuous input torque is indeed 0 Nm in the singular configurations. The maximum input torque required to move from one singular configuration to the next singular configuration is 0.035 Nm when switching between singular configurations in 5 seconds. Another observation that must be made from figure 6.6 is the clearly visible hysteresis. The difference between the (upper) forward rotation graph and the (lower) reverse rotation graph of the input cam appears to be caused by hysteresis. This hysteresis will mainly be caused by the friction of the follower rollers on the cam surface. Another origin for the visible hysteresis is a small amount of hysteresis in the torsion springs. Lastly, the peaks in the graph also represent a slight imbalance in the static balance. This is most likely caused by the 'zero' position of the springs which have to be set accurately in order to obtain a proper static balance.

6.2.4 Experiment 3: Output locking torque characteristic

In this experiment the question that needs to be answered is: What is the locking torque characteristic of the locking device?

Method

The third experiment is set up to determine the locking torque the locking device can generate. In order to conduct this experiment the locking device must be turned around in the setup such that the output of the locking device (the brake disk) is connected to the motor and the load cells. This configuration is depicted in figure 6.1. The motor performs a small radial linear incline of 0.1 rad, it holds that position for two seconds, and moves back to its original position with a radial linear decline of 0.1 rad. With this procedure the braking disk will first start to slip when static friction is overcome in one direction and then the same happens in the other direction. The resulting time against torque graph will reveal the maximum (static) locking torque in both directions as a peak before the locker overcomes static friction and moves into dynamic friction. This experiment can

be executed for different angles of the input cam, which have to be set manually. This should not be a problem as the input is stable in any configuration. This experiment will provide a graph of the input (cam) angle against locking torque (the locking characteristic if you will).

Results

The locking torque characteristic for different angles of the input cam is depicted in figure 6.7. The dots represent the measurement points and the connecting graph is a linear fit merely to show a trend. For completeness in figure E.6 in section E.3 of appendix E an individual experiment run is presented with the original data.

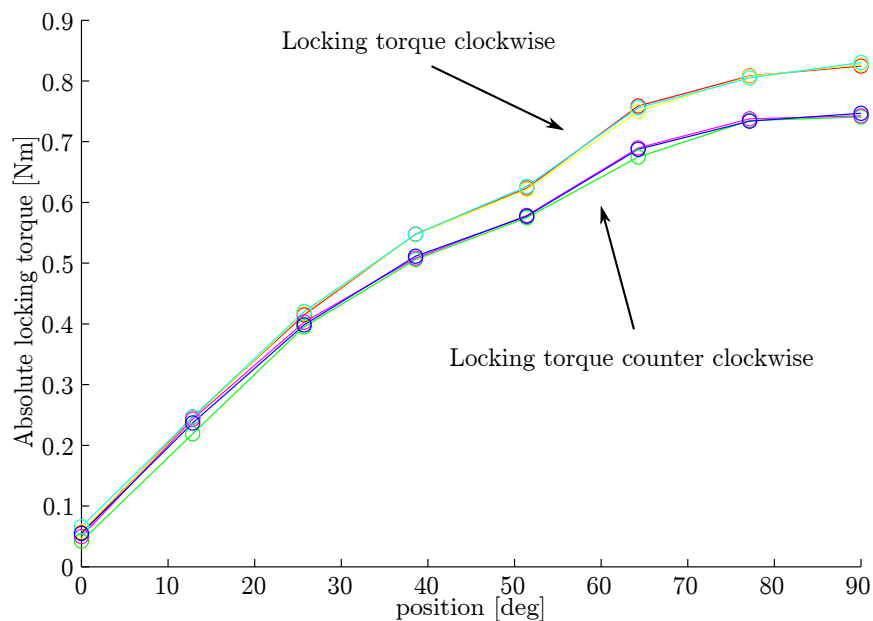


Figure 6.7: Locking torque for various angles of the input disk. Maximum locking torque is 0.83 Nm in clockwise direction and 0.75 in counter clockwise direction. The locking torque shows a sinusoidal relationship with the position of the cam shaft.

Discussion

The maximum locking torque in counter clockwise direction is 0.75 Nm and the maximum locking torque in clockwise direction is 0.83 Nm. Furthermore the locking characteristic shows a sinusoidal graph with respect to the input angle of the cam shaft. One important observation to make is that the locking torque is not equal in both directions. This is most likely caused by a self-engaging effect in the locking device. The reason for this to occur can be explained with figure 6.8 where a self-engaging brake is depicted. As can be seen the friction force vector must exactly point through the axle of the brake arm. In the case

of this locking device, section 5.1 shows that this design was intended correctly. However, the thickness of the braking material added to the braking arms was slightly more than expected. The result is that the braking arm touches the brake disk on a slightly different spot, which results in the idea that the friction force vector does not exactly point through the axle of the braking arm.

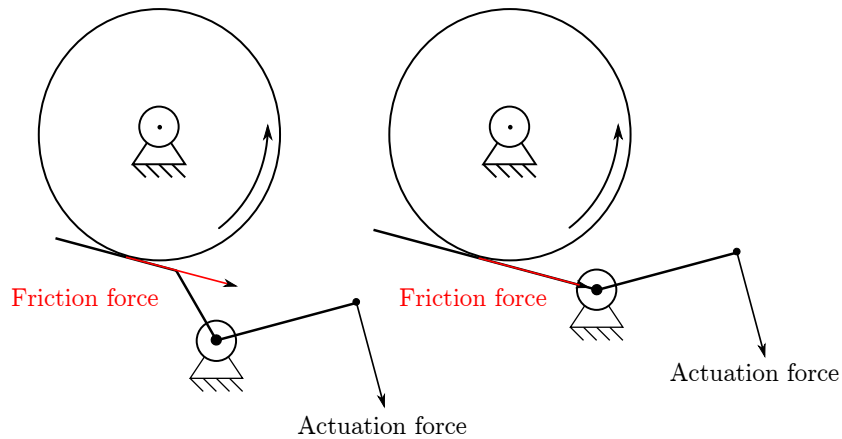


Figure 6.8: A self-engaging locking effect. The friction force vector indicated with the red arrow will cause a moment around the axis of the actuation lever. This phenomena will result in a different locking torque for both rotation directions of the disk.

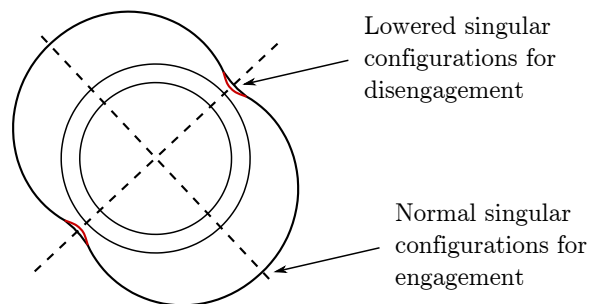


Figure 6.9: A cam shaft that allows for full disengagement of the locker. The four followers of the cam move into the four singular configurations simultaneously. The 'low' singular configurations are the configurations in which the mechanism unlocks and the springs of the follower are relaxed in this position. This means that the radius of the cam can be lowered as depicted in red. The reason not to do this initially is because the 'zero' positions of the mechanism are easier to set for the non-lowered singular configurations.

A second observation to be made is that when the locker is disengaged, it still realizes a small frictional moment. This is most likely caused by the fact that the 'disengaged' singular configuration was set such that the braking surfaces still touch, but the springs connected to the braking arms are unloaded. The reason for this procedure is that it is in this case easier to set the zero positions for the follower arms, since the followers must only just touch the surface. Now that the principle is proven to work and experience is gained in setting the zero positions, the 'disengaged' singular configurations on the input cam can be lowered. This ensures that the braking arms come loose from the friction surface. This adjustment to the cam shaft is depicted in figure 6.9.

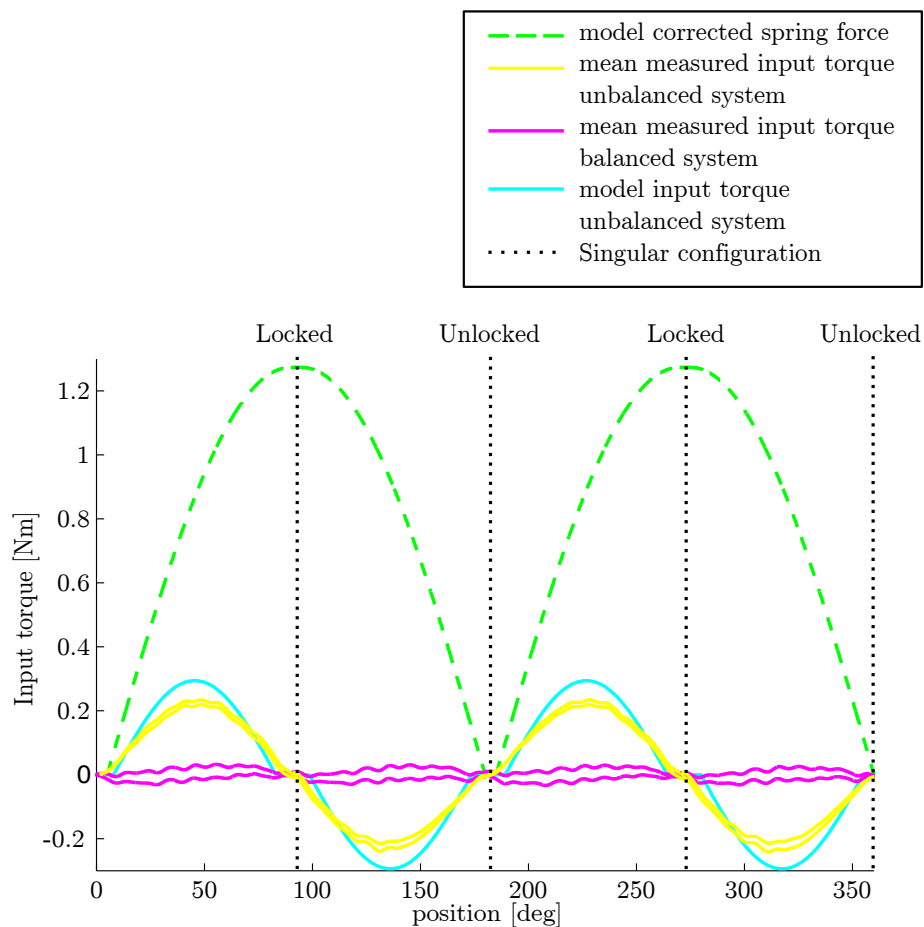


Figure 6.10: Combined overview figure of the input characteristics of the p-brake. The singular configurations are visualized with the black dotted lines, showing where the mechanism is locked and where the mechanism is unlocked. As can be seen from the purple graph the input torque is close to zero and the combined braking spring torque (green, dashed) reaches over 1.27 Nm.

6.3 Conclusion

As a conclusion to this chapter, the results indicate that the locking device has a zero actuation torque in the 'on' and 'off' (singular) configurations and a maximum actuation force of 0.035 Nm when moving at a switching speed of 3 rpm. The maximum locking torque is 0.83 Nm in clockwise direction and 0.75 Nm in counter clockwise direction. Figure 6.10 shows both the actuation torque of the cam shaft and the estimated torque in two torsion springs connected to the brake arms. In the 'on' and 'off' (singular) configurations of the locking device the actuation torque is 0 Nm which is a 100% reduction of the torque in the springs. In the non-singular configurations the maximum actuation torque on the cam shaft is 0.035 Nm which is a 97% reduction of the combined actuation torque in the torsion springs connected to the brake arms. This efficiency was calculated with the pre-defined performance criterion for the SBS-FL mechanisms:

$$\frac{\text{Input torque}_{\max}}{\text{Torque in braking springs}} = \frac{0.035}{2 \cdot 0.637} \left[\frac{Nm}{Nm} \right] = 0.0275 = 2,75\%$$

$$\frac{\text{Input torque}_{\text{cont}}}{\text{Torque in braking springs}} = \frac{0}{2 \cdot 0.637} \left[\frac{Nm}{Nm} \right] = 0 = 0\%$$

The dimensions of the locking device are a diameter of 55 mm and a length of 23 mm. This means that the volume of the locking device is 218576 mm³. This makes the final performance metric for this embodiment:

$$\frac{2,75\%}{218576} \left[\frac{1}{mm^3} \right] = 125,81 m^{-3}$$

Chapter 7

Discussion

In this report statically balanced singular-friction lockers are introduced. A categorization of all mechanism that can be used as a SBS-FL mechanism is presented. From this classification the most compact embodiment is selected. This concept is build and tested on its performance. In this chapter a discussion is provided on the performance, additional functionalities and the applications of SBS-FL mechanisms.

To comment on the performance of SBS-FL mechanisms the performance criteria for a locking device are used as presented in chapter 6. The z-force is the state of the art in statically balanced locking and therefore a comparison is made between the z-force and the p-brake with respect to the criteria from section 4.1. Table 7.1 summarizes the performance of the two statically balanced brakes. To support this table the braking torque, actuation force, size and mass are discussed.

The locking torques of the z-force is 1.08 Nm, and the p-brake has a locking force of 0.75-0.83 Nm. To increase the locking torque of both designs, the radius of the friction disk can be enlarged or stiffer springs can be incorporated. As shown in section 6.2.2 the springs in the p-brake turned out to be less stiff than expected. Incorporating springs that produce the right stiffness only enlarges the design very little. The stiffness increases greatly with only a slightly thicker wire thickness of the torsion springs, but in this prototype they just did not fit.

The maximum actuation force of the z-force is 5.9 N and the maximum actuation torque for the p-brake is 0.035 Nm. To compare the efficiency of the two locking devices, a dimensionless number is proposed for the compensated

Criterion	z-force	p-brake
Locking torque	1.08 Nm	0.75-0.83 Nm
Actuation force/torque	5.9 N (95% efficient)	0.035 Nm (97% efficient)
Bi-directionality	++	+
Size	Ø60x59 mm	Ø55x23 mm
Mass	170 g	92 g

Table 7.1: Performance of the two statically balanced lockers.

spring force or torque. The z-force compensates 95% of the spring force and the p-brake compensates 97% of the spring torque. An advantage for the p-brake is that the continuous actuation force is 0 Nm in the engaged and disengaged configurations. In both designs, the fact that the actuation force is not zero is due to hysteresis and imperfect balancing of the mechanism.

When comparing the size of the z-force to the p-brake, the conclusion must be that the z-force is significantly larger than the p-brake. As presented in chapter 4 the concept selection criteria were focussed on obtaining a very compact locking device. The result is a locking device which is 67% smaller than the z-force (667274 mm³ against 218576 mm³). A possible explanation for this size reduction is the fact that the p-brake has the entire mechanism in one plane, where the z-force is a more out-of-plane design.

The p-brake was made for a robotic application (BIC-PEA) in order to provide the energy saving mechanism with a locking device that does not consume the energy the BIC-PEA is saving. In a broader scope, SBS-FL mechanisms can be used throughout robotics. There are many applications in robotics that require a locking device. A motor can for example be locked to maintain a position instead of the motor consuming energy to achieve the same goal. Other applications include switching between configurations of the robot and robots that carry their own energy supply. Typically in the last category which includes all sorts of mobile and walking robots, the use of a component that does not consume continuous energy is beneficial.

SBS-FL mechanisms can also be used as safety brakes and bi-stable brakes. Since the designer is free to choose the shape of the cam surface or the link parameters, the characteristics can be influenced to the desired behaviour. The singular configurations are stable zones in the mechanism, when those zones are chosen cleverly, the mechanism can exhibit bi-stable behaviour, or safety behaviour. When for example the grounded springs of the p-brake are removed, the mechanism becomes a regular singular-friction locker. By removing the singular configurations the mechanism can function as a safety brake.

Generally the idea presented in this thesis is that locking currently is a force related task, but with the p-brake it almost becomes a pure position related task. This principle can be used in all sorts of fields of use, ranging from trains to bikes to cars. However especially in those applications where only a limited amount of energy is available but still a large locking force in two directions at any moment is required, a SBS-FL mechanism is favourable.

The p-brake was originally intended as a locking mechanism. The friction interface with rubber and Vulca SF-001 might not be very wear-resistant. When the thickness of either of the friction materials becomes smaller, the static balance is influenced negatively. However, the principle should also work in a brake when a friction material is found with low wear rates. When such a material turns out to be unavailable, another option to solve the wear of friction material is to incorporate a self adjusting mechanism. Such mechanisms are for example used in mountain bike oil braking systems, where the loss of oil due to use of the system has to be compensated.

Chapter 8

Conclusion

The research questions of this thesis were: 'What classes of statically balanced singular-friction lockers exist, which of these classes contains the most compact statically balanced singular-friction locking device and what is the performance of this most compact locking device?' The answer to the first of these three questions is that there are nine types of rigid body statically balanced singular-friction lockers, consisting of one linkage type class of lockers and eight cam type classes of lockers. Secondly the the most compact statically balanced singular-friction locking device is a locking mechanism with a rotational cam input and rotational followers connected to torsion springs. Thirdly the locking device has a zero actuation torque in the 'on' and 'off' (singular) configurations and a maximum actuation torque of 0.035 Nm when switching 'on' and 'off' in 5 seconds. This is a 97% reduction of the torque in the springs connected to the brake arms. The maximum locking torque is 0.83 Nm in clockwise direction and 0.75 Nm in counter clockwise direction. The locking device has a diameter of 55 mm and a length of 23 mm. This efficient and small cam based prototype seems to be the most promising approach to statically balanced locking and can find its use not only in robotics but also for example in cars, trucks, bikes and trains.

Appendices

Appendix A

Paper Statically balanced brakes

Statically Balanced Brakes

Michiel Plooij, Tom van der Hoeven, Gerard Dunning and Martijn Wisse
Delft University of Technology

Abstract—The problem with conventional brakes is that they require a powerful actuator, leading to large, heavy and in most cases energy consuming brakes. This paper introduces a fundamentally different brake concept called statically balanced brakes* (SBBs). SBBs do not require any actuation force to maintain a braking torque and only have to move a small mass to vary that torque. Therefore, their energy consumption is potentially very low. In an SBB, one of the two friction surfaces is connected through springs to a braking block. This braking block is connected through a mechanism to a second set of springs, of which the other side connects to the ground. The total energy in the two sets of springs is constant, which results in a zero-force characteristic at the braking block. The position of this statically balanced braking block determines the displacement of the first set of springs and thus the normal force between the friction surfaces. We categorize mechanisms that can be used in SBBs and show two embodiments: one with leaf springs with a negative stiffness range and one with torsional springs and a non-linear cam mechanism. Results show that the actuation force can be reduced with approximately 95-97% in comparison to regular brakes. This shows that in SBBs, the actuation force can be almost eliminated.

I. INTRODUCTION

Conventional brakes require a powerful actuator that generates a normal force between two friction surfaces [1, 2]. The amplitude of the normal force, the friction coefficient and the geometry of the brake together determine the braking torque. There are applications in which powerful actuators are undesired due to size and weight limitations or their (potentially high) energy consumption. Therefore, researchers have worked on designing brakes that require less actuation force.

Research on the reduction of the required actuation force can be split into three categories. Firstly, self-engaging brakes have been developed that use the relative motion between the friction surfaces to pull the friction surfaces together and thereby reducing the required actuation force [3–6]. Disadvantages of such brakes are that they only work in one braking direction and that they can only disengage in the opposite direction of engagement. Secondly, spring brakes (also called safety brakes or parking brakes) use a spring to keep the brake engaged without actuation force [2, 7–9]. However, these brakes still require an actuation force to keep the brake disengaged. This is solved in the third category: bi-stable brakes [10, 11]. Such brakes have a bi-stable element (e.g. a bi-stable spring), providing the brake with two stable states: the engaged state and the disengaged state. However, switching between these two states still requires a high actuation force.

*Patent pending

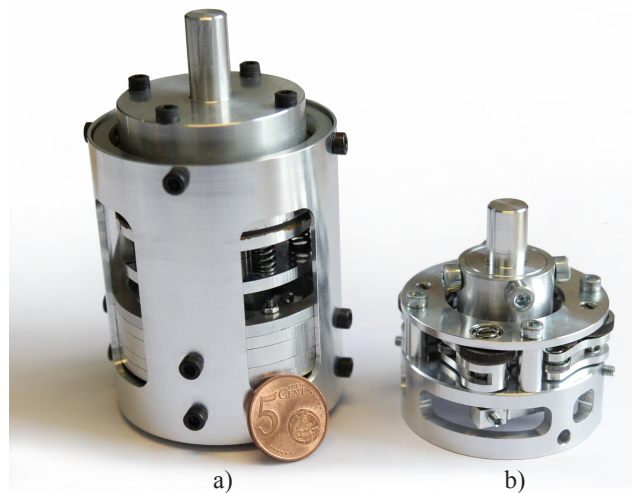


Figure 1. A picture of the two prototypes of statically balanced brakes. a) A prototype with leaf springs with a negative stiffness range. b) A prototype with torsion springs and a rotational cam mechanism.

Other researchers focused on implementing actuators with a high force density and a low energy consumption. The best example of this is piezo-actuated brakes [12–16]. Because of their high force density and low energy consumption, they are potentially very effective in solving the issues mentioned above. However, they require high voltages (that might not be available), very precise manufacturing (since they have a very small stroke) and are expensive. Furthermore, the brake construction has to be very stiff, otherwise the construction will deform, which reduces the effectiveness of piezo actuators.

The problem with the state of the art brakes is that the actuator has to be able to generate a force equal to the normal force between the friction plates. The goal of this paper is to introduce a brake concept in which the normal force and the actuation force are decoupled.

This new brake concept is fundamentally different from current brake concepts and is called statically balanced brakes (SBBs, see Fig. 1). SBBs do not require an actuation force to hold a certain braking torque and only require a small actuation force to vary that torque. Furthermore, with small adjustments, SBBs can be changed to incorporate any of the three different functionalities mentioned above (i.e. regular-, spring- and bi-stable behavior), while still only requiring a small actuation force. In a statically balanced mechanism, every position is an equilibrium position [17]. Such mechanisms have also been used amongst others for intrinsically

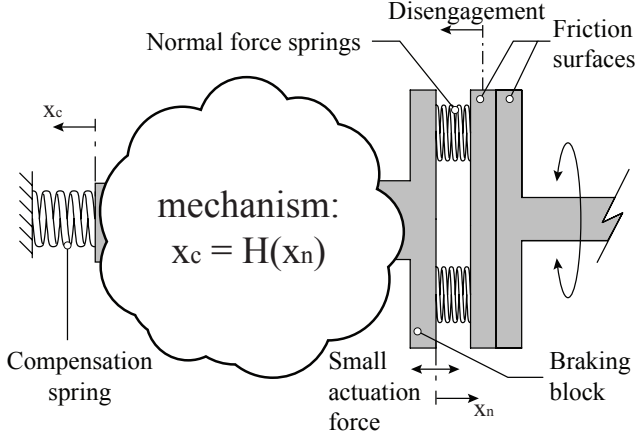


Figure 2. A schematic drawing of a statically balanced brake. The right friction surface is connected to a joint that has to be braked. The left friction surface is connected through the normal force springs with the braking block. A mechanism connects the braking block with the compensation springs and the other side of the compensation springs connects to the ground. The position of the braking block determines the normal force between the friction surfaces.

safe robotic arms [18, 19], exoskeletons [20], prostheses [21] and micro and precision mechanisms [22, 23].

The rest of this paper is structured as follows. First, section II explains the concept of SBBs in more detail. Then, section III categorizes all possible embodiments of SBBs that are relatively simple and therefore small and lightweight. Sections IV and V then show two prototypes of SBBs and their performance. Finally, the paper ends with a discussion in section VI and a conclusion in section VII.

II. THE CONCEPT OF STATICALLY BALANCED BRAKES

In this section we explain the concept of SBBs in more detail. First, we give a general formulation without assuming linear springs. Then, we work out the equations for a system with linear springs. Fig. 2 shows a schematic drawing of the concept of a SBB. The brake is engaged by pushing the two friction surfaces against each other. The friction between the surfaces is assumed to be a Coulomb type friction:

$$|F_f|_{max} = \mu F_n \quad (1)$$

where μ is the Coulomb friction coefficient, $|F_f|_{max}$ is the maximum absolute friction force before the surfaces start to slip and F_n is the normal force. The brake in Fig. 2 is statically balanced by two groups of springs. One group of springs is placed between the braking block and the left friction surface. The energy in this group of springs is equal to $E_n(x_n)$, with x_n being the displacement of the springs as shown in Fig. 2. The force in these springs is equal to the normal force between the friction surfaces:

$$F_n = \frac{\partial E_n}{\partial x_n} \quad (2)$$

Multiplying this friction force by the effective radius r of the brake, gives the braking torque:

$$|T|_{max} = \mu \frac{\partial E_n(x_n)}{\partial x_n} r \quad (3)$$

This means that the position of the braking block determines the amplitude of the braking torque. Now if this were the only group of springs, an actuator would still have to generate the force F_n to hold the braking block in a certain position. In order to decouple this normal force from the actuation force, a second spring system is used: the compensation springs. The compensation springs are placed between the ground and a mechanism that also connects to the braking block. This mechanism is depicted in Fig. 2 as a cloud with the mechanism equation $x_c = H(x_n)$. This equation assumes that the overall system has one degree of freedom (DOF). In section III, we will zoom in on this part and discuss possible mechanisms. Here we will analyse the static balance of mechanisms from an energy perspective. The energy in the group of compensation springs is $E_c(x_c)$ with x_c being the displacement of the springs as shown in Fig. 2. Now the system is statically balanced when $E = E_n + E_c$ is constant for all positions of the system. The transfer ratio from the normal force springs to the compensation springs at position x_n is equal to:

$$h(x_n) = \frac{\partial H(x_n)}{\partial x_n} = \frac{\partial x_c}{\partial x_n} \quad (4)$$

We can now write the condition for static balance as

$$\frac{\partial E}{\partial x_n} = 0 \quad (5)$$

$$\frac{\partial E_n(x_n)}{\partial x_n} + \frac{\partial E_c(x_c)}{\partial x_c} h(x_n) = 0 \quad (6)$$

Now given the two spring characteristics, this system is statically balanced for all x_n for which it holds that

$$h(x_n) = -\frac{\partial x_c}{\partial E_c(x_c)} \frac{\partial E_n(x_n)}{\partial x_n} \quad (7)$$

The force that the compensation spring applies on the braking block can be expressed as:

$$F_c = \frac{\partial E_c}{\partial x_n} = \frac{\partial E_c(x_c)}{\partial x_c} h(x_n) = -\frac{\partial E_n(x_n)}{\partial x_n} = -F_n \quad (8)$$

It is logical that $F_c = -F_n$ because this results in force equilibrium, which is another way to consider static balancing. Now assume that both the normal force springs and the compensation springs are linear:

$$E_n = \frac{1}{2} k_n \max(x_n, 0)^2 \quad (9)$$

$$E_c = \frac{1}{2} k_c x_c^2 \quad (10)$$

Where k_n and k_c are spring stiffnesses and the max operator returns the maximum value of the two inputs and models the disengagement of the friction surfaces. Eq. (7) now becomes:

$$h(x_n) = -\frac{k_n \max(x_n, 0)}{k_c x_c} \quad (11)$$

From Eq. (11) it follows that $h(x_n \leq 0) = 0$. This means that the mechanism H is in a singular position or that the mechanism contains a clutch that decouples the two motions.

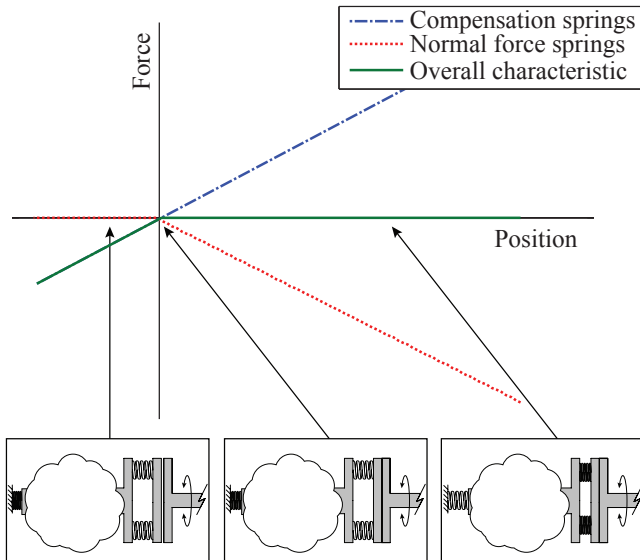


Figure 3. The working principle of a statically balanced brake. The compensation springs have a negative stiffness when measured at the braking block and the normal force springs have a positive stiffness. Since the stiffnesses cancel out and the equilibrium positions coincide, the overall characteristic has a range of zero force, which is the actuation stroke. A small actuator can position the brake at any position in this range, controlling the normal force and thus the braking torque.

From Eqs. (9) and (10) it follows that for linear springs, the mechanism should satisfy

$$x_c = \sqrt{\frac{2E - k_n x_n^2}{k_c}} \quad (12)$$

$$h(x_n) = -\frac{k_n}{k_c} \frac{x_n}{\sqrt{\frac{2E - k_n x_n^2}{k_c}}} \quad (13)$$

Fig. 3 shows a schematic explanation of the forces in such a mechanism as function of the position of the braking block. This figure shows that the overall characteristic is equal to zero for $x_n \geq 0$, while the normal force at those positions depends linearly on the position. This means that the actuator does not have to apply any force to maintain a certain normal force between the friction surfaces. Note that in this example, $h(x_n < 0) \neq 0$, meaning that the system is not statically balanced for $x_n < 0$.

The concept of SBBs depends on a decoupling of the normal force between two friction surfaces and the force required to engage or disengage the brake. Without the static balancing, the actuator that moves the braking block would also have to deliver the force that pushes the friction surfaces together. With the static balancing, the braking block can be moved by an actuator that does not have to counteract any spring force (Eq. (8)). This controlled position determines the braking torque (Eq. (3)).

III. POSSIBLE EMBODIMENTS

The previous section presented requirements on mechanisms for SBBs. This section categorizes possible embodiments of SBBs and focuses on possible mechanisms. In gen-

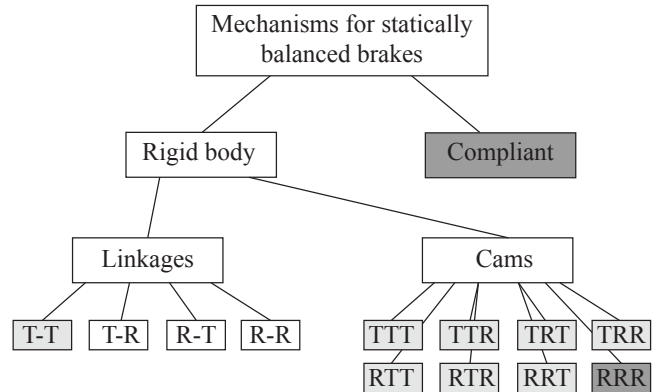


Figure 4. A visualization of the categorization of mechanisms for statically balanced brakes. A first division is made between rigid body mechanisms and compliant mechanisms. Rigid body mechanisms are split into linkages and cam mechanisms. Linkages are categorized based on the nature of their input and output (rotational or translational). Three linkage mechanisms cannot be statically balanced. Cam mechanisms are categorized on the nature of their input, output and cam movement (rotational or translational). In the grey categories it is possible to obtain perfect static balance. From the dark-grey categories we show a prototype in this paper.

eral, mechanisms can be divided into rigid mechanisms and compliant mechanisms. Rigid body mechanisms on their turn can be split into linkage mechanisms and cam mechanisms. The overall categorization of mechanisms is shown in Fig. 4. This section first discusses rigid body mechanisms and then compliant mechanisms.

A. Rigid body mechanisms for SBBs

Rigid mechanisms are mechanisms in which all the parts of the mechanism are rigid except for the springs that are either translational or rotational. Here we assume that the springs are linear and therefore the transfer function of the mechanism $h(x_n)$ must be non-linear (see Eq. (13)).

In order to categorize both one DOF linkage and cam mechanisms further, we have to realize that the mechanism should at least possess one singular position (see Eq. (11)). Therefore, we categorize both linkage and cam mechanisms further by categorizing singular mechanisms. There exists already literature on singular mechanisms and how to categorize them [24–26]. Here we introduce a categorization that only incorporates simple singular mechanisms, leading to small and lightweight designs. Our categorization of singular mechanisms is based on the notion that all one DOF singular mechanisms have one input motion and one output motion. In simple singular mechanisms, these input and output motions are either translational or rotational motions. In linkages this leads to four categories:

1. translational input - translational output
2. translational input - rotational output
3. rotational input - translational output
4. rotational input - rotational output

In cam mechanisms, the cam itself can also be translational or rotational, leading to eight categories.

B. Linkages

This section analyzes linkage mechanisms for SBBs. All mechanisms use the same notation. x_n and x_c denote the displacements of the springs and can be rotational or translational. When multiple compensation springs are used, they are denoted by x_{c1} and x_{c2} . x_i and x_o denote the position of the input and output translations or rotations. l and θ refer to a constant distance and angle respectively. k_n and k_c denote the stiffnesses of the normal force springs and compensation springs. And finally d and γ refer to distances and angles that change when the position of the mechanism changes.

The four categories of mechanisms will be discussed below. Before discussing them, it should be noted that the placement of translational normal force springs becomes impractical when they are both rotating and translating; see for example the left spring in Fig. 5a. Therefore, translational normal force springs can only connect to a slider that is in line with the spring. This also ensures that at a certain position, the force in the normal force springs becomes zero.

1) *Translational input - translational output*: A generalized version of this mechanism is shown in Fig. 5a. It consists of two sliders that intersect in O . θ_3 denotes the angle between the two sliders and x_i and x_o denote the positions of the sliders measured from O . The link between the two sliders has length l_3 and each slider connects to a spring. The other sides of the springs are connected to the ground at distances l_1 and l_2 from O under angles of θ_1 and θ_2 . The elongations of the springs are denoted by x_n and x_c and the stiffnesses are k_n and k_c . Since the left spring should be in line with the left slider, it is given that $\theta_1 = 0$. The energy in the system can be obtained by applying cosine rules:

$$\begin{aligned} x_n^2 &= l_1^2 + x_i^2 - 2l_1x_i \\ x_c^2 &= l_2^2 + x_o^2 - 2l_2x_o \cos(\theta_2) \\ l_3^2 &= x_i^2 + x_o^2 - 2x_ix_o \cos(\theta_3) \end{aligned} \quad (14)$$

$$\begin{aligned} E &= \frac{1}{2}k_nx_n^2 + \frac{1}{2}k_cx_c^2 \\ E &= C_1 + \frac{1}{2}(k_n - 1)x_i^2 + \frac{1}{2}(k_c - 1)x_o^2 \\ &\quad + x_ix_o \cos(\theta_3) - k_nl_1x_i - k_cl_2x_o \cos(\theta_2) \end{aligned} \quad (15)$$

Where C_1 is the constant term:

$$C_1 = l_3^2 + \frac{1}{2}k_nl_1^2 + \frac{1}{2}k_cl_2^2 \quad (16)$$

We can derive x_o as function of x_i from Eq. (14) and fill it into Eq. (15). Now for static balance, Eq. (5) should hold for all x_i , which is only true when $\theta_2 = \theta_3 = 0.5\pi$, $l_1 = 0$ and $k_n = k_c$. Such a mechanism is depicted in Fig. 5d, where the ground can be moved freely along the dashed line. The normal force tension spring is changed into a compression spring in this example and is connected to friction plates. This mechanism is already a well known statically balanced mechanism [17].

2) *Translational input - rotational output*: A generalized version of this mechanism is shown in Fig. 5b. It consists of one slider with a zero position $x_i = 0$ at O and a

crank mechanism with links of lengths l_1 and l_2 . One spring is placed between the slider and the ground and the other two are placed between the crank and the ground. The translational compensation spring connects to bar 1 of the crank at distance l_6 from the ground. Since the left spring should be in line with the left slider, it is given that $\theta = 0$. The energy in this system can be derived as follows. First, we define d_2 as the distance between the joint that connects the the two bars of the crank and the line d_1 :

$$\begin{aligned} d_2 &= l_1 \cos(\gamma) \\ d_1 &= \sqrt{l_1^2 - d_2^2} + \sqrt{l_2^2 - d_2^2} \\ x_i &= \sqrt{d_1^2 - l_4^2} \\ x_{c2} &= \sqrt{l_5^2 + l_6^2 - 2l_5l_6 \cos(x_o)} \\ x_n &= (x_i - l_3) \\ E &= \frac{1}{2}k_nx_n^2 + \frac{1}{2}k_{c1}(x_{c1} - x_{c1,0})^2 + \frac{1}{2}k_{c2}x_{c2}^2 \end{aligned} \quad (17)$$

where $x_{c1,0}$ is the equilibrium position of the rotational spring. Again for static balance, Eq. (5) should hold for all x_i , which is only the case when $k_n = k_{c1} = k_{c2} = 0$. Since the stiffnesses should be larger than zero, it is impossible to use this mechanism for a perfectly statically balanced brake. The use of imperfectly statically balanced mechanisms will be discussed in section VI-C.

3) *Rotational input - translational output*: This system is the same as the system with translational input and rotational output in Fig. 5b, with the difference that the input and output are switched. Now, since the right spring is rotating and is therefore impractical as a normal force spring, it is given that $k_{c2} = 0$. The energy in the system can now be calculated by:

$$\begin{aligned} x_i &= \sqrt{d_1^2 - l_4^2} \\ x_c &= \sqrt{l_5^2 + l_6^2 - 2l_5l_6 \cos(x_c)} \\ x_n^2 &= l_3^2 + x_i^2 - 2l_3x_i \cos(\theta) \\ E &= \frac{1}{2}k_nx_n^2 + \frac{1}{2}k_{c1}(x_{c1} - x_{c1,0})^2 \end{aligned} \quad (18)$$

Since it is impossible to satisfy Eq. (5) with non-zero stiffnesses, it is impossible to perfectly statically balance this system.

4) *Rotational input - rotational output*: A generalized version of this mechanism is shown in Fig. 5c. The input and output links and the link in between form a four bar mechanism with lengths l_1, l_2, l_3 and l_4 . One rotational spring is placed between link 1 and the ground. The rotational second spring is placed between link 2 and the ground. And a translational compensation spring connects to link 2 at a distance l_5 from the ground. The energy can again be calculated by applying the cosine rule:

$$\begin{aligned} x_{c2}^2 &= l_5^2 + l_6^2 - 2l_5l_6 \cos(x_o - \theta_2) \\ E &= \frac{1}{2}k_n(x_n - x_{n,0})^2 + \frac{1}{2}k_{c1}(x_{c1} - x_{c1,0})^2 + \frac{1}{2}k_{c2}x_{c2}^2 \end{aligned} \quad (19)$$

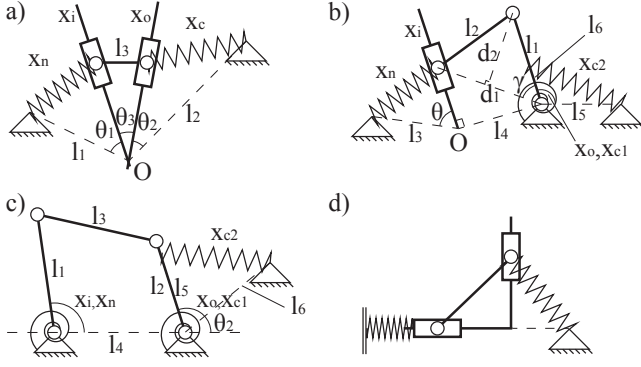


Figure 5. The collection of possible simple singular linkage mechanisms. a) A mechanism with translational input and output. This mechanism can be statically balanced. b) A mechanism with translational input and rotational output. c) A mechanism with rotational input and output. d) A statically balanced version of a.

Again, such a mechanism cannot be perfectly statically balanced.

This leads to the conclusion that the only feasible simple linkage mechanism for SBBs is the one depicted in Fig. 5d.

C. Cams

In this section we analyze possible cam mechanisms for SBBs. Figs. 6a-d show small and lightweight cam mechanisms which function as building blocks for SBBs. Eight categories can be constructed from these building blocks, based on the input, output and cam motions. Fig. 6e shows one of the eight classes with a rotational cam, a rotational storage spring and a rotational normal force spring. All eight categories are feasible, although some have clear advantages or disadvantages. Here we discuss the components of such mechanisms, which can be split into:

1. A translational spring on a translational slider (Fig. 6b)
2. A rotational spring on a translational slider (Fig. 6d)
3. A translational spring on a rotational slider (Fig. 6a)
4. A rotational spring on a rotational slider (Fig. 6c)

In the analysis, we make three assumptions for simplicity. Firstly, we assume that the rollers on the cam have a radius of zero. How the analysis changes with a non-zero radius is described in [27]. Secondly, we assume that the grounds at which the springs are connected are in line horizontally with the center of the rotational cam (see Figs. 6a and 6c). Grounds that are not in line are also possible and would add an offset to the equations. Thirdly, we assume that the translational springs are placed horizontally. Translational springs under an angle are also possible, but would make the analysis unnecessarily complicated.

The notation that is used is as follows. The lengths of the springs are denoted by x_n for the normal force springs and x_c for the compensation springs. $x_{n,0}$ and $x_{c,0}$ denote the equilibrium positions of the springs, meaning that the displacements of the springs are $x_n - x_{n,0}$ and $x_c - x_{c,0}$. x_{cam} denotes the position of the cam, which is translational or rotational. The surface of the cam is obtained in the body fixed workspace coordinates y_1 and y_2 . l_1 and l_3 denote the

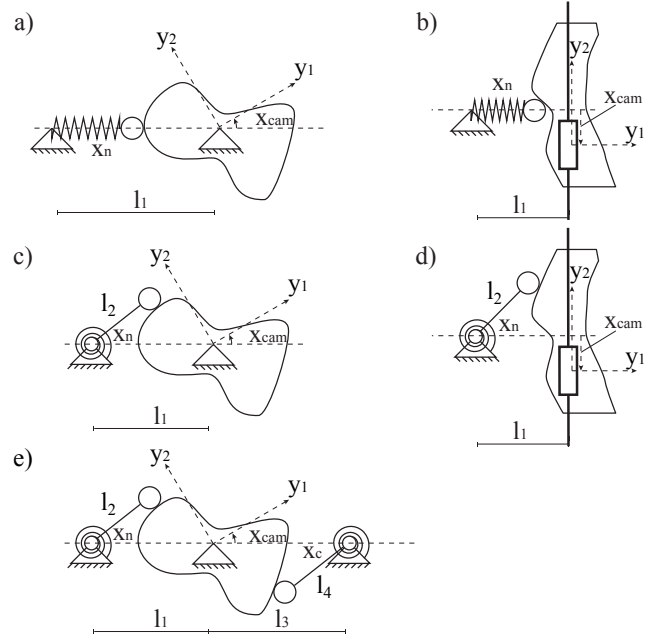


Figure 6. The collection of possible simple cam mechanisms which can be combined to form to SBBs. The mechanisms have rotational or translational inputs, outputs and cams. Combining two simple cam mechanisms to obtain a SBB leads to eight categories: a-a, a-c, c-a, c-c, b-b, b-d, d-b and d-d. e) shows a SBB of configuration c-c.

distances between the two grounds and the center of the cam. And finally, l_2 and l_4 denote the length of the links connected to the rotational springs (when present).

In statically balanced cam mechanisms, the cam determines the relationship $x_c = H(x_n)$. Now, x_n can be chosen freely as function of the position of the cam. Then, by filling in Eq. (12), we obtain:

$$x_c(x_{cam}) = \sqrt{\frac{2E - k_n(x_n(x_{cam}) - x_{n,0})^2}{k_c}} + x_{c,0} \quad (20)$$

Using Eq. (20), a trajectory for $x_c(x_{cam})$ can be found as function of the trajectory $x_n(x_{cam})$. When $x_n(x_{cam})$ and $x_c(x_{cam})$ are known, the cam surface can be obtained in the body fixed workspace coordinates y_1 and y_2 . We will now present the equations to obtaining a cam surface with the desired follower behaviour for the four building blocks in Fig. 6.

1) *Translational spring - translational cam*: An example of such a submechanism is shown in Fig. 6b. The shape of the cam surface for the normal force springs in the workspace coordinates y_1 and y_2 can now be obtained with:

$$\begin{bmatrix} y_1 \\ y_2 \end{bmatrix} = \begin{bmatrix} x_n(x_{cam}) - l_1 \\ x_{cam} \end{bmatrix} \quad (21)$$

This defines the cam surface for the side with the normal force springs. The side with the compensation springs works the same.

2) *Rotational spring - translational cam*: An example of such a submechanism is shown in Fig. 6d. The cam shape

can be obtained with:

$$\begin{bmatrix} y_1 \\ y_2 \end{bmatrix} = \begin{bmatrix} l_2 \cos(x_n(x_{cam})) - l_1 \\ l_2 \sin(x_n(x_{cam})) + x_{cam} \end{bmatrix} \quad (22)$$

3) *Translational spring - rotational cam*: An example of such a submechanism is shown in Fig. 6a. The cam shape can be obtained with:

$$\begin{bmatrix} y_1 \\ y_2 \end{bmatrix} = \begin{bmatrix} (x_n(x_{cam}) - l_1) \cos(x_{cam}) \\ (x_n(x_{cam}) - l_1) \sin(x_{cam}) \end{bmatrix} \quad (23)$$

4) *Rotational spring - rotational cam*: An example of such a submechanism is shown in Fig. 6c. The cam shape can be obtained with:

$$\begin{bmatrix} y_1 \\ y_2 \end{bmatrix} = R(x_{cam}) \cdot \begin{bmatrix} l_2 \cos(x_n(x_{cam})) - l_1 \\ l_2 \sin(x_n(x_{cam})) - l_1 \end{bmatrix} \quad (24)$$

where $R(x_{cam})$ denotes the rotation matrix for a rotation of x_{cam} .

D. Example: RRR

This mechanism is shown in Fig. 6e. For the analysis we must first choose spring displacement function, the stiffnesses and the equilibrium positions:

$$x_n(x_{cam}) = \sin(x_{cam}) \quad (25)$$

$$k_n = k_c = k \quad (26)$$

$$x_{n,0} = l_1 = x_{c,0}, l_3 \quad (27)$$

From Eq. (20) it follows that

$$x_c(x_{cam}) = \cos(x_{cam}) \quad (28)$$

The cam trajectory for both springs is obtained by filling in Eq. (24):

$$\begin{bmatrix} y_{1,n} \\ y_{2,n} \end{bmatrix} = R(x_{cam}) \cdot \begin{bmatrix} l_2 \cos(\sin(x_{cam})) - l_1 \\ l_2 \sin(\sin(x_{cam})) - l_1 \end{bmatrix} \quad (29)$$

$$\begin{bmatrix} y_{1,c} \\ y_{2,c} \end{bmatrix} = R(x_{cam}) \cdot \begin{bmatrix} l_4 \cos(\cos(x_{cam})) - l_3 \\ l_4 \sin(\cos(x_{cam})) - l_3 \end{bmatrix} \quad (30)$$

There are two options to create this cam surface. Firstly the cam can be split in two halves where one half connects to the normal force spring and the other half connects to the compensation spring. Secondly the position of the compensation spring can be altered and placed vertically in Fig. 6e. By doing so a 0.5π phase shift is obtained in x_{cam} for the compensation spring trajectory. Since $\sin(x_{cam}) = \cos(x_{cam} - 0.5\pi)$, the same cam surface can be used as for both the normal force spring and the compensation spring. Therefore, the cam is statically balanced for the complete rotation. This last option is implemented in the embodiment that will be explained in section V.

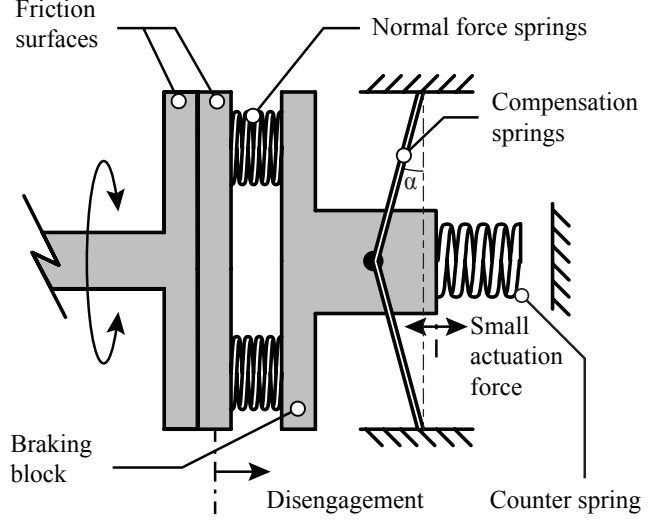


Figure 7. A schematic drawing of the statically balanced brake with leaf springs. The left friction surface is connected to a joint that has to be braked. The right friction surface is connected through the normal force springs with the braking block. The braking block is connected to the ground through leaf springs with a negative stiffness range and through the counter springs that engage when the friction surfaces disengage.

E. Compliant mechanisms for SBBs

Instead of having rotational or translational springs and a rigid body mechanism in between, compliant mechanisms could be used. Applying compliant mechanisms varies from using springs with a negative stiffness range to making the whole mechanism out of one part. Compliant mechanisms are harder to categorize than the rigid body mechanisms earlier in this section. Moreover, such a categorization will never give a complete list of all possible small and lightweight compliant mechanisms in SBBs.

In their handbook of compliant mechanisms, Howell et al. [28] categorized compliant mechanisms in two ways: based on the used components and based on their application. Here, we only indicate that there is a difference between SBBs with one compliant mechanism that fulfills the function of both the normal force springs and the compensation springs in Fig. 2 and SBBs with a spring with a negative stiffness range that is used in a configuration with two spring systems. The latter option will be exploited in the embodiment in section IV. Two common types of springs that are known to exhibit the capacity to have a negative stiffness range are leaf springs [29] and disk springs (also called Belleville springs) [30].

IV. EXAMPLE 1: COMPLIANT MECHANISM: BI-STABLE LEAF SPRINGS

This section shows our prototype of the concept with compression springs as normal force springs and leaf springs with a negative stiffness range as compensation springs (see Fig. 7). This concept also has a third group of springs, called the counter springs, to compensate for the non-linear behavior due to disengagement of the friction surfaces in Eq. (9).

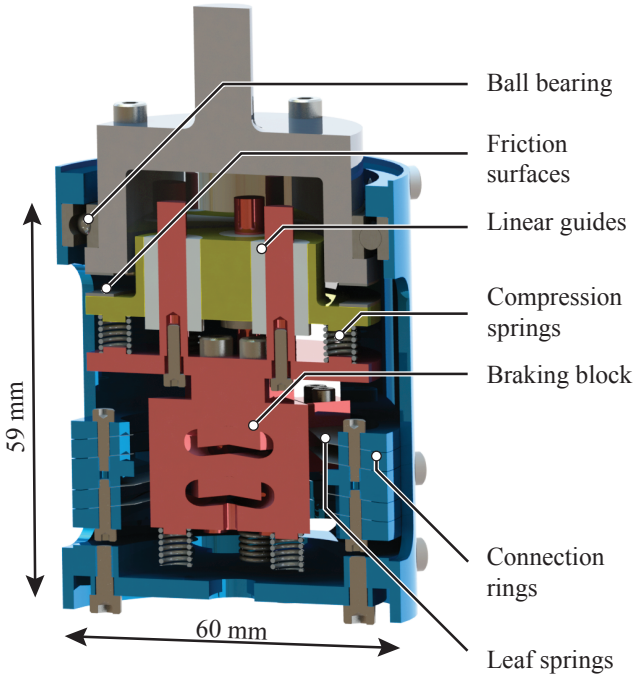


Figure 8. A section view of the embodiment with leaf springs. The leaf springs are arranged in eight pairs of two. One side of the leaf springs is connected to the braking block, the other side is connected to the housing through a set of connection rings. The braking block is connected to the bottom friction surface by seven compression springs with a total stiffness of 66.8 N/mm. Four axes that are connected to the braking block are connected to the bottom friction surface through linear ball bearings. These linear guides prevent a torsional load on the normal force springs. At the bottom of the braking block, there is a group of compression springs with a total stiffness of 54.0 N/mm. The top friction surface is connected to the joint that has to be braked, which is connected to the housing by a ball bearing.

A. Static balancing

The energy in the normal force springs is given by Eq. (9). The leaf springs with a negative stiffness range are the compensation springs in this embodiment. In the range with negative stiffness, their energy can be approximated by

$$E_c = \frac{1}{2}k_c x_c^2 + E_0 \quad (31)$$

where k_c is negative and E_0 is a constant. The third group of springs in this embodiment (i.e. the counter springs) engage when the normal force springs disengage. The energy in this spring system is equal to

$$E_{ctr} = \frac{1}{2}k_{ctr} \min(x_{ctr}, 0)^2 \quad (32)$$

where the min operator returns the lowest value of the two inputs. Now if $k_n = k_{ctr} = -k_c$ and $x_n = x_c = x_{ctr}$, the total energy in the system is constant:

$$E = E_n + E_c + E_{ctr} = E_0 \quad (33)$$

B. Detailed design

Fig. 8 shows a section view CAD drawing of this embodiment. The amount of positive stiffness of the two groups of

Table I
THE PARAMETERS OF THE SEVEN CASES

Case	l (mm)	t (mm)	α (deg)	u (mm)
Case 1	10.0	0.10	10.0	0.0
Case 2	10.2	0.10	10.0	0.0
Case 3	10.0	0.11	10.0	0.0
Case 4	10.0	0.10	10.5	0.0
Case 5	10.0	0.10	10.0	0.2
Case 6	10.2	0.09	9.5	-0.05
Case 7	9.8	0.11	10.5	0.2

compression springs was tuned manually, as will be explained in the next section.

The used friction materials are the specialized friction material Vulka SF-001 and rubber. This leads to a friction coefficient of almost 0.8 and does not lead to sticking behavior. The use of rubber has the disadvantage that rubber tends to wear fast when there is relative movement of the friction surfaces at the moment a normal force is applied. However, in clutches, there should be no relative movement when the device is engaged. If a large amount of relative motion during engagement is to be expected, SF-001 should be used for both friction surfaces, which leads to a friction coefficient of 0.5.

C. Stiffness tuning

The stiffnesses of the three groups of springs have to be balanced. Therefore, we used a leaf spring model in the software package ANSYSTM of which the correctness was verified in [29]. The used leaf springs are made of stainless steel with an E-modulus of 200 GPa and a Poisson ratio of 0.3. The springs have a width of 7.5 mm, a thickness of 0.1 mm and a length of 10 mm. The angle between the leaf springs and the vertical (see Fig. 7) is $\alpha = 10$ deg. The length and width were chosen to fit in the housing of the brake. The thickness was chosen such that the maximum stress is slightly smaller than the yield strength.

In order to test the sensitivity of the characteristic to manufacturing inaccuracies, we derived the characteristics for one pair of springs with seven slightly different parameter sets (see Table I). Case 1 uses the intended parameters. In Case 2-5, the length, thickness, angle and pretension were varied. Pre-tension means that the distance between the braking block and the ground is reduced. Then, in Case 6 and 7, the worst and best cases in terms of maximum force were tested.

Fig. 9 shows the seven characteristics. It shows that the characteristic is very sensitive to certain manufacturing inaccuracies. Especially, a pre-tension changes the characteristic drastically. The different parameter variations influence the maximum force, the stroke of the springs and the stiffness.

Since the final characteristic is very sensitive to inaccuracies, we decided to tune the stiffnesses in the final design manually. This tuning consisted of three steps. First we measured the characteristic of the group of leaf springs to determine the amount of positive stiffness k_n and k_{ctr} that should be added, which turned out to be $k_n = 66.8$ N/m and $k_{ctr} = 54.0$ N/m. The two groups of springs have a

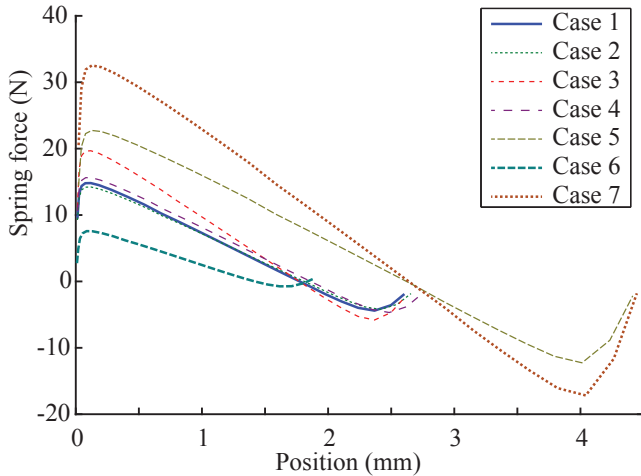


Figure 9. The characteristics of seven sets of springs with slightly varied parameters.

different total stiffness in order to better match the sinusoidal-like characteristic of the leaf springs. Second, we added the positive stiffnesses and measured the characteristic again to determine the off-set in x_n and x_{ctr} . Finally, we adjusted the off-sets in x_n and x_{ctr} accordingly and verified the balancing by measuring the overall characteristic. The result of this tuning is presented in the next section.

D. Performance

Fig. 10a shows the characteristic of the leaf springs and the tuned characteristic of the three spring systems combined. The maximum actuation force is 5.9N and the maximum normal force is 109.6N. Therefore, the actuation force is reduced with 95% in comparison to a regular brake. The average actuation force within the actuation stroke is 1.83 N, which is an improvement of 97% in comparison to a regular brake.

We measured the braking torque manually at 12 positions by applying torque until the brake starts to slip and thus measuring the static friction. Fig. 10b shows the braking torque as function of position and the fit through the data. The results show that the braking torque is a piecewise linear function of the position of the braking block. The maximum braking torque is 1.08 Nm.

V. EXAMPLE 2: CAM MECHANISMS: RRR

This section shows our prototype of the concept based on a rigid body approach. Rigid body mechanisms have the advantage that they are easier to model than compliant mechanisms. We chose to build a prototype with a rotational cam surface with torsion springs connected to the rotational input and output (see Fig. 6e). The mechanism in Fig. 6e is implemented twice, leading to a total of four torsion springs. An initial case study showed that this concept was most promising in terms of torque density.

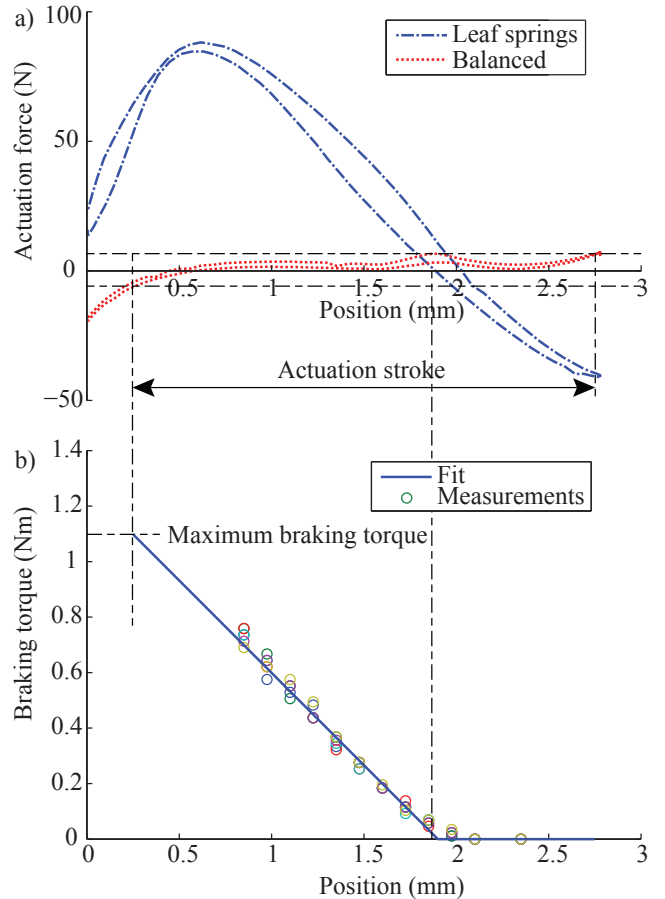


Figure 10. Measurements on prototype 1. a) The characteristics of the leaf springs and the complete statically balanced mechanism. In both cases, the force is measured while moving in both directions. The difference between the two measurements is due to hysteresis. b) The braking torque as function of the position.

A. Detailed design

Fig. 11a shows a CAD drawing of this prototype. The cam shaft is the braking block to which an actuator can be connected. When the cam shaft is rotated, the four followers track the motion induced by the cam surface and the torsion springs are deflected accordingly. The axles running through the followers connect to two components: two connect to the braking arms, the other two connect to the ground. This connection is clarified in Fig. 11b. The axles are connected to the followers through torsion springs with an individual stiffness of 0.637 Nm/rad.

Fig. 11b depicts the braking side of the mechanism with the brake arms and the friction surface disk of the robot axis. Clearly, the robot axis can pass through the entire braking device without obstructions. This has the advantage that this type of brake can also be used in the middle of an axis. The used friction materials are the specialized friction material Vulka SF-001 and rubber (the same as embodiment 1).

B. Performance

Fig. 12 shows the actuation torque for the this embodiment when only the two normal force springs are connected. The

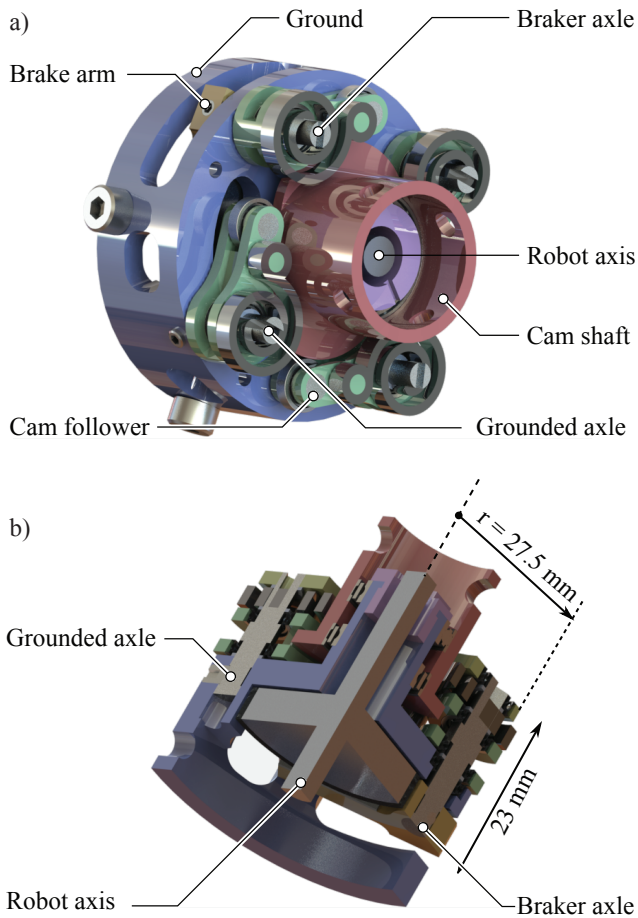


Figure 11. Two CAD drawings of the second embodiment. a) An inside view of the embodiment with torsion springs. b) A section view of the embodiment with torsion springs showing the connection with the braking arms.

resulting actuation torque can be used to estimate the actual stiffness of the torsion springs. The calculated maximum input torque was 0.29 Nm and the actual maximum input torque was 0.24 Nm. This leads to the conclusion that the springs have a 20% lower stiffness than expected from the model and the maximum torque the springs produce is 0.64 Nm per spring instead of the calculated 0.80 Nm. Note however, that although the springs do not have the same stiffness as modelled, the brake is still statically balanced as long as the springs are linear.

Fig. 12 also shows both the actuation torque of the cam shaft and the estimated torque in two torsion springs connected to the brake arms. every 90 degrees, the system has a singular configuration in which the brake is either fully braking or disengaged. In those singular configurations, the actuation torque is 0 Nm which is a 100% reduction of the torque in the springs. In the non-singular configurations the maximum actuation torque on the cam shaft is 0.04 Nm which is a 97% reduction of the combined actuation torque in the torsion springs connected to the brake arms.

Fig. 13 shows the braking torque as function of the position of the cam. The maximum braking torque in clockwise

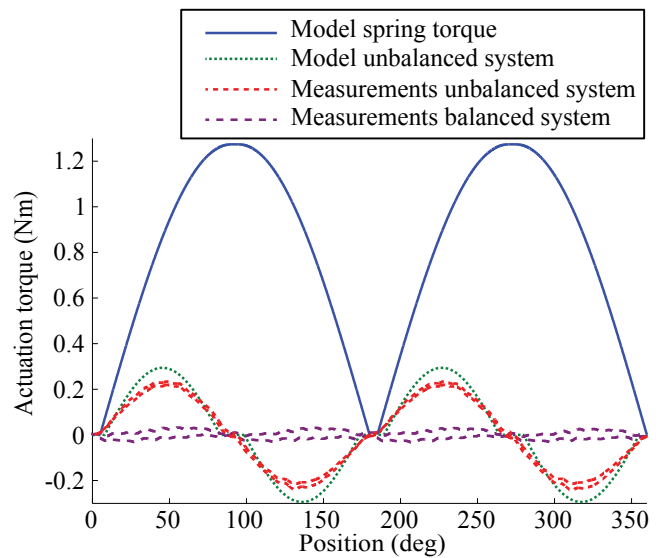


Figure 12. Actuation torque of embodiment 2 for a full rotation of the input cam. The blue solid graph is the estimated torque in the braking springs, the purple dashed graph is the measured input torque.

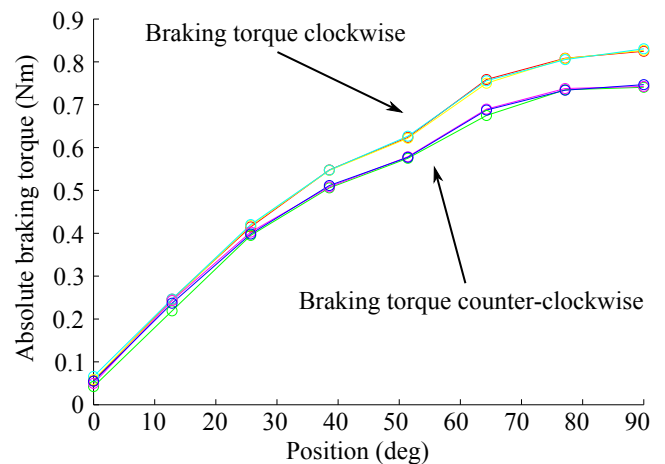


Figure 13. Braking torque of embodiment 2 over a range between 0 degrees (disengaged) to 90 degrees (fully braking) of the cam.

direction is 0.83 Nm and the maximum braking torque in counter clockwise direction is 0.75 Nm. This difference between the braking torque in different directions is caused by a slight self-engaging effect in the brake. This effect is most likely caused by the fact that the SF-001 friction material was slightly thicker than expected.

VI. DISCUSSION

This paper introduced the concept of SBBs, categorized all relatively simple mechanisms that can be used in SBBs and showed two embodiments. We will now discuss the performance, mechanism selection, the use of imperfectly balanced mechanisms, the energy consumption of SBBs and the applications.

Table II
PERFORMANCE OF THE EMBODIMENTS

Criterion	Leaf springs	Rotational cam
Braking torque	1.08 Nm	0.83 Nm
Actuation	5.9 N (= -95%)	0.035 Nm (= -97 %)
Bi-directionality	++	+
Size	Ø60x59 mm	Ø55x23 mm
Mass	170 g	92 g

A. Performance

Table II summarizes the performance of the two embodiments in terms of the braking torque, actuation force/torque, bi-directionality, size, mass. We will now discuss those performance criteria separately.

The braking torques of the embodiments are 1.08 Nm, and 0.83 Nm. There are two options to increase the braking torque. The first option is to increase the radii of the friction surfaces and the second option is to increase the stiffnesses of the springs.

The maximum actuation force and torque are 5.9 N and 0.035 Nm for the two embodiments. Since one embodiment has an actuation force and the other has an actuation torque, the two numbers are hard to compare. However, in embodiment 1, the actuation force is only 5 % of the force in the normal force springs and in embodiment 2, the actuation torque is only 3 % of the torque in the normal force springs. This means that the brakes reach reductions of 95 % and 97 % in comparison to regular brakes. In both cases, the fact that the actuation force is not zero is due to hysteresis and imperfect balancing. Both account for approximately 50% of the maximum actuation force/torque.

The size and mass of embodiment 1 are significantly larger than that of embodiment 2. The challenge in both designs is to miniaturize the mechanism for the compensation springs. In embodiment 1, the leaf springs and their mounting contribute most to mass and size. One possibility to lower the mass and size would be to replace the leaf springs by Belleville springs (also known as disk springs) [30]. More space and mass can be saved by optimizing the design. For example, the braking block, friction surfaces and housing are not optimized for mass and size. In embodiment 2, the cam mechanism and springs are all in one plane, making the design more compact.

B. Mechanism selection

In section III, we categorized all relatively simple mechanisms that can be used between the braking block and the compensation springs. There are no hard rules that, when followed, will automatically lead to the best design. However, here we provide three considerations for selection of a suitable mechanism.

Firstly, rigid body mechanisms in combination with regular springs are easier to model than compliant mechanisms. As shown in section IV, compliant mechanisms can be very sensitive to manufacturing inaccuracies. On the other hand, compliant mechanisms are potentially very compact because the whole mechanism can be made out of one part.

Secondly, rigid body designs are in general smaller when the spring, the actuator and the input and output match. For instance, when a linear actuator is used, it is inconvenient to connect it to a rotational DOF.

Thirdly, the actuator should not be placed on a joint that can reach a singular position. For instance in Fig. 5b, placing a linear actuator on the vertical slider is not a good idea, because it will not be able to leave the position where the bar is vertical. Instead, a rotational actuator could be placed between the bar and one of the sliders.

C. Imperfectly balanced mechanisms

Section III-B discusses three categories of linkage mechanisms that cannot be perfectly statically balanced. Therefore, we did not consider them to be applicable. However, these mechanisms can be used when an approximately statically balanced mechanism suffices. Moreover, with imperfectly balanced mechanisms, the different functionalities mentioned in the introduction can be obtained: the regular brake, the safety brake and the bi-stable brake. These functionalities can also be obtained in cam mechanisms and compliant mechanisms. Here we explain how these adjustments can be obtained in embodiment 1.

The characteristic in Fig. 10 shows an almost statically balanced mechanism. At positions smaller than 0.5mm, the spring force is negative and at all other positions, the spring force is slightly larger than zero. This means that without any actuation force, the system will move to the 0.5mm position, at which the brake is engaged. This behavior is equal to that of a safety brake: when not actuated, the brake engages.

Changing the zero positions of the normal force or counter springs does not change the stiffness and thus it only shifts the total characteristic up and down. The amplitude of the shift influences the maximum actuation force. When the position at which the counter springs engage with the ground is changed, the behavior can be changed to that of a bi-stable brake. Such a brake has two stable positions: one in which the brake is engaged and one in which the brake is disengaged. When also changing the position at which the friction surfaces engage (and thus effectively changing the zero position of the normal springs), the behavior can be changed to that of a regular brake, which is only braking when actuated.

D. Energy consumption

Throughout this paper we only considered the actuation force and suggested that this relates to the energy consumption. Only considering the actuation force has the advantage that it is independent of the specific actuator that is used. To get an idea of the actual energy consumption, we will now briefly discuss the power consumption of a DC motor as a brake actuator. The power of a DC motor that is standing still is equal to:

$$P = \frac{F_n^2 \cdot R}{n^2 \cdot k_t^2} \quad (34)$$

where R is the motor resistance, n is the transfer ratio from the position of the motor to the position of the brake and k_t

is the motor constant. This power consumption goes to zero when the transfer ratio n goes to infinity. However, since this also increases friction, size and mass, this transfer ratio cannot be chosen too large. Now given a certain n , k_t and R , we see that the power consumption scales quadratically with the actuation force. In most other actuators, the energy consumption will scale with the actuation force and therefore, a higher actuation force will result in a higher energy consumption.

There are actuators in which the energy consumption (theoretically) is independent of the actuation force. Examples are electro-static and piezo-electric actuators. However, those actuators have other disadvantages that make them less suitable for application in brakes, as explained in the introduction.

E. Applications

The intended application of the brakes we introduced in this paper is robotics. The use of locking devices in robotics is increasing [31]. Such locking devices are mainly used to reconfigure robots, decrease actuator load when standing still, and control the energy release of springs. Especially in mobile robots, such as household robots or walking robots, components that do not consume energy are advantageous.

The main reason for using a SBB in comparison to other brakes is when only a small actuation force is available and the brake should be able to brake in two directions. Other possible applications for statically balanced brakes include torque limiters, cars, trains, buses, trucks and bikes. Especially the safety/parking brake version of the brake that we showed in this paper is applicable in vehicles such as buses and trucks that often use such brakes to stand still.

As stated in [31], brakes are often used as locking mechanisms or clutches. Using a brake as a clutch (instead of quickly switching clutches such as ratchets) has two advantages. Firstly, a brake can disengage while under load and secondly, the braking torque is independent of the position of the joint.

VII. CONCLUSION

In this paper we introduced a new type of brakes: statically balanced brakes. The goal of SBBs is to eliminate the actuation force required in regular brakes. With small adjustments, SBBs can also be used as safety brakes or bi-stable brakes, with a reduced actuation force. We conclude that the concept of SBBs is promising and that the required actuation force can be reduced with 95-97% in comparison to regular brakes. Furthermore, cam mechanisms seem to be the most promising approach for balancing of the two spring systems because of their design freedom and the fact that they are relatively easy to model.

ACKNOWLEDGEMENT

This work is part of the research programme STW, which is (partly) financed by the Netherlands Organisation for Scientific Research (NWO).

REFERENCES

- [1] W. C. Orthwein, *Clutches and brakes: design and selection*. CRC Press, 2004.
- [2] R. Limpert, *Brake design and safety*, 1992, vol. 120.
- [3] J. Kim and S. B. Choi, "Design and modeling of a clutch actuator system with self-energizing mechanism," *Mechatronics, IEEE/ASME Transactions on*, vol. 16, no. 5, pp. 953–966, 2011.
- [4] B. Peerdeman, G. Pieterse, S. Stramigioli, H. Rietman, E. Hekman, D. Brouwer, and S. Misra, "Design of joint locks for underactuated fingers," in *Biomedical Robotics and Biomechanics (BioRob), 2012 4th IEEE RAS EMBS International Conference on*, June 2012, pp. 488–493.
- [5] D. F. B. Haeufle, M. D. Taylor, S. Schmitt, and H. Geyer, "A clutched parallel elastic actuator concept: Towards energy efficient powered legs in prosthetics and robotics," in *IEEE RAS EMBS International Conference 4th on Biomedical Robotics and Biomechanics (BioRob), 2012*, pp. 1614–1619.
- [6] P. Guarneri, G. Mastinu, M. Gobbi, C. Cantoni, and R. Sicigliano, "Brake energy efficiency," *Journal of Mechanical Design*, 2014.
- [7] C. G. Peabody and R. W. Roberts, "Automatic parking brake," Feb. 18 1936, uS Patent 2,031,062.
- [8] S. L. Kurichh and L. R. Acre, "Air operated spring brake," Dec. 16 1975, uS Patent 3,926,094.
- [9] J. H. Arnold, M. D. DeWitt, R. J. Perisho, and W. L. Soucie, "Electronically controlled parking brake system," Jan. 19 1993, uS Patent 5,180,038.
- [10] J. K. Parmerlee *et al.*, "Bi-stable brake," 1973, uS Patent 3,741,353.
- [11] J. B. Chou, K. Yu, and M. C. Wu, "Electrothermally actuated lens scanner and latching brake for free-space board-to-board optical interconnects," 2012.
- [12] G. Hirzinger, M. Fischer, B. Brunner, R. Koeppel, M. Otter, M. Grebenstein, and I. Schfer, "Advances in robotics: The dlr experience," *The International Journal of Robotics Research*, vol. 18, no. 11, pp. 1064–1087, 1999.
- [13] K. Yamatoh, M. Ogura, K. Kanbe, and Y. Isogai, "Piezoelectric brake device," Aug. 8 1989, uS Patent 4,854,424.
- [14] M. G. Hanley, G. P. Caliendo, and D. B. Anderson, "Actuator having piezoelectric braking element," Nov. 16 1999, uS Patent 5,986,369.
- [15] S. Munir, L. Tognetti, and W. Book, "Experimental evaluation of a new braking system for use in passive haptic displays," in *American Control Conference, 1999. Proceedings of the 1999*, vol. 6, 1999, pp. 4456–4460 vol.6.
- [16] M. Laffranchi, N. Tsagarakis, and D. Caldwell, "A variable physical damping actuator (vpda) for compliant robotic joints," in *Robotics and Automation (ICRA), 2010 IEEE International Conference on*, 2010, pp. 1668–1674.

- [17] J. L. Herder, "Energy-free systems. theory, conception and design of statically balanced spring mechanisms," Ph.D. dissertation, Delft University of Technology, 2001.
- [18] G. J. Tuijthof and J. L. Herder, "Design, actuation and control of an anthropomorphic robot arm," *Mechanism and machine theory*, vol. 35, no. 7, pp. 945–962, 2000.
- [19] M. Vermeulen and M. Wisse, "Intrinsically safe robot arm: Adjustable static balancing and low power actuation," *International Journal of Social Robotics*, vol. 2, no. 3, pp. 275–288, 2010.
- [20] J. L. Herder, "Development of a statically balanced arm support: Armon," in *Rehabilitation Robotics, 2005. ICORR 2005. 9th International Conference on.* IEEE, 2005, pp. 281–286.
- [21] N. Tolou, G. Smit, A. A. Nikooyan, D. H. Plettenburg, and J. L. Herder, "Stiffness compensation mechanism for body powered hand prostheses with cosmetic covering," *Journal of medical devices*, vol. 6, no. 1, 2012.
- [22] N. Tolou, V. A. Henneken, and J. L. Herder, "Statically balanced compliant micro mechanisms (sb-mems): Concepts and simulation," in *ASME 2010 International Design Engineering Technical Conferences and Computers and Information in Engineering Conference.* American Society of Mechanical Engineers, 2010, pp. 447–454.
- [23] A. Dunning, N. Tolou, and J. Herder, "A compact low-stiffness six degrees of freedom compliant precision stage," *Precision Engineering*, vol. 37, no. 2, pp. 380 – 388, 2013.
- [24] C. Gosselin and J. Angeles, "Singularity analysis of closed-loop kinematic chains," *Robotics and Automation, IEEE Transactions on*, vol. 6, no. 3, pp. 281–290, Jun 1990.
- [25] D. Zlatanov, R. Fenton, and B. Benhabib, "Identification and classification of the singular configurations of mechanisms," *Mechanism and Machine Theory*, vol. 33, no. 6, pp. 743 – 760, 1998.
- [26] F. Park and J. W. Kim, "Manipulability and singularity analysis of multiple robot systems: a geometric approach," in *Robotics and Automation, 1998. Proceedings. 1998 IEEE International Conference on*, vol. 2, May 1998, pp. 1032–1037 vol.2.
- [27] D. Tsay and B. Lin, "Profile determination of planar and spatial cams with cylindrical roller-followers," *Proceedings of the Institution of Mechanical Engineers, Part C: Journal of Mechanical Engineering Science*, vol. 210, no. 6, pp. 565–574, 1996.
- [28] L. L. Howell, S. P. Magleby, and B. M. Olsen, *Handbook of compliant mechanisms.* Wiley Online Library, 2013.
- [29] A. Dunning, N. Tolou, P. Pluimers, L. Kluit, and J. Herder, "Bistable compliant mechanisms: Corrected finite element modeling for stiffness tuning and preloading incorporation," *Journal of Mechanical Design*, vol. 134, no. 8, p. 084502, 2012.
- [30] J. Almen and A. Laszlo, "The uniform-section disk spring," *Trans. ASME*, vol. 58, pp. 305–314, 1936.
- [31] M. Plooij, G. Mathijssen, P. Cherelle, D. Lefeber, and B. Vanderborght, "Lock your robot: A review of locking devices in robotics," *Robotics Automation Magazine, IEEE*, vol. 22, no. 1, pp. 106–117, March 2015.

Appendix B

Additions to chapter 2

B.1 Actuation force singular-friction locker

In this appendix section the actuation force trajectory of a typical singular-friction locking linkage is analysed. In figure B.1 such a typical singular-friction locking linkage is depicted. As can be seen, the input force is directed vertically in downward direction on the middle joint and the output force is generated in horizontal direction on the red joint. With the principle of virtual work, the actuation force characteristic is derived for this typical mechanism.

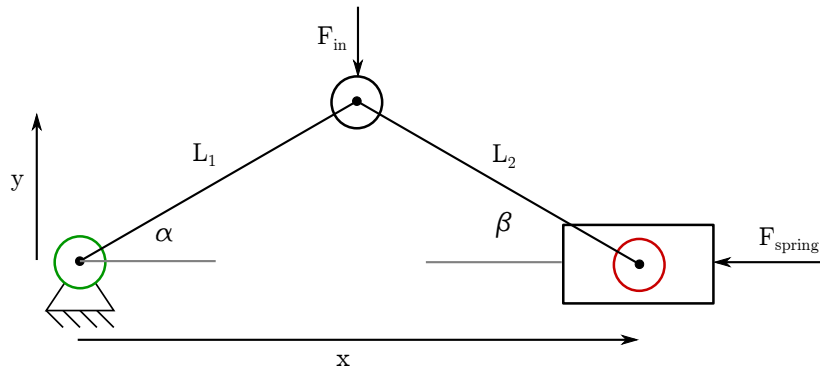


Figure B.1: A schematic representation of a singular-friction locker with a rotational input (green) and a translational output (red). The resulting actuation force characteristic of this mechanism is depicted in fig 2.3. Of course lengths L_1 and L_2 are variables in this mechanism.

$$\begin{aligned}
0 &= F_{in}(-\delta y) + F_{spring}(-\delta x) \\
x &= L_1 \cos(\alpha) + L_2 \cos(\beta) \\
y &= L_1 \sin(\alpha) \\
L_1 \sin(\alpha) &= L_2 \sin(\beta) \\
\cos^2(\beta) &= 1 - \sin^2(\beta) \\
\cos(\beta) &= \pm \sqrt{1 - \left(\frac{L_1}{L_2}\right)^2 \sin^2(\alpha)}
\end{aligned}$$

$$\begin{aligned}
\delta(x) &= -L_1 \sin(\alpha)\delta(\alpha) - L_2 \sin(\beta)\delta(\beta) \\
\delta(y) &= L_1 \cos(\alpha)\delta(\alpha) \\
L_1 \cos(\alpha)\delta(\alpha) &= L_2 \cos(\beta)\delta(\beta) \\
\delta(\beta) &= \frac{L_1 \cos(\alpha)}{L_2 \cos(\beta)} \delta\alpha
\end{aligned}$$

$$\begin{aligned}
F_{in} - (-L_1 \cos(\alpha)\delta(\alpha)) + F_{spring}(-L_1 \sin(\alpha)\delta(\alpha) - L_2 \sin(\beta)\delta(\beta)) &= 0 \\
F_{in} - (-L_1 \cos(\alpha)\delta(\alpha)) + F_{spring}(-L_1 \sin(\alpha)\delta(\alpha) - L_1 \tan(\beta) \cos(\alpha)\delta(\alpha)) &= 0
\end{aligned}$$

where:

$$\tan(\beta) = \frac{\frac{L_1 \sin(\alpha)}{L_2}}{\pm \sqrt{1 - \left(\frac{L_1}{L_2}\right)^2 \sin^2(\alpha)}}$$

Resulting in:

$$F_{in} = F_{spring} \frac{-L_1 \sin(\alpha) - L_1 \tan(\beta) \cos(\alpha)}{-L_1 \cos(\alpha)}$$

Where:

$$F_{spring} = k(x - x_0)$$

Where:

$$x_{(0)} = L_1 \cos(\alpha) + L_2 \cos(\beta)$$

Appendix C

Additions to chapter 3

C.1 Actuation force of a double singular-friction locker

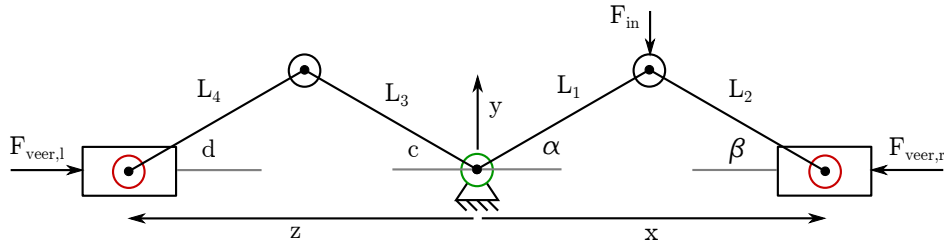


Figure C.1: Double singular-friction locker with a rotational actuated joint and a translational output.

$$\begin{aligned}
 0 &= F_{in}(-\delta y) + F_{veer,r}(-\delta x) + F_{veer,l}(-\delta z) \\
 x &= L_1 \cos(\alpha) + L_2 \cos(\beta) \\
 y &= L_1 \sin(\alpha) \\
 L_1 \sin(\alpha) &= L_2 \sin(\beta) \\
 \cos^2(\beta) &= 1 - \sin^2(\beta) \\
 \cos(\beta) &= \pm \sqrt{1 - \left(\frac{L_1}{L_2}\right)^2 \sin^2(\alpha)}
 \end{aligned}$$

The left side is added to the right side of the mechanism as follows:

$$\begin{aligned}
 z &= L_3 \cos(c) + L_4 \cos(d) \\
 L_3 \sin(c) &= L_4 \sin(d) \\
 \cos^2(d) &= 1 - \sin^2(d) \\
 \cos(d) &= \pm \sqrt{1 - \left(\frac{L_3}{L_4}\right)^2 \sin^2(c)}
 \end{aligned}$$

Variations of the variable z :

$$\begin{aligned}\delta(z) &= -L_3 \sin(c)\delta(c) - L_4 \sin(d)\delta(d) \\ L_3 \cos(c)\delta(c) &= L_4 \cos(d)\delta(d) \\ \delta(d) &= \frac{L_3 \cos(c)}{L_4 \cos(d)}\delta(c)\end{aligned}$$

We know c in terms of α and the initial value of α , α_0 :

$$\begin{aligned}c &= -\alpha + \alpha_0 \\ \delta(c) &= -\delta(\alpha) \\ z &= L_3 \cos(-\alpha + \alpha_0) + L_4 \cos(d) \\ \cos(d) &= \pm \sqrt{1 - \left(\frac{L_3}{L_4}\right)^2 \sin^2(-\alpha + \alpha_0)}\end{aligned}$$

$$\begin{aligned}F_{veer,l} &= k(z - z_0) \\ z_{(0)} &= L_3 \cos(-\alpha + \alpha_0) + L_4 \cos(d)\end{aligned}$$

These values can be substituted back into the original equations:

$$\begin{aligned}F_{in} - (-L_1 \cos(\alpha)\delta(\alpha)) + F_{veer,r}(-L_1 \sin(\alpha)\delta(\alpha) \\ - L_2 \sin(\beta)\delta(\beta)) + F_{veer,l}(-L_3 \sin(c)\delta(c) - L_4 \sin(d)\delta(d)) &= 0 \\ F_{in}(L_1 \cos(\alpha)\delta(\alpha)) + F_{veer,r}(-L_1 \sin(\alpha)\delta(\alpha) - L_1 \tan(\beta) \cos(\alpha)\delta(\alpha) \\ + F_{veer,l}(+L_3 \sin(c)\delta(\alpha) + L_3 \tan(d) \cos(c)\delta(\alpha)) &= 0\end{aligned}$$

where:

$$\tan(d) = \frac{\frac{L_3 \sin(c)}{L_4}}{\pm \sqrt{1 - \left(\frac{L_3}{L_4}\right)^2 \sin^2(c)}}$$

Resulting in the final expression for the input force:

$$F_{in} = \frac{F_{veer,r}(-L_1 \sin(\alpha) - L_1 \tan(\beta) \cos(\alpha)) + F_{veer,l}(L_3 \sin(c) + L_3 \tan(d) \cos(c))}{-L_1 \cos(\alpha)}$$

When fully written in terms of α and α_0 this expression becomes:

$$F_{in} = \frac{\cos(\alpha) \left(L_3 k_2 \left(\sin(\alpha - \alpha_0) + \frac{L_4 \cos(\alpha - \alpha_0) \sin(\alpha - \alpha_0)}{L_4 \sqrt{1 - \frac{L_3^2 \sin(\alpha_0)^2}{L_4^2}}} \right) \left(L_4 \sqrt{1 - \frac{L_3^2 \sin(\alpha_0)^2}{L_4^2}} + L_3 \cos(\alpha_0) - L_4 \sqrt{1 - \frac{L_3^2 \sin(\alpha - \alpha_0)^2}{L_4^2}} - L_3 \cos(\alpha - \alpha_0) \right) - L_1 k_1 \left(\sin(\alpha) + \frac{L_1 \cos(\alpha) \sin(\alpha)}{L_2 \sqrt{1 - \frac{L_1^2 \sin(\alpha)^2}{L_2^2}}} \right) \left(L_2 \sqrt{1 - \frac{L_1^2 \sin(\alpha)^2}{L_2^2}} - L_2 \sqrt{1 - \frac{L_1^2 \sin(\alpha_0)^2}{L_2^2}} + L_1 \cos(\alpha) - L_1 \cos(\alpha_0) \right) \right)}{L_1}$$

Appendix D

Additions to chapter 5

D.1 Friction disk and arm in reality

The practical implementation of the calculations have led to the design of the brake disk and the brake arms depicted in figures D.1 and D.2 respectively. In order to achieve the friction coefficient of 0.8 between the brake disk and the brake arm, rubber was applied to the brake disk and Vulca SF-001 from the workshop was applied to the brake arms.



Figure D.1: The braking disk produced from Alu7075 with braking rubber glued on the outer surface.



Figure D.2: The braking lever produced from Alu7075 with braking material glued on the inner surface.

D.2 Cam surface generation

This procedure is described literally in the work by Tsay and Lin [31]. Refer to figure 5.6 for the schematic representation of the cam and the follower. Length b is the length of the follower arm, length a is the distance from the follower axle to the cam axle and r is the radius of the roller of the follower. Angle ϕ_2 is the rotation of the cam and ϕ_1 is the follower angle.

The center of the roller can be located with the first equation where δ is the parameter along the axis of the roller. Using the rigid-body transformation, the pitch surface can be derived by rotating the follower in the opposite direction to the rotation of the cam. It can be written as:

$$\begin{aligned}
 S_0(\phi_2, \delta) &= (a - b \cos(\phi_1))i + b \sin(\phi_1)j + \delta k \\
 S_0(\phi_2, \delta) &= [a - b \cos(\phi_1), b \sin(\phi_1), \delta] \times \begin{bmatrix} \cos(\phi_2) & -\sin(\phi_2) & 0 \\ \sin(\phi_2) & \cos(\phi_2) & 0 \\ 0 & 0 & 1 \end{bmatrix} \\
 &= [a \cos(\phi_2) - b \cos(\phi_1 + \phi_2)]i + [-a \sin(\phi_2) + b \sin(\phi_1 + \phi_2)]j + \delta k
 \end{aligned}$$

Differentiating the above equation with respect to ϕ_2 as well as δ and taking the cross-product, the unit normal vector of the pitch surface is obtained as:

$$\begin{aligned}
 n &= \frac{\frac{\partial S_c}{\partial \delta} \times \frac{\partial S_c}{\partial \phi_2}}{\left| \frac{\partial S_c}{\partial \delta} \times \frac{\partial S_c}{\partial \phi_2} \right|} = n_x i + n_y j \\
 n_x &= \frac{a \cos(\phi_2) - b(1 + \phi_1') \cos(\phi_1 + \phi_2)}{\sqrt{a^2 - 2ab(1 + \phi_1') \cos(\phi_1) + b^2(1 + \phi_1')^2}} \\
 n_y &= \frac{b(1 + \phi_1') \sin(\phi_1 + \phi_2) - \sin(\phi_2)}{\sqrt{a^2 - 2ab(1 + \phi_1') \cos(\phi_1) + b^2(1 + \phi_1')^2}} \\
 \phi_1' &= \frac{d\phi_1}{d\phi_2}
 \end{aligned}$$

Then the surface equation of the disk cam profile with an oscillating roller-follower can be presented by the offset surface of the pitch surface with a distance equal to the radius of the roller.

$$\begin{aligned}
 S(\phi_2, \delta) &= S_c(\phi_2, \delta) \pm rn \\
 &= S_x(\phi_2, \delta)i + S_y(\phi_2, \delta)j + S_z(\phi_2, \delta)k \\
 S_x(\phi_2, \delta) &= [a \cos(\phi_2) - b \cos(\phi_1 + \phi_2)] \pm rn_x \\
 S_y(\phi_2, \delta) &= [-a \sin(\phi_2) + b \sin(\phi_1 + \phi_2)] \pm rn_y \\
 S_z(\phi_2, \delta) &= \delta
 \end{aligned}$$

This equation will result in the grooved cam surface with two walls.

D.3 Follower trajectory and cam model

In this appendix section the cam follower trajectory and the energy graph are presented in figures D.3 and D.4. the red stripes mark the singular configurations in the mechanism.

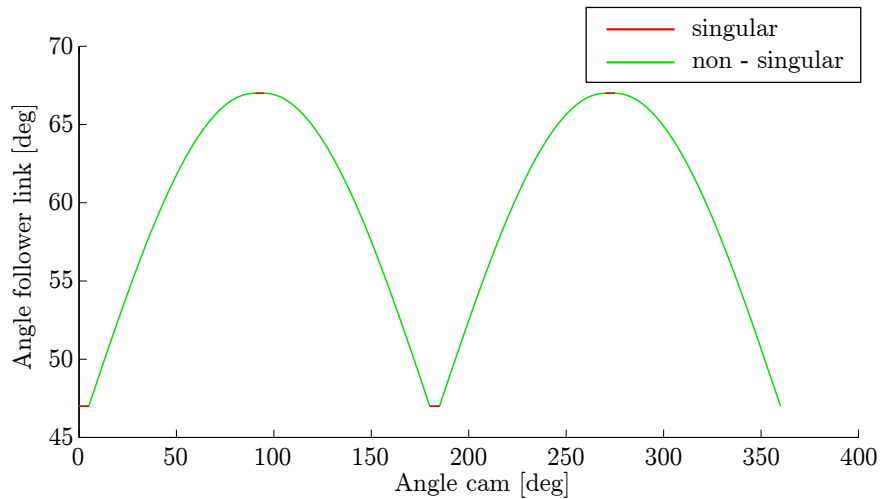


Figure D.3: The output follower angle as a function of the angle of the input cam shaft. Note that in the regions for ϕ_2 of 0-5, 90-95, 180-185 and 270-275 singular configurations are built into the trajectory for ϕ_1 .

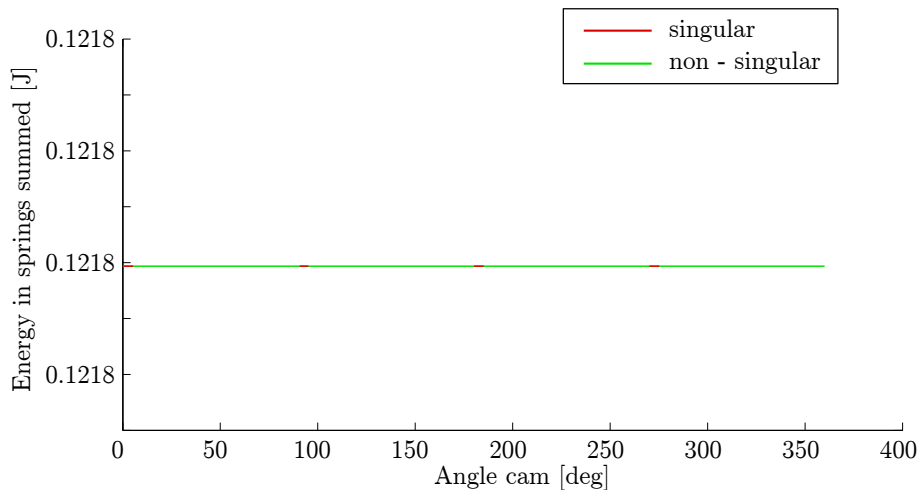


Figure D.4: The summed energy in all four springs in Joules for a full rotation of the input cam shaft.

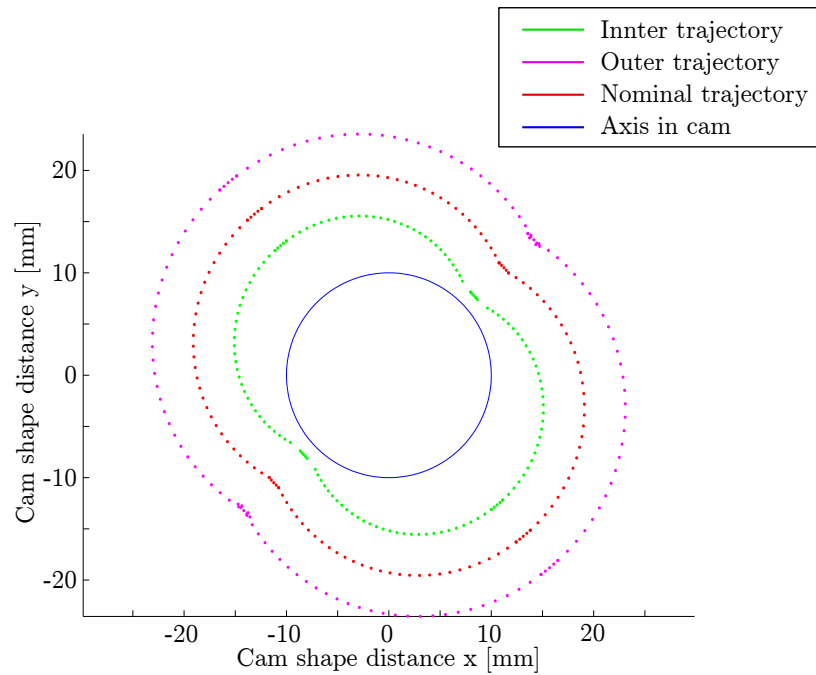


Figure D.5: A plot of the points as they were exported to solidworks to produce an actual cam shaft.

Real model

As described the cam model was produced into a real cam by means of cnc milling. The resulting camshaft is depicted in figure D.6. Interestingly, the first cam that was produced did not provide a perfect static balance, but a small but clear stiffness could be felt when rotating the input cam shaft. The answer to this problem lies in the fact that though the cam may look symmetrical, it certainly is not! As can be seen from figure D.6 the cam surface has a bush attached to it. When the bush is attached to the cam like it is in the figure, one image of the 2D cam plane is obtained where if the bush is attached to the other side of the cam plane, the other image is obtained. The difference in outcome (or cam shape) is very little, however the effect is quite big. To solve the initial issues, a new cam shaft was produced and used for a second round of measurements as presented in chapter 6.



Figure D.6: Cam disk produced in Alu7075 to the matlab model. Two thin section ball bearings are incorporated to deal with the forces and moments exerted on the cam surface.

D.4 Other components

In this section the other various components of the design are presented. The sections are little and contain some basic information on the design and materials used.

D.4.1 Main body elements

The 'ground' of the locking device consists of two parts, a main body as depicted in figure D.7 and a secondary body as depicted in figure D.8. The main body connects all parts together. In the middle the cam shaft can rotate about the centre axle of the main body.

The ground axles are also directly fitted to this body with set screws to be able to adjust the 'zero' position for the springs. This is the position where the springs are fully relaxed and only just make contact with the cam surface. The axles connected to the braking arm are supported by means of small roller bearings. These braking axles are connected to the braking arms in the same manner with set screws as the grounded axles to the main body.

The secondary body is mainly for stability. The axles that hold the followers have to be precisely in place due to all small tolerances. By adding the secondary ground, the axles are supported on two places and the loads on the axles are divided.

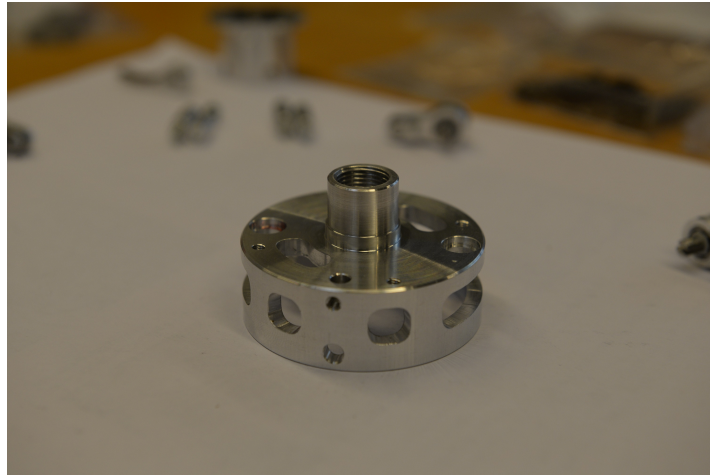


Figure D.7: Main body milled and turned from Alu7075. This part is the heart of the locking device to which everything is connected.



Figure D.8: Secondary body machined from Alu7075.

D.4.2 Follower links

In figure D.9 a follower of the cam shaft is depicted. The connection to the torsion springs becomes clear when studying the image. When the follower is rotated, the spring is put under tension and a torque is applied to the center axle. This axle is sprung with two bearings in the follower to compensate for the out of plane load introduced by the torsion spring.



Figure D.9: Follower link with spring attached. The follower is machined from Alu7075 and features three roller bearings. One to roll over the cam surface, and two on the main axle to compensate for the load introduced by the torsion spring.

D.4.3 Locknut

Last but not least the part that holds the cam shaft in place. In the very center of figure D.10 the locknut can be seen. This nut is screwed into the main body by means of the thread depicted in figure D.7. In that way the bearings supporting the cam shaft are locked into place.

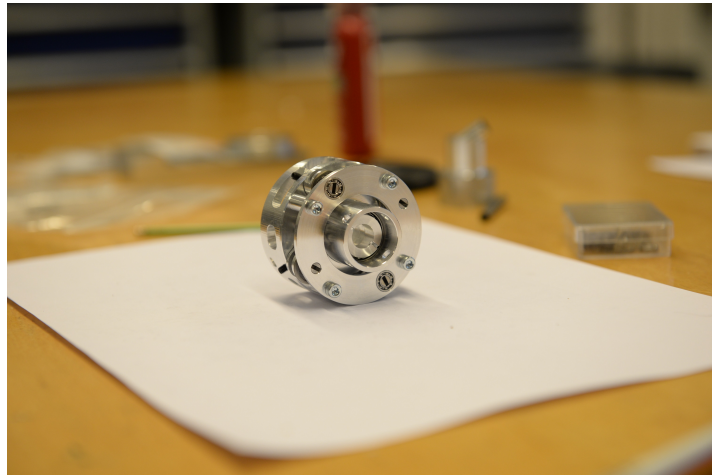


Figure D.10: Cam installed on the main body with the locknut. The locknut was also produced from Alu7075

Appendix E

Additions to chapter 6

E.1 Additional images test setup

In this section the solidworks model of the measurement setup and the real measurement setup are presented. In figure E.1 the solidworks model is shown. This model was used to make the p-brake exactly fit in the (existing) measurement setup. The measurement setup without the locking devise in it is depicted in figure E.2.

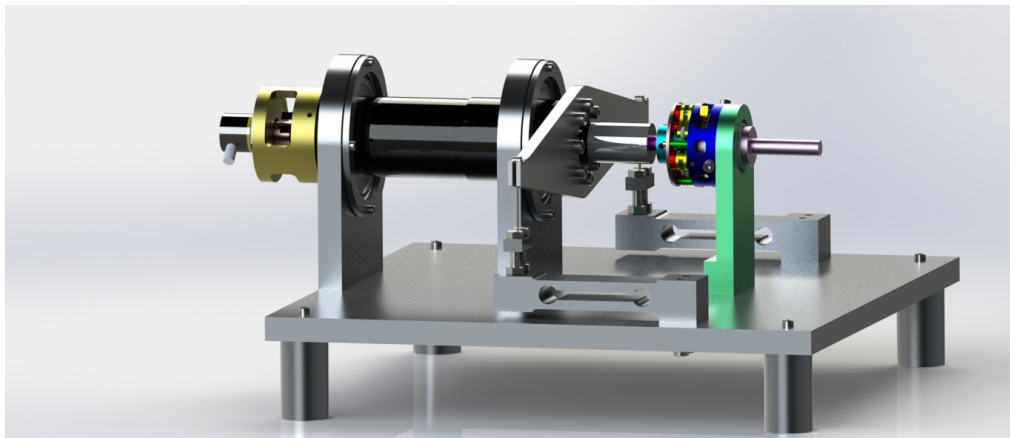


Figure E.1: Rendered solidworks image of the test setup. The non coloured parts are from a previous setup and the coloured parts are the locking devise and an encoder on the motor.

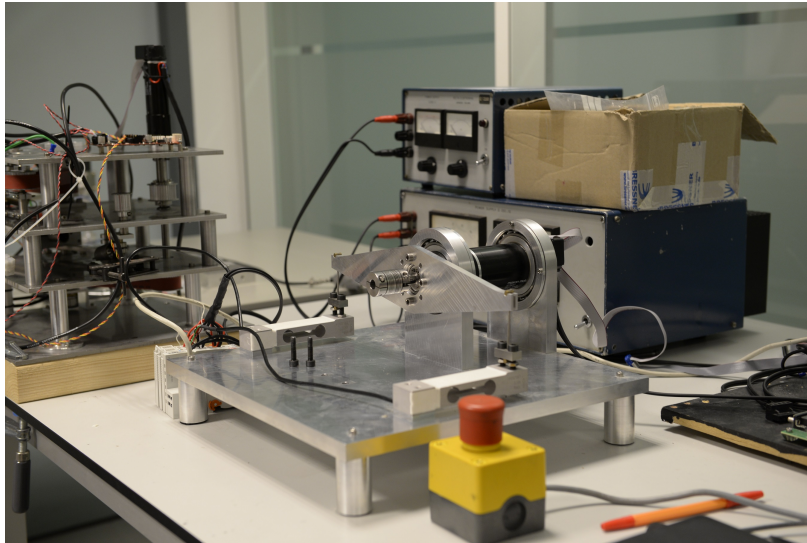


Figure E.2: Test setup in reality. A safety button was included to be able to stop the motor at any given moment. This ensured that the locking device would not easily be damaged.

E.2 Calibration: No-load conditions

Experiment 1 identifies any offsets in the measurement setup. As described the first measurement is the torque measured in the load cells when the measurement is at standstill for a short instance of time (16 seconds to be precise). The result of this measurement is depicted in figure E.3. The mean offset torque is -0.0833 Nm and the standard deviation torque is 0.0063 Nm.

The second experiment to be conducted is the measurement of the torque on the load cells when the motor is slowly rotating. In this way any other forms of hysteresis or misconfiguration can be identified. The results of his experiment are presented in figure E.4. The mean offset torque is -0.0817 Nm and the standard deviation torque is 0.0061 Nm.

Discussion

From both sub experiments the conclusion can be drawn that the static offset is determined -0.0833 Nm. When the motor is moving a very small neglectable term is added to this static offset, but for the reversed direction it will be in the opposite direction. Therefore only a static offset of -0.0833 Nm is added to the rest of the measurements.

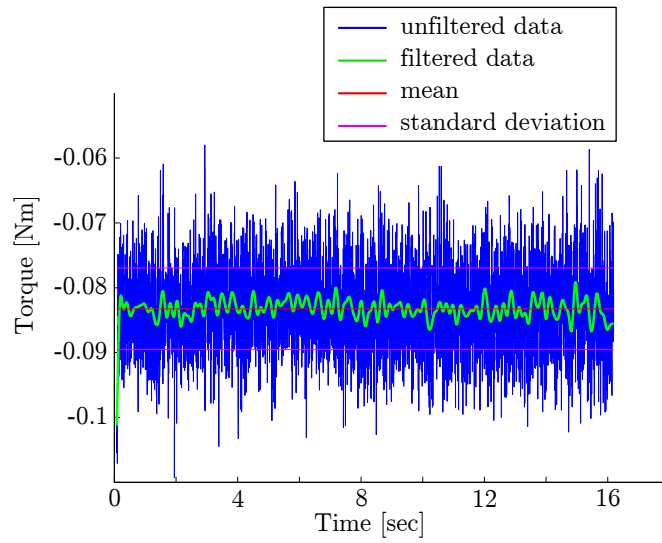


Figure E.3: No-load conditions at standstill. Data are filtered with a seventh order lowpass butterworth filter with a cutoff frequency of 5Hz and sample rate of 1000 samples per second. The mean offset torque is -0.0833 Nm and the standard deviation torque is 0.0063 Nm.

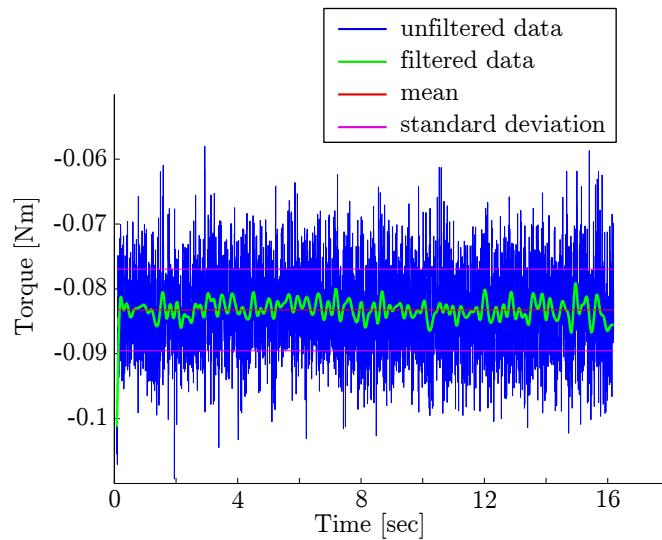


Figure E.4: No-load conditions while moving at 5 rpm. Data are filtered with a seventh order lowpass butterworth filter with a cutoff frequency of 5Hz and sample rate of 1000 samples per second. The mean offset torque is -0.0817 Nm and the standard deviation torque is 0.0061 Nm.

E.3 Single runs

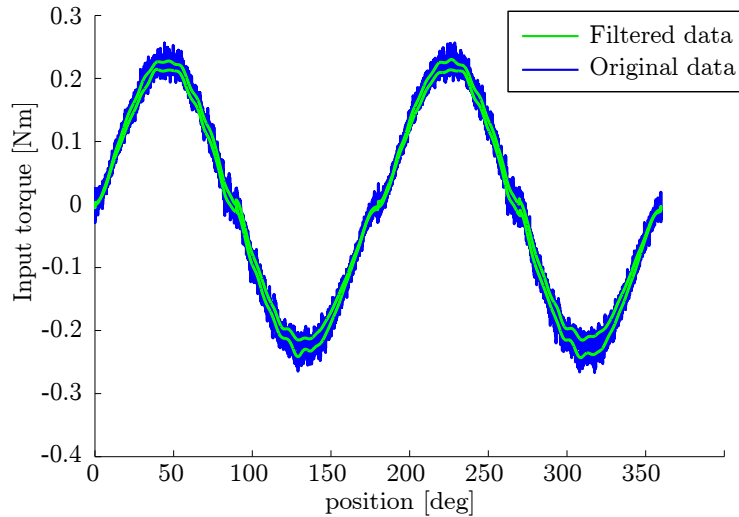


Figure E.5: Single run of the spring characteristic measured against position corresponding to measurement 1 in figure 6.4. Data are filtered with a seventh order lowpass butterworth filter with a cutoff frequency of 5Hz and sample rate of 1000 samples per second. The trajectory of the motor is depicted in figure 6.3

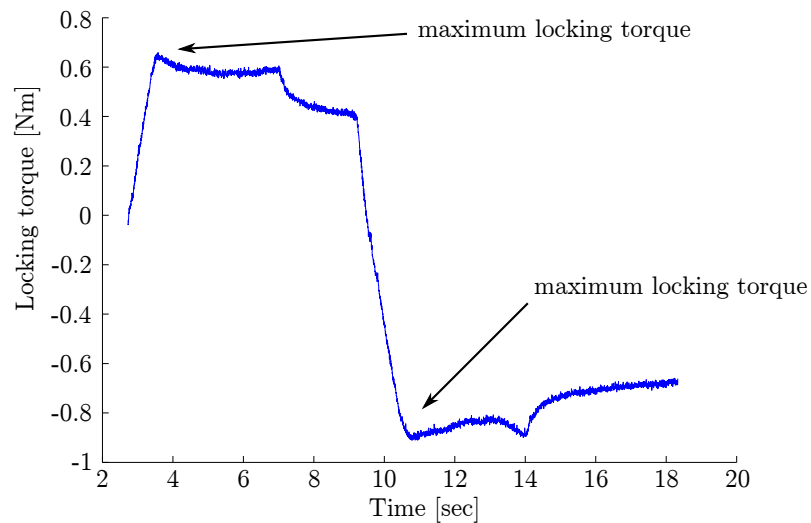


Figure E.6: A single run of the locking torque measurement. While the locker is switched on the brake disk moves 0.1 rad in one direction and then returns to the starting position. The two peaks in the graph represent the maximum locking torque in both directions

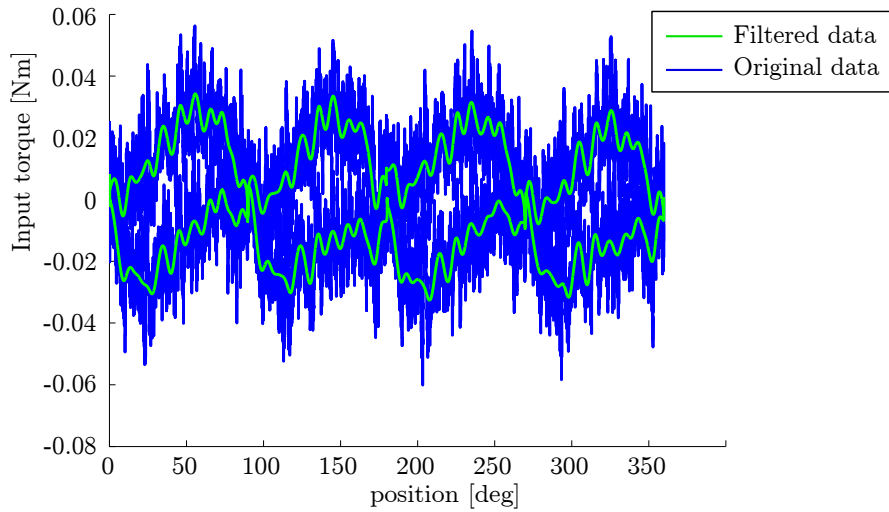


Figure E.7: A single run of the input torque plotted over the input angle. Data are filtered with a seventh order lowpass butterworth filter with a cutoff frequency of 5Hz and sample rate of 1000 samples per second. The trajectory of the motor is depicted in figure 6.3

E.4 Overview measurement runs

This appendix contains an index of all experimental runs conducted with the locking device in the test setup. Unfortunately the accompanying paperwork of the very first measurement runs with the flawed cam were lost. Therefore the runs with the new (and correct) cam are presented only. The year, month, day and time refer to the name of the .mat file since it is a combination of these data (the first run is for example 201503021636.mat).

year	month	day	time	description
2015	03	02	16:36	first input run new cam
2015	03	02	16:44	second input run new cam
2015	03	02	16:58	no load brake side
2015	03	02	16:58	no load brake side 2
2015	03	02	17:00	locked braking
2015	03	02	17:02	locked braking 2
2015	03	02	17:05	no load braker config. 2
2015	03	02	17:09	loaded config. 2
2015	03	02	17:12	loaded config. 2

Table E.1: Overview of all measurement runs.

year	month	day	time	description
2015	03	03	12:42	New cam input side
2015	03	03	12:47	New cam input side #2
2015	03	03	13:08	Loose ground spring stiffness
2015	03	03	13:12	Loose ground spring stiffness #2
2015	03	03	17:43	Nothing connected
2015	03	03	17:46	Nothing connected #2
2015	03	03	17:50	No movement
				gearbox corrected from 1:25 to 1:26!
2015	03	04	09:26	no load braker without cam connected
2015	03	04	09:28	no load braker without cam connected #2
2015	03	04	11:21	no load braker
2015	03	04	11:24	braker but flawed
2015	03	04	11:26	braker #1
2015	03	04	11:40	Long run brake side
2015	03	04	11:45	Braking squeak side
2015	03	04	12:49	Braking squeak side #2
2015	03	04	12:21	Input new
2015	03	04	14:23	Input new #2
2015	03	04	14:33	Two 1mm springs input
2015	03	04	14:36	Two 1mm springs input #2
2015	03	04	14:41	No load brake side
2015	03	04	14:42	braked 2 springs #1
2015	03	04	14:45	braked 2 springs #2
2015	03	04	14:47	braked 2 springs #1 squeak side
2015	03	04	14:48	braked 2 springs #2 squeak side
2015	03	04	16:06	input 3mm springs #1
2015	03	04	16:10	input 3mm springs #2
2015	03	04	16:17	brake side no load
2015	03	04	16:20	brake side loaded (0.5)
2015	03	04	16:23	brake side loaded (0.6)
2015	03	04	16:25	brake side loaded (0.6)
2015	03	04	16:27	brake side loaded squeak (0.4)
2015	03	04	16:28	brake side loaded squeak (0.45)
2015	03	05	09:18	springs only 3mm
2015	03	05	09:21	prings only 3mm #2
2015	03	05	10:10	prings only 3mm unwinding
2015	03	05	10:12	prings only 3mm unwinding #2
2015	03	06	11:09	long run input side 3mm springs

Table E.2: Overview of all measurement runs.

year	month	day	time	description
				corrected new spring type!
2015	03	09	12:25	long run 1mm spring input
2015	03	09	12:37	short run 1mm spring input
2015	03	09	12:52	spring characteristic 1mm spring
2015	03	09	12:53	brake torque 1mm
2015	03	09	12:54	brake torque 1mm #2
2015	03	09	12:55	brake torque 1mm #3
2015	03	09	12:58	brake torque 1mm squeak side
2015	03	09	12:59	brake torque 1mm squeak side #2
2015	03	09	13:00	brake torque 1mm squeak side #3
2015	03	09	13:44	3mm new input #1
2015	03	09	13:48	3mm new input #2
2015	03	09	13:51	3mm new input #3
2015	03	09	13:52	3mm new input #4
2015	03	09	13:54	3mm new input #5
2015	03	09	13:57	long run input side
2015	03	09	14:06	brake torque #1
2015	03	09	14:09	brake torque #2
2015	03	09	14:10	brake torque #3
2015	03	09	14:12	brake torque #4
2015	03	09	14:14	brake torque squeak side #1
2015	03	09	14:16	brake torque squeak side #2
2015	03	09	14:19	brake torque squeak side #3
2015	03	09	14:43	input redone #1
2015	03	09	14:45	input redone #2
2015	03	09	14:48	long run inout redone
2015	03	09	14:52	spring characteristic
2015	03	09	15:49	Brake torque pos 0 (off)
2015	03	09	15:50	Brake torque pos 1
2015	03	09	15:51	Brake torque pos 2
2015	03	09	15:52	Brake torque pos 3
2015	03	09	15:53	Brake torque pos 4
2015	03	09	15:54	Brake torque pos 5
2015	03	09	15:55	Brake torque pos 6
2015	03	09	15:56	Brake torque pos 7 (on)
2015	03	09	16:10	springs only #2
2015	03	09	16:13	springs only #3

Table E.3: Overview of all measurement runs.

year	month	day	time	description
				torque controller is implemented!
2015	03	10	13:21	180 degree return input side
2015	03	10	13:23	90 degree return input side
2015	03	10	13:28	90 degree return input side #2
2015	03	10	13:30	90 degree return input side #3
2015	03	10	13:39	90 degree return input side #4
2015	03	10	13:43	90 degree return input side #5 (nice run)
2015	03	10	14:18	position contour 360 degree return
2015	03	10	14:31	full 360 degree run
2015	03	10	14:50	full 360 degree run (different start)
2015	03	10	16:04	full 360 degree run #2
2015	03	10	16:06	full 360 degree run #3
2015	03	10	16:10	full 360 degree run #4
2015	03	10	16:12	full 360 degree run #5
2015	03	10	16:38	full 360 degree run #6
2015	03	10	17:11	Braking new pos 0
2015	03	10	17:28	Braking new pos 0 #2
2015	03	10	17:29	Braking new pos 0 #3
2015	03	10	17:31	Braking new pos 0 #4
2015	03	10	17:33	Braking new pos 0 #5
2015	03	10	17:35	Braking new pos 1 #1
2015	03	10	17:36	Braking new pos 1 #1
2015	03	10	17:38	Braking new pos 2 #1
2015	03	10	17:39	Braking new pos 2 #2
2015	03	10	17:40	Braking new pos 3 #1
2015	03	10	17:41	Braking new pos 3 #2
2015	03	10	17:43	Braking new pos 4 #1
2015	03	10	17:44	Braking new pos 4 #2
2015	03	10	17:46	Braking new pos 5 #1
2015	03	10	17:48	Braking new pos 5 #2
2015	03	10	17:51	Braking new pos 6 #1
2015	03	10	17:52	Braking new pos 6 #2
2015	03	10	17:53	Braking new pos 7 #1
2015	03	10	17:54	Braking new pos 7 #2
2015	03	10	18:01	springs only full 360 degrees #1
2015	03	10	18:04	springs only full 360 degrees #2
2015	03	10	18:06	springs only full 360 degrees #3
2015	03	10	18:09	springs only full 360 degrees #4
2015	03	10	18:10	springs only full 360 degrees #5

Table E.4: Overview of all measurement runs.

year	month	day	time	description
2015	03	13	14:45	no load switch 1 sec
2015	03	13	14:42	no load switch 2 sec
2015	03	13	14:40	no load switch 3 sec
2015	03	13	14:38	no load switch 4 sec
2015	03	13	14:50	loaded switch 1 sec
2015	03	13	14:55	loaded switch 2 sec
2015	03	13	14:57	loaded switch 3 sec
2015	03	13	14:59	loaded switch 4 sec
2015	03	13	15:02	loaded switch 5 sec #1
2015	03	13	15:10	loaded switch 5 sec #2
2015	03	13	15:12	loaded switch 5 sec #3
2015	03	13	15:14	loaded switch 5 sec #4
2015	03	13	15:16	loaded switch 5 sec #5
2015	03	13	15:18	loaded switch 5 sec #6
2015	03	13	15:20	loaded switch 5 sec #7
2015	03	13	15:38	loaded switch 4 sec #2
2015	03	13	15:40	loaded switch 4 sec #3
2015	03	13	15:43	loaded switch 3 sec #2
2015	03	13	15:44	loaded switch 3 sec #3
2015	03	13	15:46	loaded switch 2 sec #2
2015	03	13	15:47	loaded switch 2 sec #3
2015	03	13	15:49	loaded switch 1 sec #2
2015	03	13	15:51	loaded switch 1 sec #3
2015	03	13	16:09	loaded switch 0.5 sec #1
2015	03	13	16:11	loaded switch 0.5 sec #2
2015	03	13	16:12	loaded switch 0.5 sec #3
2015	03	13	16:14	loaded switch 0.25 sec #1
2015	03	13	16:16	loaded switch 0.25 sec #2
2015	03	13	16:17	loaded switch 0.25 sec #3
2015	03	17	09:29	Braking #1
2015	03	17	09:31	no load brake side
2015	03	17	09:33	Braking #2
2015	03	17	09:35	Braking #3
2015	03	17	09:39	Braking #4
2015	03	17	09:41	Braking #5

Table E.5: Overview of all measurement runs.

year	month	day	time	description
2015	03	17	09:49	Braking final position 0 #1
2015	03	17	09:50	Braking final position 0 #2
2015	03	17	09:51	Braking final position 0 #3
2015	03	17	09:53	Braking final position 1 #1
2015	03	17	09:54	Braking final position 1 #2
2015	03	17	09:55	Braking final position 1 #3
2015	03	17	09:57	Braking final position 2 #1
2015	03	17	09:58	Braking final position 2 #2
2015	03	17	10:00	Braking final position 2 #3
2015	03	17	10:02	Braking final position 3 #1
2015	03	17	10:03	Braking final position 3 #2
2015	03	17	10:04	Braking final position 3 #3
2015	03	17	10:06	Braking final position 4 #1
2015	03	17	10:08	Braking final position 4 #2
2015	03	17	10:09	Braking final position 4 #3
2015	03	17	10:11	Braking final position 5 #1
2015	03	17	10:12	Braking final position 5 #2
2015	03	17	10:13	Braking final position 5 #3
2015	03	17	10:15	Braking final position 6 #1
2015	03	17	10:16	Braking final position 6 #2
2015	03	17	10:17	Braking final position 6 #3
2015	03	17	10:18	Braking final position 7 #1
2015	03	17	10:19	Braking final position 7 #2
2015	03	17	10:21	Braking final position 7 #3

Table E.6: Overview of all measurement runs.

Bibliography

- [1] J. Geeroms, L. Flynn, R. Jimenez-Fabian, B. Vanderborght, and D. Lefeber, “Ankle-knee prosthesis with powered ankle and energy transfer for cyberlegs -prototype,” in *Rehabilitation Robotics (ICORR), 2013 IEEE International Conference on*, pp. 1–6, June 2013.
- [2] J. Hurst and A. Rizzi, “Series compliance for an efficient running gait,” *Robotics Automation Magazine, IEEE*, vol. 15, pp. 42–51, September 2008.
- [3] B. Vanderborght, B. Verrelst, R. Van Ham, M. Van Damme, D. Lefeber, B. M. Y. Duran, and P. Beyl, “Exploiting natural dynamics to reduce energy consumption by controlling the compliance of soft actuators,” *The International Journal of Robotics Research*, vol. 25, no. 4, pp. 343–358, 2006.
- [4] G. Pratt and M. Williamson, “Series elastic actuators,” in *Intelligent Robots and Systems 95. 'Human Robot Interaction and Cooperative Robots', Proceedings. 1995 IEEE/RSJ International Conference on*, vol. 1, pp. 399–406 vol.1, Aug 1995.
- [5] G. van Oort, R. Carloni, D. Borgerink, and S. Stramigioli, “An energy efficient knee locking mechanism for a dynamically walking robot,” in *Robotics and Automation (ICRA), 2011 IEEE International Conference on*, pp. 2003–2008, May 2011.
- [6] M. Plooij and M. Wisse, “A novel spring mechanism to reduce energy consumption of robotic arms,” in *Intelligent Robots and Systems (IROS), 2012 IEEE/RSJ International Conference on*, pp. 2901–2908, Oct 2012.
- [7] U. Mettin, P. X. La Hera, L. B. Freidovich, and A. S. Shiriaev, “Parallel elastic actuators as a control tool for preplanned trajectories of underactuated mechanical systems,” *The International Journal of Robotics Research*, vol. 29, no. 9, pp. 1186–1198, 2010.
- [8] M. Plooij, H. Vallery, and M. Wisse, “Bips: a bi-directional parallel spring mechanism that reduces the energy consumption of robots,” *under review*.
- [9] M. Plooij, G. Mathijssen, P. Cherule, D. Lefeber, and B. Vanderborght, “Lock your robot: a review of locking devices in robotics,” *IEEE Robotics and Automation Magazine*, vol. 22, March 2015.

-
- [10] M. Wisse, G. Feliksdal, J. Van Frankkenhuyzen, and B. Moyer, "Passive-based walking robot," *Robotics Automation Magazine, IEEE*, vol. 14, pp. 52–62, June 2007.
- [11] M. Design, "Mechanisms for intermittent motion," *Part*, vol. 3, pp. 146–155, 1952.
- [12] T. Lindberg, "Electromagnetic brake," Feb. 16 1993. US Patent 5,186,286.
- [13] D. W. Mckinley and J. K. Parmerlee, "Bi-stable brake," June 1973.
- [14] O. Baser and E. I. Konukseven, "Theoretical and experimental determination of capstan drive slip error," *Mechanism and Machine Theory*, vol. 45, no. 6, pp. 815 – 827, 2010.
- [15] K. Yamatoh, M. Ogura, K. Kanbe, and Y. Isogai, "Piezoelectric brake device," Aug. 1989.
- [16] G. D. Michiel Plooij and M. Wisse, "Z-force: a zero force brake, based on statically balancing," *under review*.
- [17] J. Hieronymus and R. Wadlinger, "Edge folding device having self-locking mechanism," July 8 2003. US Patent 6,588,341.
- [18] T. van der Hoeven, "Using mechanical singularities for friction locking," *Literature survey, Delft University of Technology*, 2014.
- [19] J. J. Uicker, G. R. Pennock, and J. E. Shigley, *Theory of machines and mechanisms*. Oxford University Press Oxford, 2011.
- [20] F. Park and J. W. Kim, "Singularity analysis of closed kinematic chains," *Journal of mechanical design*, vol. 121, no. 1, pp. 32–38, 1999.
- [21] C. Gosselin and J. Angeles, "Singularity analysis of closed-loop kinematic chains," *Robotics and Automation, IEEE Transactions on*, vol. 6, pp. 281–290, Jun 1990.
- [22] D. Zlatanov, R. Fenton, and B. Benhabib, "Identification and classification of the singular configurations of mechanisms," *Mechanism and Machine Theory*, vol. 33, no. 6, pp. 743 – 760, 1998.
- [23] F. Park and J. W. Kim, "Manipulability and singularity analysis of multiple robot systems: a geometric approach," in *Robotics and Automation, 1998. Proceedings. 1998 IEEE International Conference on*, vol. 2, pp. 1032–1037 vol.2, May 1998.
- [24] J. L. Herder, *Energy-free Systems. Theory, conception and design of statically*. 2001.
- [25] R. Barents, M. Schenk, W. D. van Dorsser, B. M. Wisse, and J. L. Herder, "Spring-to-spring balancing as energy-free adjustment method in gravity equilibrators," *Journal of Mechanical Design*, vol. 133, no. 6, p. 061010, 2011.

-
- [26] W.-H. Zhu, T. Lamarche, and P. Barnard, "Modular robot manipulators with preloadable modules," in *Mechatronics and Automation, 2007. ICMA 2007. International Conference on*, pp. 7–12, IEEE, 2007.
- [27] F. J. van Osch and J. L. Herder, "Design of an adjustable gravity equilibrator using torsion bars," *Master thesis, Delft University of Technology*, 2011.
- [28] G. Radaelli, J. A. Gallego, and J. L. Herder, "An energy approach to static balancing of systems with torsion stiffness," *Journal of Mechanical Design*, vol. 133, no. 9, p. 091006, 2011.
- [29] M. Plooij, T. van der Hoeven, G. Dunning, and M. Wisse, "Statically balanced brakes," *under construction*.
- [30] B. T. Knox and J. P. Schmiedeler, "A unidirectional series-elastic actuator design using a spiral torsion spring," *Journal of Mechanical Design*, vol. 131, no. 12, p. 125001, 2009.
- [31] D. Tsay and B. Lin, "Profile determination of planar and spatial cams with cylindrical roller-followers," *Proceedings of the Institution of Mechanical Engineers, Part C: Journal of Mechanical Engineering Science*, vol. 210, no. 6, pp. 565–574, 1996.
- [32] A. M. D. G. Steinhörsson, A and J. Herder, "Draft: Review, categorization and comparison of 1 dof static balancers," *Proceedings of of the ASME 2015 ASME 2015 International Design Engineering Technical Conferences and Computers and Information in Engineering Conference*, 2015, under review.